A ^{89}Y NMR Study of Substitution for Copper in $YBa_2Cu_3O_{7-\delta}$ and $YBa_2Cu_4O_8$.

Azmi Gençten

A thesis submitted to the University of Warwick
for the degree of Doctor of Philosophy.

Department of Physics
October 1992

List of Contents

Contents		i
List of Tables		iv
List of Figures		vi
Acknowledgements		xii
Declaration		xiii
Abstract		xiv

Chapter 1: Introduction.

1.1	Introduction to Superconductivity.	1
1.2	High T_c Superconductivity.	4
	1.2.1 General Introduction.	4
	1.2.2 $YBa_2Cu_3O_{7-\delta}$ and $YBa_2Cu_4O_8$.	7
	1.2.3 Substitution for Copper in $YBa_2Cu_3O_{7-\delta}$ and $YBa_2Cu_4O_8$.	13
1.3	Introduction to NMR.	14
1.4	NMR and Superconductivity.	15
1.5	A Brief Review of the NMR studies of High T_c Superconductors.	16
	1.5.1 NMR Studies in $YBa_2Cu_3O_{7-\delta}$ and $YBa_2Cu_4O_8$ systems.	16
	1.5.1.1 ^{89}Y NMR Approach.	16
	1.5.1.2 The Other Nuclei in $YBa_2Cu_3O_{7-\delta}$ and $YBa_2Cu_4O_8$.	18
	1.5.2 NMR Studies in the Other High T_c Superconductors.	19
1.6	The Aim of the Present Work.	20
	References.	21

Chapter 2: Theory.

2.1	Basic Principles of NMR.	26
2.2	Nuclear Spin Interactions in Solids.	31
	2.2.1 Dipole Dipole Interaction.	31
	2.2.2 The Chemical Shift Interaction.	34
	2.2.3 The Knight Shift Interaction.	38
	2.2.4 The Quadrupolar Interaction.	40
	2.2.5 RKKY Interaction.	41
2.3	Spin Lattice Relaxation.	43
2.4	MAS and Averaging of the Anisotropic Interactions.	45
2.5	NMR Theory of High T_c Superconductivity.	49
	2.5.1 General Introduction.	49
	2.5.2 One Component Model and the Spin Hamiltonian.	50

2.5.3 The Knight Shift and Relaxation Rate. 52
References. 54

Chapter 3: Experimental.

3.1 Pulsed FT NMR. 56
3.2 The Bruker MSL-360 Spectrometer. 60
3.2.1 The NMR Probes and Spinners. 61
3.3 Setting and Operation of the Spectrometer. 63
3.3.1 Setting up on a Nucleus. 63
3.3.2 Magic Angle Spinning. 63
3.3.3 Spin-Echo Method. 68
3.3.4 Data Collection. 69
3.3.5 Data Manipulation. 71
3.4 Variable Temperature Experiments. 71
3.5 T_1 Measurements. 72
3.6 Sample Preparation and Characterization 74
3.6.1. Sample Preparation. 75
3.6.1.1 Preparation of $YBa_2(Cu_{1-x}M_x)_3O_{7-\delta}$. 75
3.6.1.2 Preparation of $YBa_2(Cu_{1-y}M_y)_4O_8$. 75
3.6.2 X-Ray Diffraction. 76
3.6.3 A.C. Susceptibility. 79
References. 83

Chapter 4: $YBa_2(Cu_{1-x}M_x)_3O_{7-\delta}$ System.

4.1 Introduction to $YBa_2(Cu_{1-x}M_x)_3O_{7-\delta}$ System. 84
4.2 XRD Results and Transition Temperatures. 85
4.3 ^{89}Y Shifts. 90
4.3.1 General. 90
4.3.2 Room Temperature Results and Discussion. 91
4.3.3 Temperature Dependence. 95
4.3.3.1 Results. 95
4.3.3.2 Discussion. 104
4.3.3.2.(a) Chain Site Substitution. 104
4.3.3.2.(b) Plane Site Substitution (Zn and Ni). 107
4.3.3.2.(c) V Substitution. 107
4.4 Evidence for O-T Transition for Fe, Co, Ga and Al Substitutions. 109
4.5 ^{89}Y spin lattice relaxation. 115
4.5.1 Results. 115

	4.5.2 Discussion.	116
	4.5.2.(a) Chain Site Substitution.	116
	4.5.2.(b) Plane Site Substitution.	116
4.6	Correlation Between T_c and ^{89}Y NMR Data (Shift and Relaxation).	123
	4.6.1 Chain Site Substitution.	123
	4.6.2 Plane Site Substitution.	127
4.7	^{51}V NMR in $YBa_2(Cu_{1-x}V_x)_3O_{7-\delta}$.	127
4.8	^{27}Al NMR in $YBa_2(Cu_{1-x}Al_x)_3O_{7-\delta}$.	130
4.9	General Discussion of $YBa_2(Cu_{1-x}M_x)_3O_{7-\delta}$ System.	132
	References.	136

Chapter 5: $YBa_2(Cu_{1-y}M_y)_4O_8$ System.

5.1	Introduction to $YBa_2(Cu_{1-y}M_y)_4O_8$ System.	138
5.2	XRD Results and Transition Temperatures.	139
5.3	^{89}Y Shifts:	144
	5.3.1 Room Temperature Results and Discussion.	144
	5.3.2 Temperature Dependence.	147
5.4	^{89}Y Spin Lattice Relaxation.	150
	5.4.1 Results.	150
	5.4.2 Discussion.	155
5.5	General Discussion of $YBa_2(Cu_{1-y}M_y)_4O_8$ System.	158
	References.	162

Chapter 6: Conclusions.

6.1	Comparison of These Two Systems.	163
6.2	General Conclusions.	164
	6.2.1 $YBa_2(Cu_{1-x}M_x)_3O_{7-\delta}$ System.	164
	6.2.2 $YBa_2(Cu_{1-y}M_y)_4O_8$ System.	165
6.3	Suggestions for Further Work.	166
	References.	168

List of Tables.

1.1 Some of the high T_c superconductors with their T_c values and the year discovered. 6

1.2 The positions of the atoms in $YBa_2Cu_3O_{7-\delta}$[5]. 10

1.3 The positions of the atoms in $YBa_2Cu_4O_8$[22]. 10

3.1 Larmor frequencies of the nuclei and their reference samples used in this study together with their abundances and spin numbers. 64

4.1 The reduction rates in T_c for a variety of substitutions in $YBa_2(Cu_{1-x}M_x)_3O_{7-\delta}$. 90

4.2 The comparison of the experimental and the theoretical (in terms of transferred hyperfine field) values of total shift for the case of Ni and Zn substitution in $YBa_2Cu_3O_{7-\delta}$. 94

4.3 K^2T_1T versus dopant concentration for $YBa_2(Cu_{1-x}Co_x)_3O_7$ at room temperature. 120

4.4 K^2T_1T versus dopant concentration for $YBa_2(Cu_{1-x}Fe_x)_3O_7$ at room temperature. 120

4.5 K^2T_1T versus dopant concentration for $YBa_2(Cu_{1-x}Al_x)_3O_7$ at room temperature. 121

4.6 K^2T_1T versus dopant concentration for $YBa_2(Cu_{1-x}Ga_x)_3O_7$ at room temperature. 121

4.7 Summary of ^{89}Y data for $YBa_2(Cu_{1-x}M_x)_3O_{7-\delta}$ system. 133

5.1 MAS line widths for Zn and Fe substituted $YBa_2(Cu_{1-y}M_y)_4O_8$ at room temperature. 147

5.2 K^2T_1T versus dopant concentration for $YBa_2(Cu_{1-y}Fe_y)_4O_8$ at room

temperature. 155

6.1 The changes in relaxation rate and T_c with Zn substitution for Cu in $YBa_2Cu_3O_{7-\delta}$ and $YBa_2Cu_4O_8$. 163

6.2 The changes in shift and T_c with Fe substitution for Cu in $YBa_2Cu_3O_{7-\delta}$ and $YBa_2Cu_4O_8$. 163

List of Figures.

1.1 Magnetization curves for (a) the type I and (b) the type II superconductors. 5

1.2 The crystal structure of orthorhombic $YBa_2Cu_3O_{7-\delta}$[14]. 8

1.3 The phase diagram of $YBa_2Cu_3O_{7-\delta}$[15]. 11

1.4 The crystal structure of $YBa_2Cu_4O_8$[21]. 12

2.1 The energy levels for the nuclei with I=1/2. 28

2.2 Precession of the magnetic moment around the direction of applied field B_0. 28

2.3 Anisotropic powder patterns for (a) cubic symmetry (b) axial symmetry and (c) the general cases. 37

2.4 (a) Separation of energy levels and (b) the schematic spectrum for a nucleus I=3/2 in the case of first order quadrupolar interaction. 42

2.5 (a) The conduction electron wave functions and (b) the distribution of conduction electron spin density around the impurity atom in RKKY interactions[13]. 44

2.6 Definition of angle geometry for Magic Angle Spinning technique. 47

2.7 ^{51}V NMR spectra in 2.5 % V doped $YBa_2Cu_3O_{7-\delta}$ with different spinning rates. The asterisks denote the spinning side bands. 48

2.8 The illustration of the hyperfine couplings in the CuO_2 planes[33]. 51

3.1 The effect of (a) a $\pi/2$ and (b) a π pulse. 58

3.2 (a) Typical FID signal and (b) its Fourier transformation. 58

3.3	The block diagram of the Pulsed FT NMR spectrometer.	59
3.4	The block diagram of the Bruker MSL-360 spectrometer system[7].	62
3.5	The spinners used in (a) DB MAS and (b) Doty and Woty probes.	64
3.6	^{89}Y Static and MAS NMR spectra in $YBa_2Cu_4O_8$.	66
3.7	^{51}V Static and MAS, with different spinning rates, NMR spectra in $YBa_2(Cu_{1-x}V_x)_3O_{7-\delta}$ (x=0.2).	67
3.8	The illustration of the simplest form of spin echo sequence.	70
3.9	The vectorial representation of the extended spin echo sequence.	70
3.10	The illustration of saturation combs sequence for T_1 measurements.	73
3.11	XRD powder pattern of orthorhombic $YBa_2Cu_3O_7$ at room temperature.	77
3.12	XRD powder pattern of $YBa_2Cu_4O_8$ at room temperature.	78
3.13	Basic schematic diagram of the A.C. susceptibility system.	80
3.14	A.C. susceptibility vs. temperature curve for $YBa_2Cu_3O_7$.	82
4.1	XRD powder patterns for $YBa_2(Cu_{1-x}Co_x)_3O_7$ with x=0–0.1 and 2θ=45–50.	86
4.2	XRD powder patterns for $YBa_2(Cu_{1-x}M_x)_3O_7$ with 2θ=45–50. Where x=0.1 and M=Cu, V, Ni, Zn, Fe, Co, Ga and Al.	87
4.3	(a) The transition temperatures as a function of dopant concentration x for Al, Ga, Fe and Co substitution in $YBa_2(Cu_{1-x}M_x)_3O_7$.The lines are drawn to guide the eye.	88
4.3	(b) The transition temperatures as a function of dopant concentration	

x for V, Ni and Zn substitution in $YBa_2(Cu_{1-x}M_x)_3O_7$. The lines are drawn to guide the eye. 89

4.4 ^{89}Y MAS NMR spectra in $YBa_2(Cu_{1-x}Co_x)_3O_7$ with x=0–0.1. The asterisks denote an unknown phase. 92

4.5 ^{89}Y shift at room temperature vs. concentration x for $YBa_2(Cu_{1-x}M_x)_3O_7$ with M=Co, Ga, Fe, Al, V, Ni and Zn. 93

4.6 ^{89}Y shift as a function of temperature in $YBa_2(Cu_{1-x}Co_x)_3O_7$ with x=0–0.1. The lines are drawn to guide the eye. 96

4.7 ^{89}Y shift as a function of temperature in $YBa_2(Cu_{1-x}Al_x)_3O_7$ with x=0–0.1. The lines are drawn to guide the eye. 97

4.8 ^{89}Y shift as a function of temperature in $YBa_2(Cu_{1-x}Ga_x)_3O_7$ with x=0–0.1. The lines are drawn to guide the eye. 98

4.9 ^{89}Y shift as a function of temperature in $YBa_2(Cu_{1-x}V_x)_3O_7$ with x=0–0.1. The lines are drawn to guide the eye. 99

4.10 The temperature dependence of the ^{89}Y NMR shift for the 2.5% substituted samples. The lines are drawn to guide the eye. 100

4.11 The temperature dependence of the ^{89}Y NMR shift for the 5% substituted samples. The lines are drawn to guide the eye. 101

4.12 (a) The ^{89}Y MAS NMR line width in $YBa_2Cu_3O_7$ and for 2.5% Al,Co,Ga and Zn substituted $YBa_2Cu_3O_7$. The lines are drawn to guide the eye. 102

4.12 (b) The ^{89}Y MAS NMR line width for 2.5% substituted Fe,Ni and V. The lines are drawn to guide the eye. 103

4.13 The ^{89}Y MAS NMR line width vs. 1/T for $YBa_2Cu_3O_7$ and for 2.5% Al, Co and Ga substituted $YBa_2(Cu_{1-x}M_x)_3O_7$. 106

4.14 The ^{89}Y MAS NMR line width vs. 1/T for pure $YBa_2Cu_3O_7$ and for 2.5% and 5% Zn substituted $YBa_2(Cu_{1-x}Zn_x)_3O_7$. 108

4.15 ^{89}Y shift at room temperature as a function of the dopant concentration x for $YBa_2(Cu_{1-x}M_x)_3O_7$ with M=Co, Ga, Al and V. 110

4.16 ^{89}Y shift at 200K as a function of the dopant concentration x for $YBa_2(Cu_{1-x}M_x)_3O_7$ with M=Co, Ga, Al and V. 112

4.17 ^{89}Y chemical shift at room temperature as a function of the dopant concentration x for $YBa_2(Cu_{1-x}Co_x)_3O_7$. 113

4.18 T_c versus ^{89}Y shift at room temperature for Co and Al substituted $YBa_2Cu_3O_7$ with x as the implicit parameter. 114

4.19 (a) ^{89}Y spin lattice relaxation rates at room temperature versus concentration for Ga, Al, Fe and Co substituted $YBa_2Cu_3O_7$. The lines are drawn to guide the eye. 116

4.19 (b) ^{89}Y spin lattice relaxation rates at room temperature versus concentration for Zn, Ni and V substituted $YBa_2Cu_3O_7$. The lines are drawn to guide the eye. 117

4.20 (T_1T) as a function of temperature for 2.5% Co and Zn substituted $YBa_2Cu_3O_7$ and for pure $YBa_2Cu_3O_7$. The lines are drawn to guide the eye. 118

4.21 K^2T_1T as a function of temperature for 2.5% Co substituted $YBa_2Cu_3O_7$ and for pure $YBa_2Cu_3O_7$. 122

4.22 The reduction in T_c as a function of the change in ^{89}Y shift in $YBa_2(Cu_{1-x}M_x)_3O_7$ with M=Co,Fe,Ga, Al and V. 125

4.23 The ^{89}Y NMR shift in $YBa_2Cu_3O_{6.75}$ vs. $YBa_2(Cu_{1-x}Co_x)_3O_7$ (x=0.05) which both have T_c=70K with temperature as the implicit parameter. Also shown is the ^{89}Y NMR shift for $YBa_2(Cu_{1-x}V_x)_3O_7$ (x=0.05) vs. $YBa_2(Cu_{1-x}Al_x)_3O_7$ (x=0.025), both of which have a

T_c=89K. 126

4.24 The reduction rate in Tc as a function of the change in relaxation rate in $YBa_2(Cu_{1-x}M_x)_3O_7$ with M=Cu, Ni and Zn. 128

4.25 ^{51}V NMR spectra of $YBa_2(Cu_{1-x}V_x)_3O_7$ with x=0.025,0.05 and 0.10 (a) static, (b) spinning at 3.5kHz, asterisks denote the spinning sidebands. 129

4.26 ^{27}Al MAS NMR spectra of $YBa_2(Cu_{1-x}Al_x)_3O_7$ with x=0.025, 0.05, and 0.10, asterisks donate the second phase Al_2O_3. 131

5.1 XRD powder patterns in $YBa_2(Cu_{1-y}M_y)_4O_8$ for M= (a) Zn and (b) Fe for y=0–0.03 and 2θ=45–50. 140

5.2 (a) The lattice parameters of $YBa_2(Cu_{1-y}Zn_y)_4O_8$ as a function of dopant concentration y. The lines are drawn to guide the eye. 141

5.2 (b) The lattice parameters of $YBa_2(Cu_{1-y}Fe_y)_4O_8$ as a function of dopant concentration y. The lines are drawn to guide the eye. 142

5.3 The transition temperatures as a function of dopant concentration y for Zn and Fe substitution in $YBa_2(Cu_{1-y}M_y)_4O_8$. The line is drawn to guide the eye. 143

5.4 ^{89}Y MAS NMR spectra in $YBa_2(Cu_{1-y}Zn_y)_4O_8$ with x=0-0.03. The asterisks denote the unknown phase. 145

5.5 ^{89}Y MAS NMR spectra in $YBa_2(Cu_{1-y}Fe_y)_4O_8$ with x=0-0.03. The asterisks denote the additional phases. 146

5.6 ^{89}Y shift at room temperature versus dopant concentration y for $YBa_2(Cu_{1-y}M_y)_4O_8$ with M=Fe and Zn. 148

5.7 ^{89}Y shift as a function of temperature for 1.8% and 3% Zn substituted $YBa_2(Cu_{1-y}Zn_y)_4O_8$ and for pure $YBa_2Cu_4O_8$. The lines are drawn to guide the eye. 149

5.8 ^{89}Y shift as a function of temperature for 1.8% Zn and Fe substituted $YBa_2(Cu_{1-y}M_y)_4O_8$ and for pure $YBa_2Cu_4O_8$. The line is drawn to guide the eye. 151

5.9 The ^{89}Y MAS NMR line width as a function of temperature for 1.8% Zn and Fe substituted $YBa_2(Cu_{1-y}M_y)_4O_8$ and for pure $YBa_2Cu_4O_8$. The lines ara drawn to guide the eye. 152

5.10 ^{89}Y MAS NMR line width versus 1/T for pure $YBa_2Cu_4O_8$ and 1.8% Zn doped $YBa_2Cu_4O_8$. 153

5.11 ^{89}Y T_1^{-1} at room temperature versus dopant concentration y for $YBa_2(Cu_{1-y}M_y)_4O_8$ with M=Fe and Zn. The lines are drawn to guide the eye. 154

5.12 (T_1T) as a function of temperature for 1.8% Zn and Fe substituted $YBa_2(Cu_{1-y}M_y)_4O_8$ and for pure $YBa_2Cu_4O_8$[8]. 156

5.13 T_1^{-1} as a function of T_c for $YBa_2(Cu_{1-y}Zn_y)_4O_8$ with y as the implicit parameter. 157

5.14 K^2T_1T as a function of temperature for 1.8% Fe substituted $YBa_2(Cu_{1-y}M_y)_4O_8$ and for pure $YBa_2Cu_4O_8$[8]. 159

Acknowledgements.

I wish to acknowledge the Turkish Higher Education Council (YÖK)and Ondokuz Mayıs University (Turkey) consortium for a studentship.

I would like to thank my friends from Turkey at this University and at the other Universities in UK for their close friendships and their encouragements. I am especially grateful to the ones doing Physics:AB,EB and MEY for their interest and their support.

The NMR coffee club was providing an enjoyable environment everyday and I would like to thank all its members (past and present): GAS, GB, PD, TK, ZPH, MES, SK, ML, MGM, RE, DK, JR, DG, LCA. I would especially like to thank Dr. A.P. Howes and L.W.J. Caves for their suggestions in preparation and characterisation of the samples at the beginning of this study and I am grateful to Prof. D.McK. Paul for his invaluable suggestions.

I would like to thank Dr T.G.N. Babu and Dr C. Greaves of Birmingham University for their suggestions in preparation of $YBa_2(Cu_{1-y}M_y)_4O_8$ samples. I would like to express my gratitude to Prof. R. Dupree, my supervisor, for his perfect guidance and help during this study.

Declaration.

The work for this thesis was carried out in the Department of Physics at the University of Warwick from March 1989 to March 1992. It contains an account of my own independent research except where specifically referenced in the text and has not been submitted for any other degree.

Some parts of this thesis have been published or are to be published as follows:

1- "A ^{89}Y NMR study of substitution for copper in $YBa_2(Cu_{1-x}M_x)_3O_7$." R. Dupree, A. Gencten and D.McK. Paul, Physica C 193 (1992) 81.

2- "A ^{89}Y NMR Investigation in Zn and Fe doped $YBa_2Cu_4O_8$." A. Gencten, R. Dupree and D.McK. Paul, to be published.

It is anticipated that other parts of this thesis will be submitted for publication in the future.

Abstract

^{89}Y MAS NMR has been used to study the effects of substitution for Cu in $YBa_2(Cu_{1-x}M_x)_3O_7$ (M=V,Fe,Co,Ni,Zn,Al and Ga) and $YBa_2(Cu_{1-y}M_y)_4O_8$ (M=Zn and Fe). Substituted $YBa_2(Cu_{1-x}M_x)_3O_7$ and $YBa_2(Cu_{1-y}M_y)_4O_8$ samples have been characterized by means of XRD and A.C. susceptibility measurements.

For $YBa_2(Cu_{1-x}M_x)_3O_7$, a different behaviour is observed for the substitutions (Fe,Co,Al and Ga) which go into the chain site and change the structure to tetragonal, compared to the other substitutions (Ni and Zn). For chain site substitutions the room temperature shift increases linearly with concentration and the relaxation rate decreases whilst the shifts become more positive with decreasing temperature. For these chain site substitutions, changes in ^{89}Y chemical shift have provided evidence for the existence of a true O–T transition. For these substitutions the shift and relaxation appear to obey a Korringa relation and the reduction in T_c is correlated with the change in shift indicating that suppression of T_c is due to the changes in $N(E_F)$. A similar temperature dependence of shift for chain site substituted samples with similar T_cs suggests that the T_c is related to the spin susceptibility in the CuO_2 planes. Plane site substitutions have only a small effect on the shift,whilst increasing the relaxation rate at room temperature. The increased relaxation rate indicates that some form of magnetic scattering is produced by these substitutions and this combined with the small changes in shift and with the correlation between the reduction in T_c and the change in relaxation rate indicates that magnetic effects rather than hole doping are the cause of the reduction in T_c. In addition, MAS NMR data for ^{51}V and ^{27}Al in V and Al substituted $YBa_2Cu_3O_7$ are presented. Both the ^{89}Y behaviour and ^{51}V data suggest that vanadium substitutes on the chain sites even though the structure remains orthorhombic.

In the case of Fe and Zn substitution for Cu in $YBa_2(Cu_{1-y}M_y)_4O_8$ a rapid decrease in T_c has been obtained. For Fe, as the dopant concentration increases, a nearly Korringa like behaviour has been observed, at room temperature, with an increase in shift and a decrease in relaxation rate. Zn substitution caused only a very small change in shift but an increase in relaxation rate. As was found for the plane site substituted $YBa_2(Cu_{1-x}M_x)_3O_7$, this rapid increase in relaxation rate is again an indication for the existence of fluctuating magnetic fields. The correlation between T_1^{-1} and T_c with Zn substitution suggests that magnetic effects are responsible for the rapid decrease in T_c. ^{89}Y NMR data for $YBa_2Cu_4O_8$ doped with Zn and Fe combined with that for $YBa_2Cu_3O_7$ doped with Zn and Fe have suggested that Zn occupies the Cu(2) site and Fe substitutes into both Cu(1) and Cu(2) sites.

Chapter 1. Introduction.

1.1. Introduction to Superconductivity.

Superconductivity is the total disappearance of the electrical resistance as the material is cooled below a certain temperature called the transition temperature, T_c. The superconducting state is a phase of a superconductor as ice is a phase of water.

In 1911 the phenomenon of superconductivity was first discovered by Kamerling Onnes who liquefied helium in 1908. He found that the electrical resistance of mercury abruptly vanishes when it is cooled down to 4.2K.

The discovery of the Meissner effect by Meissner and Ochsenfeld in 1933 showed that a superconductor is not just an ideal conductor, but also a perfect diamagnet. They found that the magnetic field lines are expelled from (the inside of) a superconductor in the superconducting state. A theoretical description of these two anomalous behaviours based on the two fluid model, namely; zero resistance and Meissner effect was first achieved by the F. and H. London brothers in 1935.

In 1950 it was suggested[1] that superconductivity is connected with the interaction between the electrons and lattice vibrations. The microscopic theory of superconductivity was established by Bardeen, Cooper and Schrieffer in 1957[2] and is now called BCS theory. Historical reviews on superconductivity can be found elsewhere[3].

The basic principle of the BCS theory is based on the existence of a pair of electrons, called a Cooper pair, whose energy is lower than that of two individual electrons. It is assumed that there is an attractive interaction (larger than the repulsive Coulomb interaction) between these two electrons. In BCS type

superconductors a gap appears in the density of states centred about the Fermi energy in the superconducting state. In the BCS theory the transition temperature and the energy gap E_g are expressed as[4]

$$k_B T_c = 1.14 \hbar\omega_c e^{-\frac{1}{N(E_F)V-\mu^*}} \tag{1.1}$$

$$E_g = 4\hbar\omega_c e^{-\frac{1}{N(E_F)V-\mu^*}} \tag{1.2}$$

Where $N(E_F)$, $\hbar\omega_c$ and V are the density of normal state electrons at the Fermi level, the phonon energy and electron electron attractive potential, respectively. μ^* is the coulomb interaction pseudopotential given as;

$$\mu^* = \frac{\mu}{1+\mu\ln(\frac{E_F}{\hbar\omega_c})} \tag{1.3}$$

with a Coulomb constant $\mu = \langle V_c \rangle N(E_F)$. From the equations 1.1 and 1.2, the ratio between the energy gap and the critical temperature is given by

$$\frac{E_g}{k_B T_c} = 3.528 \tag{1.4}$$

In the superconducting state as a result of a gap in the electronic density of states there exists an electronic specific heat different from that of a normal metal. BCS theory predicts that at the transition temperature there is a jump in the specific heat proportional to T_c given by[5]

$$\frac{\Delta C}{\gamma T_c}=1.43 \tag{1.5}$$

Where $\Delta C=C_s-C_n$ and $C_n=\gamma T_c$. The subscripts s and n refer to the superconducting and normal states respectively.

The Ginsburg-London parameter is defined as $\kappa=\lambda/\xi$. Where λ and ξ are penetration depth and coherence length, respectively. The penetration depth is the distance into a superconducting material where 1/e of the external dc magnetic field penetrates. The coherence length is the average separation between two electrons which form a Cooper pair. The Ginsburg-London parameter is used to classify superconductors as type I or type II:

$$\kappa=\frac{\lambda}{\xi}\begin{cases}<\frac{1}{\sqrt{2}} & \text{type I}\\ >\frac{1}{\sqrt{2}} & \text{type II}\end{cases} \tag{1.6}$$

The basic characteristic properties of superconductivity can be summarized as follows:

(a) Zero resistivity: capability of carrying current with absolutely no

resistance.

(b) The transition temperature: below which the superconducting state is entered.

(c) Perfect diamagnetism or Meissner effect: in the superconducting state, the exclusion of magnetic fields from the sample.

(d) Critical magnetic field and critical current: superconductivity can be destroyed by either a large enough magnetic field $H>H_c$ or a large enough current density $J>J_c$. H_c and J_c are called critical magnetic field and critical current density, respectively. In type II superconductors , two critical magnetic fields exist namely; the first (H_{c1}) and the second (H_{c2}). The region between these fields is called the mixed state in which the magnetic field partially penetrates into the material. This partial penetration forms a flux lattice with superconducting regions between the flux lines. Magnetization curves for the two types of superconductors are illustrated in fig.1.1.

1.2. High T_c Superconductivity.

1.2.1. General Introduction.

The discovery of a superconducting copper oxide $(La,Ba)_2CuO_4$ with a T_c of 35 K in 1986 by Bednorz and Müller[6] started a new era in the study of superconductivity. After their work many new high T_c superconductors were found. In table 1.1 some of these high T_c superconductors are listed with their T_c values and the year of the discovery. Because their T_c values are much higher than that of old superconductors, they are called high T_c superconductors. Before 1986, the recorded highest T_c was 23.2 K for Nb_3Ge superconductor[7,8]. At the present time

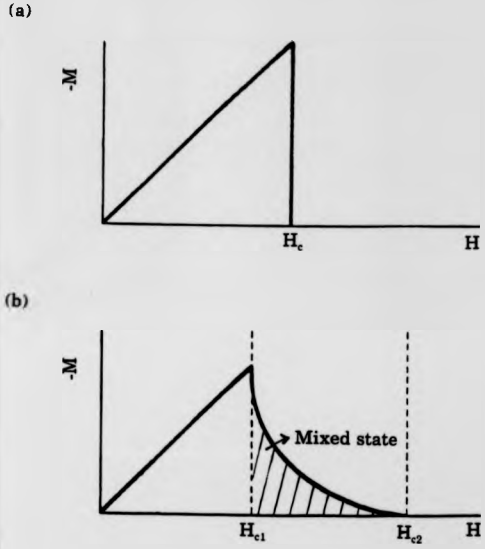

Fig.1.1. Magnetization curves for (a) the type I and (b) the type II superconductors.

Table 1.1. Some of the high T_c superconductors with their T_c values and the year discovered.

Compounds	T_c(K)	Year Discovered
$(La,Ba)_2CuO_4$	35	1986
$(Ba_{1-x}K_x)BiO_3$ (x=0.4)	30	1988
$Nd_{2-x}Ce_xCuO_4$ (x=0.15)	30	1989
$YBa_2Cu_3O_7$	92	1987
$YBa_2Cu_4O_8$	80	1988
$Bi_2Sr_2CaCu_2O_8$	85	1987
$Bi_2Sr_2Ca_2Cu_3O_{10}$	110	1987
$Tl_2Ba_2CaCu_2O_8$	112	1988
$Tl_2Ba_2Ca_2Cu_3O_{10}$	125	1988

the highest T_c is 125 K for the $Tl_2Ba_2Ca_2Cu_3O_{10}$ superconductor. Some other oxide (e.g. $Ba_{1-x}K_xBiO_3$[9]) and fullerene (e.g.$Cs_2Rb_1C_{60}$[10]) superconductors with T_c>20K have been discovered. They are also considered as high T_c superconductors.

All the copper oxide superconductors have perovskite-like structures[5,11] with the existence of CuO_2 planes being a distinctive characteristic in all of them. It is now believed that superconductivity occurs in these planes. The crystal structure of these high T_c superconductors is given elsewhere[4,12].

It appears that all high T_c copper oxide superconductors are related to an insulating antiferromagnetic phase. As an example, $YBa_2Cu_3O_6$ is the antiferromagnetic phase of $YBa_2Cu_3O_7$. In $YBa_2Cu_3O_6$ doping with the oxygen removes the electrons from the copper oxygen planes, leaving behind holes. Then the holes make the CuO_2 layers metallic and superconducting. Apart from $Nd_{2-x}Ce_xCuO_4$ in table 1, in all of these high T_c copper oxides the charge carriers are holes. They all are type II superconductors.

The normal state properties of high T_c superconductors are anomalous in many ways such as a linear temperature dependence of the resistivity and temperature dependent Hall coefficient. Therefore an explanation of normal state properties of these high T_c superconductors is required in order to develop a theory for the high T_c superconductivity.

1.2.2. $YBa_2Cu_3O_{7-\delta}$ and $YBa_2Cu_4O_8$.

The discovery of $YBa_2Cu_3O_{7-\delta}$ superconductor[13] was significant because its T_c (92K) is higher than the boiling point of nitrogen (77K). $YBa_2Cu_3O_{7-\delta}$ is the most studied among the high T_c copper oxide superconductors. Sometimes it is also

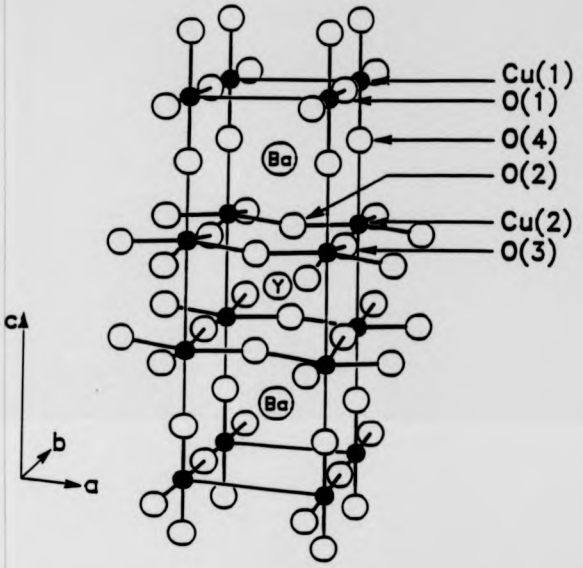

Fig.1.2. The crystal structure of orthorhombic $YBa_2Cu_3O_{7-\delta}$[14].

called "Y123". It is orthorhombic if $\delta<0.6$ and the lattice parameters for $\delta=0$ are a=3.827, b=3.882 c=11.682 Å. The crystal structure for this phase is shown in fig.1.2[14] and the positions of the atoms are given in table.1.2[5]. As seen from the structure (fig.1.2) Cu has two sites: namely; Cu(1) chain site (CuO) and Cu(2) plane site (CuO_2) with one Cu(1) and two Cu(2) sites in a unit cell. The Y atom sits at the centre of the unit cell between the CuO_2 planes.

The oxygen stoichiometry is not stable, thus δ in $YBa_2Cu_3O_{7-\delta}$ can take any value between 0 and 1. As a result of this, the structure and superconductivity are sensitive to the oxygen stoichiometry. The phase diagram of this compound is shown in fig.1.3[15]. For $0<\delta<0.6$, the compound is superconducting, orthorhombic and metallic but for $0.6<\delta<1$, it has a tetragonal structure and is semiconducting and antiferromagnetic. The reduction in oxygen content (in δ) is due to oxygen depletion in the CuO chains.

The first evidence for the existence of $YBa_2Cu_4O_8$ came from the electron microscopy study of lattice defects in $YBa_2Cu_3O_{7-\delta}$[16]. Later it was prepared as a bulk superconductor by several research groups using a high oxygen pressure[17,18] and finally under one atmosphere pressure[19]. The crystal structure of this compound was determined by X-ray diffraction[20]. $YBa_2Cu_4O_8$ has a T_c of 80K. As shown in Fig.1.4[21], the crystal structure of this compound is closely related to $YBa_2Cu_3O_{7-\delta}$ having an additional CuO chain. The existence of additional CuO chains results in a much longer c lattice parameter and thermally stable oxygen content. The lattice parameters of $YBa_2Cu_4O_8$ are a=3.8364 b=3.8635 c=27.2083Å (chapter 3). The positions of the atoms in $YBa_2Cu_4O_8$ are provided in table 1.3[22]. Since $YBa_2Cu_4O_8$

Table 1.2. The positions of the atoms in $YBa_2Cu_3O_{7-\delta}$[5].

Atom	x	y	z
Y	0.5	0.5	0.5
Ba	0.5	0.5	±0.1854
Cu(1)	0.0	0.0	0.0
Cu(2)	0.0	0.0	±0.3555
O(1)	0.0	0.5	0.0
O(2)	0.5	0.0	±0.3781
O(3)	0.0	0.5	±0.3790
O(4)	0.0	0.0	±0.1568

Table 1.3. The positions of the atoms in $YBa_2Cu_4O_8$[22].

Atom	x	y	z
Y	0.5	0.5	0.0
Ba	0.5	0.5	±0.13485
Cu(1)	0.0	0.0	±0.21328
Cu(2)	0.0	0.0	±0.06153
O(1)	0.0	0.5	±0.21802
O(2)	0.5	0.0	±0.05262
O(3)	0.0	0.5	±0.05240
O(4)	0.0	0.0	±0.14527

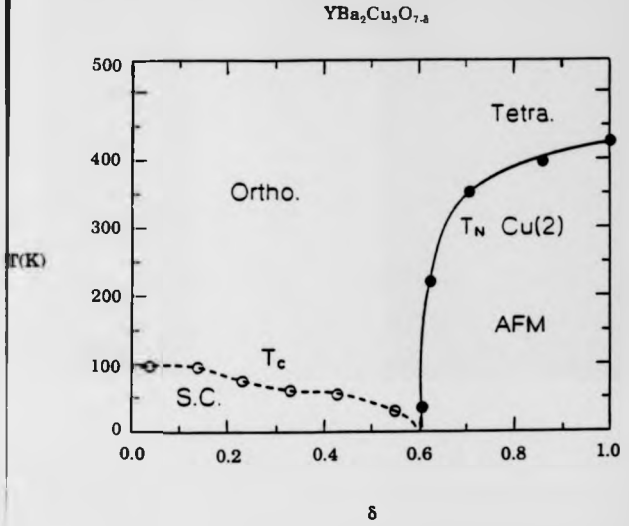

Fig.1.3. The phase diagram of $YBa_2Cu_3O_{7-\delta}$[15].

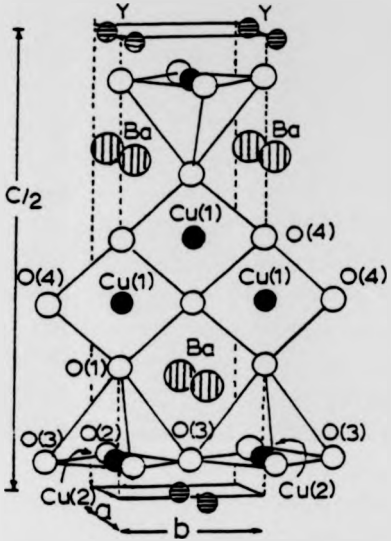

Fig.1.4. The crystal structure of $YBa_2Cu_4O_8$[21].

is stable in terms of oxygen content and structure, the experimental results are not effected either by oxygen stoichiometry or by the structural transition contrary to $YBa_2Cu_3O_{7-\delta}$.

1.2.3. Substitution for Copper in $YBa_2Cu_3O_{7-\delta}$ and $YBa_2Cu_4O_8$.

Substitution for Cu in $YBa_2Cu_3O_{7-\delta}$ was first carried out with the aim of increasing T_c as with other substitution studies. But now the main aim is to study the mechanism of high T_c superconductivity. It was found that the T_c was reduced with different substitutions for Cu in $YBa_2Cu_3O_{7-\delta}$ (for data see chapter 4).

There have been many studies by different research groups on the effect of substitution for Cu in $YBa_2(Cu_{1-x}M_x)_3O_{7-\delta}$ (M=Ti, V, Cr, Mn, Fe, Co, Ni, Zn, Al and Ga)[23–27]. Structural effects have been studied by using X-ray diffraction[23–26] and neutron diffraction[24,26,28]. It was found that substitution of Fe, Co, Al and Ga causes a structural change from orthorhombic to tetragonal for about 2-3% of substituent[24,26]. Site occupancies have been investigated by using neutron diffraction[24,26,28–35], EXAFS[32,36,37] and Mössbauer spectroscopy[26,38–40]. There have been disagreements about the site preference of a particular substituent, but it has been agreed by most research groups that Co[26,31,36], Al[26,41] and Ga[24] substitute for the Cu(1) site whereas Ni[33,34] goes onto the Cu(2) site. In the case of Fe, most substitution occurs onto the Cu(1) site although at higher concentrations Fe substitutes on both sites[35,36,42,43]. For Zn the situation is still controversial with the balance of opinion seeming to favour substitution on the Cu(2) site[24,32,34,44]. Discussions in detail on substitution effects are given in chapter 4 together with NMR results.

It was reported that 10% Ca substitution on the Y site in $YBa_2Cu_4O_8$ increases the T_c to 90K[45] and Y can be replaced by the rare earth metals with small changes in T_c[18].

Because of the difficulties in preparation of $YBa_2Cu_4O_8$, there have been only a few studies on substitution for Cu[21,46–52]. These showed that T_c in $YBa_2Cu_4O_8$ is very sensitive to the substitution for Cu. For example, for both Zn and Fe substitutions the reduction rate in T_c is 20–23K/% (see chapter 5). It seems that Zn substitution does not make any change in the crystal structure whereas in the case of Fe substitution the structure eventually becomes tetragonal at around 5% substitution (see Chapter 5). Site occupancies and other effects of Zn and Fe substitutions are discussed in chapter 5 by comparing our ^{89}Y NMR results with the results of other techniques.

1.3. Introduction to NMR.

NMR involves the transitions between magnetic energy levels of nuclei separated by a magnetic field. NMR was first performed in 1946 by Purcell and his colleagues[53] in paraffin wax and by Bloch and his co-workers in liquid water[54], independently. They were both awarded the 1952 Nobel price for their discovery.

In 1949 it was observed by Knight[55] that the resonance frequency of a given nucleus in a metal is shifted with respect to its frequency in a non–metal. This is due to an additional effect from the interaction between the conduction electrons and the nucleus and is called the Knight shift. Knight shift effects have been widely used to study the electronic and magnetic properties of metallic specimens (for a review see references 56–58). A detailed theoretical description of the Knight shift is given in

section 2.2.3.

It has been found (in 1950) that the resonance frequency of a particular nucleus depends on its chemical environment[59–61]. As a result of the discovery of this effect called the chemical shift (see section 2.2.2), NMR became a powerful technique for studying chemical compounds. The chemical shift is usually smaller than the Knight shift.

Solid state NMR has been applied to the study of superconductivity before (section 1.4) and after (section 1.5) the discovery of high T_c superconductivity.

1.4. NMR and Superconductivity.

It is well known that NMR has played a significant role in understanding the mechanism of low T_c superconductors and thus confirming BCS theory. The spin lattice relaxation rate has a sharp peak just below the transition temperature in conventional superconductors as first measured by Hebel and Slichter[62] in superconducting aluminum. They found that their experimental results were consistent with the calculations based on the coherence effect of the BCS theory[63]. The observation of this peak called the coherence peak or the Hebel–Slichter peak confirmed BCS theory in the old superconductors. Another feature of the spin lattice relaxation rate consistent with the BCS theory is that it decreases exponentially at low temperatures ($T \ll T_c$) as given by

$$\frac{1}{T_1} \propto \exp\left(-\frac{E_g}{2k_B T}\right) \qquad (1.7)$$

The electronic susceptibility in the superconducting state is measured by means of the Knight shift in an NMR experiment. The temperature dependence of the Knight shift in the superconducting state for BCS superconductors was first given by Yoshida[64]. But the experimental Knight shift data in superconducting mercury colloids presented by Reif[65] was in contradiction with Yoshida theory. Therefore a simple modification was made in Yoshida theory[66,67]. For more detailed information on the magnetic resonance studies of conventional superconductors the reader is referred to the general review by MacLaughlin[68].

1.5. A Brief Review of the NMR Studies of High T_c Superconductors.

In the previous section, the significant contribution of NMR for establishing the BCS theory has been discussed. In this section, NMR studies on high T_c superconductors (concentrating on $YBa_2Cu_3O_{7-\delta}$ and $YBa_2Cu_4O_8$) are reviewed.

The experimental studies on high T_c superconductors using different techniques showed that these new superconductors are very unusual. It was believed that NMR was one of the most important tools for the study of high T_c superconductors. During the last six years there have been many NMR and NQR studies of ^{139}La, ^{89}Y, $^{63}Cu/^{65}Cu$, ^{17}O, ^{205}Tl and so on in these new materials (see table 1.1).

1.5.1. NMR Studies in $YBa_2Cu_3O_{7-\delta}$ and $YBa_2Cu_4O_8$.

1.5.1.1. ^{89}Y NMR Approach.

The first ^{89}Y NMR measurements of fully oxygenated $YBa_2Cu_3O_{7-\delta}$ were reported by Markert et al[69] in the normal and mixed states. They observed a small

Knight shift and T_1T=constant in the normal state, with a decrease in $1/T_1$ in the superconducting state faster than in the BCS superconductors, and with no coherence peak. A ^{89}Y NMR study of $YBa_2Cu_3O_{7-\delta}$ with δ=0-1, in the normal state was first presented by Balakrishnan et al[70], using the Magic Angle Spinning (MAS) technique. Similar results were reported by Alloul et al[71]. It was reported by Alloul et al[72] and Dupree et al[73] that the negative Knight shift at room temperature in $YBa_2Cu_3O_{7-\delta}$ decreases with decreasing oxygen content. ^{89}Y NMR has been used in order to study the flux lattice in $YBa_2Cu_3O_7$[74].

^{89}Y NMR data at room temperature on Zn and Ga substitutions for Cu in fully oxygenated $YBa_2Cu_3O_{7-\delta}$ were presented by Balakrishnan et al[75]. They suggested that the source for the reduction in T_c with Zn substitution is related to the magnetic moments induced by Zn doping. Also several ^{89}Y NMR studies for some substitutions onto Cu sites in $YBa_2Cu_3O_{7-\delta}$ have been reported recently by several research groups[76,77]. These results are discussed in detail with our results in chapter 4. Pr and Nd doped $YBa_2Cu_3O_{7-\delta}$ (into Y site) have also been studied by ^{89}Y NMR[78].

The first ^{89}Y NMR measurements in $YBa_2Cu_4O_8$ were reported by Dupree et al[79]. They observed that the ^{89}Y shift in $YBa_2Cu_4O_8$ has the same temperature dependence as oxygen depleted $YBa_2Cu_3O_{7-\delta}$ with the same $T_c(\delta$=0.2). Similar results were reported by Carretta et al[80]. Vortex lattice and vortex dynamics in $YBa_2Cu_4O_8$ have also been studied by using ^{89}Y NMR[81].

1.5.1.2. The Other Nuclei in $YBa_2Cu_3O_{7-\delta}$ and $YBa_2Cu_4O_8$.

The first Cu NQR study in $YBa_2Cu_3O_{7-\delta}$ with δ close to zero was reported by Lütgemeier and Pieper[82]. Early Cu NMR and NQR studies in 90K superconductor $YBa_2Cu_3O_{7-\delta}$ presenting both Knight shift and spin lattice relaxation data were reported by several research groups[e.g.83-85]. It was found that the spin lattice relaxation rate did not show BCS type behaviour. Similar results were observed by Kitaoka et al[86] and Imai et al[87]. The Cu Knight shift measurements in the superconducting state of $YBa_2Cu_3O_{7-\delta}$ were reported by Barrett et al[88]. A Cu NMR study in $YBa_2Cu_3O_{6.64}$ (T_c=60K) was presented by Walstedt et al[89]. Analysis of Cu NMR data as a function of oxygen concentration in $YBa_2Cu_3O_{7-\delta}$ were reported by Horvatic et al[90]. Cu NMR and NQR in substituted $YBa_2Cu_3O_{7-\delta}$ were also studied by several research groups[e.g.44,91,92]. Their results will be discussed in chapter 4.

Cu NMR and NQR in $YBa_2Cu_4O_8$ have been obtained by several research groups[e.g.93,94] who presented temperature dependencies of the ^{63}Cu nuclear spin lattice relaxation rate and Knight shifts.

^{17}O NMR in $YBa_2Cu_3O_{7-\delta}$ (T_c=92K) have been studied and site assignments have been presented[95-100]. ^{17}O NMR was also used to study the oxygen exchange in $YBa_2Cu_3O_{7-\delta}$ with different preparation processes[101]. ^{17}O NMR and NQR studies in $YBa_2Cu_4O_8$ have been performed by Zheng et al[102] and Mangelschots et al[103]. Mangelschots et al have distinguished four inequivalent oxygen sites in $YBa_2Cu_4O_8$.

1.5.2. NMR Studies in the Other High T_c Superconductors.

Since there have been numerous NMR studies on High T_c superconductors, it is not possible to mention all of them here. Extensive reviews can be found elsewhere[e.g.104–108]. In this section some of ^{17}O, ^{63}Cu and ^{205}Tl NMR studies in high T_c superconductors (apart from $YBa_2Cu_3O_{7-\delta}$ and $YBa_2Cu_4O_8$ systems) are mentioned.

^{17}O NMR data for $La_{1.85}Sr_{0.15}CuO_4$ have been presented[96,109]. Oldfield et al[96] have also reported ^{17}O NMR of $Bi_2Sr_2CaCu_2O_8$, $Tl_2Ba_2CaCu_2O_8$ and $Ba_{0.6}K_{0.4}BiO_3$ superconductors. ^{17}O NMR results for $Bi_2Sr_2Ca_{n-1}Cu_nO_{4+2n}$ (n=1, 2, 3) phases have been reported by Dupree et al[110]. They identified the different oxygen sites in these phases. Similar results were presented by Trokiner et al[111]. The temperature dependence of shift and spin lattice relaxation measurements of ^{17}O in the CuO_2 planes of $Bi_2Sr_2Ca_2Cu_3O_{10}$ was presented[112]. The ^{17}O NMR in $Tl_2Ba_2Ca_2Cu_3O_{10}$ system was studied[113] reporting the temperature dependence of Knight shift and spin lattice relaxation.

Cu NMR and NQR studies have been performed in $(La,M)_2CuO_4$ (M=Sr and Ba) system[e.g.114,115]. There have been several studies on ^{63}Cu NMR and NQR studies of $Bi_2Sr_2Ca_{n-1}Cu_nO_{4+2n}$ (n=1, 2, 3)[e.g.116–118] and $Tl_2Ba_2CuO_6$[119,120] systems. Walstedt et al[118] have reported the temperature dependence of Knight shift and spin lattice relaxation of ^{63}Cu in $Bi_2Sr_2CaCu_2O_8$.

^{205}Tl shift and relaxation rate measurements in $Tl_2Ba_2Ca_{n-1}Cu_nO_{4+2n}$ (n=1, 2, 3) phases were reported[121–123]. ^{205}Tl NMR has been used to investigate the flux

lattice in $Tl_2Ba_2CuO_6$[124] and in $Tl_2Ba_2Ca_2Cu_3O_{10}$[125].

1.6. The Aim of the Present Work.

An understanding of the behaviour of CuO_2 planes which exist in all high T_c copper oxide superconductors is of importance. It is believed that elemental substitution may play a significant role in achieving this understanding and clarifying the mechanism responsible for these new superconductors. Since $YBa_2Cu_3O_{7-\delta}$ and $YBa_2Cu_4O_8$ have two copper sites, the contrasting effects of substitution for Cu in these two sites of these superconductors are of considerable interest. Also it is of importance to determine the role of the chains versus the planes in the superconductivity of $YBa_2Cu_3O_{7-\delta}$ and $YBa_2Cu_4O_8$.

NMR is a powerful technique in studying substitution effects since it is a microscopic probe sensitive to any fluctuating and static magnetic fields and also sensitive to any structural change by means of chemical shift.

^{89}Y has proved to be a good probe in Yttrium Oxides[126,127] and in the Yttrium based high T_c superconductors for the study of electronic and local magnetic properties of the Cu–O planes and chains[e.g.70–72,75–79]. Because of its location sitting at the centre of 2 CuO_2 planes (8 Cu atoms) of $YBa_2Cu_3O_{7-\delta}$ and $YBa_2Cu_4O_8$, ^{89}Y is a very good probe to detect the substitution effects. Therefore ^{89}Y MAS NMR has been used in substituted $YBa_2(Cu_{1-x}M_x)_3O_{7-\delta}$ and $YBa_2(Cu_{1-y}M_y)_4O_8$ in order to investigate the effects of substitution for Cu, namely; the reduction in T_c, structural changes with some substitutions, and site preference of the substituent.

References.

1. H. Fröhlich, Phys. Rev. **79** (1950) 845
2. J. Bardeen, L.N. Cooper and J.R. Schrieffer, Phys. Rev. **108** (1957) 1175.
3. H. Thomas, in Earlier and Recent Aspect of Superconductivity (Eds. J.G. Bednorz and K.A. Müller) Springer-Verlag, Berlin, 1990, p.2.
4. G. Burns, High Temperature Superconductivity, Academic Press, San Diego, 1992.
5. Jr C.P. Poole, T. Datta and H.A. Farach, Copper Oxide Superconductors, John Wiley & Sons, Inc. 1988.
6. J.G. Bednorz and K.A. Müller, Z. Phys. B **64** (1986) 189.
7. L.R. Testardi, J.H. Wernick and W.A. Royer, Sol. State. Comm. **15** (1974) 1.
8. J.R. Gavaler, M.A. Janocko and C.K. Jones, J. Appl. Phys. **45** (1974) 3009.
9. R.J. Cava, B. Batlogg, J.J. Krajewski, R. Farrow, L.W. Rupp, A.E. White, K. Short, W.F. Peck and T. Kometani, Nature **332** (1988) 814.
10. K. Tanigaki, T.W. Ebbesen, S. Saito, J. Mizuki, J.S. Tsai, Y. Kubo and S. Kuroshima, Nature **352** (1991) 222.
11. R.M. Hazen, Scien. Amer. **258** (6) (1988) 52.
12. K. Yvon and M. François, Z. Phys. B **76** (1989) 413.
13. M.K. Wu, J.R. Ashburn, C.J. Torng, P.H. Hor, R.L. Meng, L. Gaw, Z.J. Huang, Y.Q. Wang and C.W. Chu, Phys. Rev. Lett. **58** (1987) 908.
14. R. Beyers and T.M. Shaw, in Solid state Physics vol.42, Academic Press, New York 1989, p.135
15. I. Felner, E.R. Baumінger, D. Hechel, U. Yaron and I. Nowik, Physica A **168** (1990) 229.
16. H.W. Zandbergen, R. Gronsky, K. Wang and G. Thomas, Nature **331** (1988) 596.
17. J. Karpinski, E. Kaldis, E. Jilek, S. Rusiecki and B. Bucker, Nature **336** (1988) 660.
18. D.E. Morris, J.H. Nickel, J.Y.T. Wei, N.G. Asmar, J.S. Scott, U.M. Scheven, C.T. Hultgren and A. G. Markelz, Phys. Rev. B **39** (1989) 7347.
19. R.J. Cava, J.J. Krajewski, W.F. Peck Jr, B. Batlogg, L.W. Rupp Jr, R.M. Fleeming, A.C.W.P. James and P. Marsh, Nature **338** (1989) 328.
20. P. Marsh, R.M. Fleming, M.L. Mandick, A.M. DeSantolo, J. Kwo, M. Hong and L.J. Martinez-Miranda, Nature **334** (1988) 141.
21. P. Boolchand, S. Pradhan, Y. Wu, M. Abdelgadir, W. Huff, D. Farrell, R. Coussement and D. McDaniel, Phys. Rev B **45** (1992) 921.
22. Y. Yamada, J.D. Jorgensen, S. Pei, P. Lightfoot, Y. Kodama, T. Matsumoto and F. Izumi, Physica C **173** (1991) 185.
23. G.Xiao, M.Z.Cieplak, A.Gavrin, F.H.Streitz, A.Bakhshai and C.L.Chien, Reviews of Solid State Science, Vol.1, No.2 (1987) 323–328.
24. G.Xiao, M.Z.Cieplak, D.Musser, A.Gavrin, F.H.Streitz, C.L. Chien, J.J.Rhyne and J.A.Gotaas, Nature **332** (1988) 238.
25. Y.Maeno, T.Tomita, M.Kyogoku, S.Awaji, Y.Aoki, K.Hoshino, A.Minami and T.Fujita, Nature **238** (1987) 512.
26. J.M.Tarascon, P.Barboux, P.F.Miceli, L.H.Greene, G.W. Hull, M.Eibschutz and S.A.Sunshine, Phys.Rev.B **37** (1988) 7458.

27. Y.Xu, R.L.Sabatini, A.R.Moodenbaugh, Y.Zhu, S.G.Shyu, M. Suenaga, K.W.Dennis and R.W.McCallum, Physica C **169** (1990) 205.
28. P.Bordet, J.L.Hodeau, P.Strobel, M.Marezio and A.Santoro, Solid State Comm. **66** (1988) 435.
29. A.M.Balagurov, G.M.Mironova, A.Pajaczkowskas and H. Zymczak, Physica C **158** (1989) 265.
30. G.Roth, G.Heger, B.Renker, J.Pannetier, V.Cargnaert, M. Hervieu and B.Raveau, Z.Phys.B **71** (1988) 43.
31. R.Sonntag, D.Hohlwein, A.Hoser, W.Prandl, W.Schäfer, R. Kiemel, S.Kemmler-Sack, S.Lösch and M.Schlichenmaier, Physica C **159** (1989) 141.
32. H.Maeda, A.Koizumi, N.Bamba, E.Takayama-Murocmachi, F. Izumi, H.Asano, K.Shimizu, H.Moriwaki, H.Maruyama, Y.Kuroda and H.Yamazaki, Physica C **157** (1989) 483.
33. H.Shaked, J.Faber Jr, B.W.Veal, R.L.Hitterman and A.P. Paulikas, Solid State Commun. **75** (1990) 445.
34. T.Kajitani, K.Kusaba, M.Kikuchi, Y.Syono and M. Hirabayashi, Jpn.J.Appl.Phys. **27** (1988) L354.
35. S.Katano, T.Matsumoto, A.Matsushita, T.Hatano and S. Funahashi, Phys.Rev.B **41** (1990) 2009.
36. F.Bridges, J.B.Boyce, T.Claeson, T.H.Geballe and J.M. Tarascon, Phys.Rev.B **39** (1989) 11603.
37. M.Qian, E.A.Stern, Y.Ma and R.Ingalls, Phys.Rev.B **39** (1989) 9192.
38. A.Simopoulos and D.Niarchos, Phys.Rev.B **38** (1988) 8931.
39. E.R.Bauminger, M.Kowitt, I.Felner and I.Nowik, Solid State Commun. **65** (1988) 123.
40. D.Heckel, I.Nowik, E.R.Bauminger and I.Felner,Phys.Rev. B **42** (1990) 2166.
41. T.Siegrist, L.F.Schneemeyer, J.V.Waszczak, N.P.Singh, R.L.Opila, B.Batlogg, L.W.Rupp and D.W.Murphy, Phys.Rev.B **36** (1987) 8365.
42. Y.Kohori, Y.Oda, H.Shibai, N.Okamoto, T.Kohara and K. Asayama, J.Phys.Soc.Jpn. **57** (1988) 2632.
43. M.E.Lines and M.Eibschutz, Physica C **166** (1990) 235.
44. (a)H.Alloul, T.Ohno, H.Casalta, J.F.Marucco, P.Mendels, J.Arabski, G.Collin and M Mehbod, Physica C **171** (1990) 419.
(b)P.Mendels, H.Alloul, J.F.Marucco, J.Arabski, and G.Collin, Physica C **171** (1990) 429.
45. T. Miyatake, S. Gotoh, N. Koshizuka and S. Tanaka, Nature **341** (1989) 41.
46. I. Felner, I. Nowik, B. Brosh, D. Heckel and E.R. Bauminger, Phys. Rev. B **43** (1991) 8737.
47. I. Felner, B. Brosh, Phys. Rev. B **43** (1991) 10364.
48. Y. Wu, S. Pradhan and P. Boolchand, Phys. Rev. Lett. **67** (1991) 3184.
49. T. Miyatake, K. Yamaguchi, T. Takata, N Koshizuka and S. Tanaka, Phys. Rev. B **44** (1991) 10139.
50. D.E. Morris, A.P. Marathe and A.P.B. Sinha, Phsica C **169** (1990) 386.
51. K. Yanagisawa, Y. Matsui, Y. Kodama, Y. Yamada and T. Matsumoto, Phsica C **183** (1991) 197.
52. K. Yanagisawa, Y. Matsui, Y. Kodama, Y. Yamada and T. Matsumoto, Phsica C **191** (1992) 32.

53. E.M. Purcell, H.C. Torroy and P.V. Pound, Phys. Rev. **69** (1946) 37.
54. F. Bloch, W.W. Hansen and M. Packard, Phys. Rev. **69** (1946) 127.
55. W.D. Knight, Phys. Rev. **76** (1949) 1259.
56. L.E. Drain, Metall. Rev. **119** (1967) 195.
57. T.J. Rowland, Prog. Mat. Sci. **9** (1961) 1.
58. L.H. Bennett, R.E. Watson and G.C. Carter, J.Res. NBS **74A** (1970) 569.
59. W.C Dickinson, Phys. Rev. **77** (1950) 736.
60. G. Lindström, Phys. Rev. **78** (1950) 817.
61. W.G. Proctor and F.C. Yu, Phys. Rev. **77** (1950) 717.
62. L.C. Hebel and C.S. Slichter, Phys. Rev. **113** (1959) 1504.
63. J.R. Schrieffer, Theory of Superconductivity, W.A. Benjamin, 1964.
64. K. Yoshida, Phys. Rev. **110** (1958) 769.
65. F. Reif, Phys. Rev. **106** (1957) 208.
66. R.A. Ferrell, Phys. Rev. Lett. **3** (1959) 262.
67. P.W. Anderson, Phys. Rev. Lett. **3** (1959) 325.
68. D.E. Maclaughlin, in Solid State Physics, Vol.31, eds.H. Ehrenreich, F. Seitz and D. Turnbull (Academic Press, New York, 1976) p.1-69.
69. J.T. Markert, T.W. Noh, S.E. Russek and R.M. Cotts, Solid State Comm. **63** (1987) 847.
70. G. Balakrishnan, R. Dupree, I. Farnan, D.McK. Paul and M.E. Smith, J. Phys. C **21** (1988) L847.
71. H. Alloul, T. Ohno and P. Mendels, Phys. Rev. Lett. **63** (1989) 1700.
72. H. Alloul, T. Ohno and P. Mendels, Phys. Rev. Lett. **61** (1988) 746.
73. R. Dupree, D. McK. Paul, M.E. Smith and G. Balakrishnan, Phy. Rev. Lett. **63** (1989) 688.
74. H.B. Brom and H. Alloul, Physica C **177** (1991) 297.
75. G. Balakrishnan, L.W.J. Caves, R. Dupree, D.McK. Paul and M.E. Smith, Physica C **161** (1989) 9.
76. H. Alloul, P. Mendels, H. Casalta, J.F. Marucco and J. Arabski, Phys. Rev. Lett. **67** (1991) 3140.
77. W.J. Webster, D.P. Tunstall, P.F. Freeman and J.R. Cooper, Physica C **185-189** (1991) 1079.
78. Z.P. Han, R. Dupree, D.McK. Paul, A.P. Howes and L.W.J. Caves, Physica C **181** (1991) 355.
79. R. Dupree, Z.P. Han, D.McK. Paul, T.G.N. Babu and C. Greaves, Phsica C **179** (1991) 311.
80. P. Carretta, M. Corti, A. Rigamonti, R.De Renzi, F. Licci, C. Paris, L. Bonoldi, M. Sparpaglione and L. Zini, Physica C **191** (1992) 97.
81. P. Carretta, Phys. Rev. B **45** (1992) 5760.
82. H. Lütgemeier and M.W. Pieper, Sol. State Comm. **64** (1987) 267.
83. M. Mali, D. Brinkmann, L. Pauli, J. Roos, H. Zimmermann and J. Hulliger, Phys. Lett A **124** (1987) 112.
84. R.E. Walstedt, W.W. Warren Jr., R.F. Bell,G.F. Brennert, G.P. Espinosa, J.P. Remeika, R.J. Cava and E.A. Rietman, Phys. Rev. B **36** (1987) 5727.
85. W.W. Warren Jr., R.E. Walstedt,G.F. Brennert, G.P. Espinosa and J.P. Remeika, Phys. Rev. Lett. **59** (1987) 1860.
86. Y. Kitaoka, S. Hiramatsu, T. Kondo and K. Asayama, J. Phys. Soc. Japan **57** (1988) 30.

87. T. Imai, T. Shimizu, T. Tsuda, H. Yasuoka, T. Tabatake, Y. Nakazawa and M. Ishikawa, J. Phys. Soc. Japan **57** (1988) 1771.
88. (1990a) S.E. Barrett, D.J. Durand, C. H. Pennington, C.P. Slichter, T.A. Friedmann, J.P. Rice, D.M. Ginsberg, Phys. Rev. B **41** (1990) 6283.
89. (1990a) R.E. Walstedt, W.W. Warren Jr., R.F. Bell, R.J. Cava, G.P. Espinosa, L.F. Schneemeyer and J. V. Waszczak, Phys. Rev. B **41** (1990) 9574.
90. M. Horvatic, P. Butaud, P. Segransan, Y. Berthier, C. Berthier , J. Y. Henry and M. Couach, Physica C **166** (1990) 151.
91. Y. Kohori, Y. Oda, H. Shibai, N. Okamoto, T. Kohara and K. Asayama, J. Phys. Soc. Jpn. **57** (1988) 2632.
92. M. Matsumura, H. Yamagata and Y. Oda, Physica C **185-189** (1991) 1135.
93. H. Zimmermann, M. Mali, D. Brinkmann, J. Karpinski, E. Kaldis and S. Rusiecki, Physica C **159** (1989) 681.
94. T. Machi, I. Tomeno, T. Miyateka, N. Koshizuka, S. Tanaka, T. Imai and H. Yasuoka, Physica C **173** (1991) 32.
95. M. Horvatić, Y Berthier, P Butaud, Y. Kitaoka, P. Segransan and C. Berthier, Physica C **159** (1989) 689.
96. E. Oldfield, C. Coretsopoulos, S. Yang, L. Reven, H.C. Lee, J. Shore, O.H. Han and E. Ramli, Phys. Rev. B **40** (1989) 6832.
97. M. Takigawa, P.C. Hammel, R.M. Heffner, Z. Fisk, K.C. Ott and J.D. Thompson, Phys. Rev. Lett. **63** (1989) 1865.
98. P.C. Hammel, M. Takigawa, R.M. Heffner, Z. Fisk and K.C. Ott, Phys. Rev. Lett. **63** (1989) 1992.
99. Y. Yoshinari, H. Yasuoka, Y. Ueda, K. Koga and K. Kosuge, J. Phys. Soc. Jpn. **59** (1990) 3698.
100. M. Takigawa, A.P. Reyes, P.C. Hammel, J.D. Thompson, R.H. Heffner, Z. Fisk and K.C. Ott, Phys. Rev. B **43** (1991) 247.
101. E. Ramli, E.A. Ganja, L. Reven, E. Oldfield and T.B. Rauchhfuss, J. Solid State Chem. **86** (1990) 279.
102. G.-q. Zheng, Y. Kitaoka, K. Asayama, Y. Kodama and Y Yamada, Physica C **193** (1991) 154.
103. I. Mangelschots, M. Mali, J. Roos, D. Brinkmann, S. Rusiecki, J. Karpinski and E. Kaldis, Physica C **194** (1992) 277.
104. M. Mehring, IBM J. Res. Develop. **33** (1989) 342.
105. Y. Kitaoka, K. Ishida, K. Fujiwara, K. Asayama, H. Katayama-Yoshida, Y. Okabe and T. Takahashi, IBM J. Res. Develop. **33** (1989) 277.
106. C.H. Pennington and C.P. Slichter, in Physical Properties of High Temperature Superconductors II, Ed. D.M. Ginsberg, World Sciemtific Publishing Co., Singapore, 1989, p.269
107. R.E. Walstedt, W.W. Warren Jr., Science **248** (1990) 1082.
108. Y. Kitaoka, K. Ishida, S. Ohsugi, K. Fujiwara and K. Asayama, Physica C **185-189** (1991) 98.
109. Y. Kitaoka, Y. Berthier, P. Butaud, M. Horvatic, P. Segransan and C. Berthier, Physica C 162-164 (1989) 195.
110. R. Dupree, Z.P. Han, A.P. Howes, D.M. Paul, M.E. Smith and S. Male, Physica C **175** (1991) 269.
111. A. Trokiner, R. Mellet, A.M. Pougnet, D. Morrin, Y.M. Gao, J. Primot and J. Schneck, Phys. Rev. B **41** (1990) 9570.

112. A.P. Howes, R. Dupree, D.M. Paul and S. Male, Phsica C **193** (1992) 189.
113. A.P. Howes, PhD Thesis, University of Warwick, 1992.
114. Y. Kitaoka, S. Ohsugi, K. Ishida and K. Asayama, Physica C **170** (1990) 189.
115. S. Ohsugi, Y. Kitaoka, K. Ishida and K. Asayama, Physica C **185-189** (1991) 1099.
116. R. Michalak, M. Rosenberg and H. Lütgemeier, Physica C **162-164** (1989) 267.
117. A.K. Rajarajan, V.R. Palkar, N.C. Mishra, M.S. Multani, R. Vijayaraghavan and L.C. Gupta, Sol. State Comm. **71** (1989) 835.
118. R.E. Walstedt, R.F. Bell and D.B. Mitzi, Phys. Rev. B **44** (1991) 7760.
119. Y. Kitaoka, K. Fujiwara, K. Ishida, K. Asayama, Y. Shimakawa, T. Manako and Y. Kubo, Physica C **179** (1991) 107.
120. K. Fujiwara, Y. Kitaoka, K. Ishida, K. Asayama, Y. Shimakawa, T. Manako and Y. Kubo, Physica C **184** (1991) 207.
121. F. Hentsch, N. Winzek, M. Mehring, H. Mattausch and A. Simon, Physica C **158** (1989) 137.
122. N. Winzek, F. Hentsch, M. Mehring, H. Mattausch, R. Kremer and A. Simon, Physica C **168** (1990) 327.
123. F. Hentsch, N. Winzek, M. Mehring, H. Mattausch, A. Simon and R. Kremer, Physica C **165** (1990) 485.
124. M. Mehring, F. Hentsch, H. Mattausch and A. Simon, Z. Phys. B **77** (1989) 355.
125. Y.Q. Song, M. Lee, W.P. Halperin, L.M. Tonge and T.J. Marks, Phys. Rev. B **44** (1991) 914.
126. R. Dupree and M.E. Smith, Chem. Phys. Lett. **148** (1988) 41.
127. A.R. Thompson and E. Oldfield, J. Chem. Soc. Chem. Comm. (1987) 27.

Chapter 2. Theory.

2.1. Basic Principles of NMR.

The basic principle of NMR is based on the existence of the interaction between magnetic moments of atomic nuclei and magnetic fields. The connection between the spin quantum number I and the magnetic moment μ is

$$\mu = \gamma \hbar I \tag{2.1}$$

for a nucleus with nonzero spin (γ is the magnetogyric ratio of the nucleus). In an external magnetic field B_0 the interaction energy between the magnetic moment and the field can be given by the Hamiltonian

$$H = -\mu \cdot B \tag{2.2}$$

By using equation.2.1 and considering B_0 along the z axis, we obtain:

$$H = -\gamma \hbar B_0 I_z \tag{2.3}$$

From this Hamiltonian (2I+1) allowed energies exist and they are given by

$$E_m = -\gamma\hbar B_o m \qquad (2.4)$$

Where the (2I+1) values of m are :

$$I, I-1, I-2, \ldots\ldots, -I$$

By considering the energy levels (Eq.2.4), together with the selection rule $\Delta m = \pm 1$, one can write the energy difference between two levels as:

$$\Delta E = h\nu = \gamma\hbar B_o \qquad (2.5)$$

Fig.2.1. illustrates the energy levels for a nucleus with I=1/2. The basic equation of the nuclear magnetic resonance can be written as

$$\omega_o = \gamma B_o \qquad (2.6)$$

where ω_0 is the Larmor frequency at which the magnetic moment of the nucleus precesses around the magnetic field B_0. This precession is illustrated in fig.2.2. The precessing magnetic moment in a field B_0 experiences a torque, $\mu \times B_0$ which is equal to the rate of change in angular momentum, given by

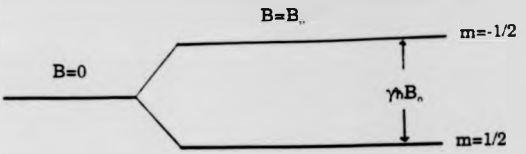

Fig.2.1. The energy levels for the nuclei with I=1/2.

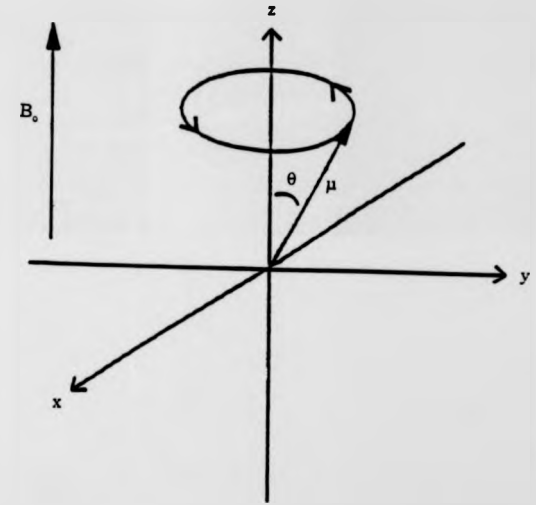

Fig.2.2. Precession of the magnetic moment around the direction of applied field B_0.

$$\frac{dJ}{dt} = \mu \times B_o \tag{2.7}$$

It can be expressed in terms of the nuclear gyromagnetic ratio by using $\mu=\gamma J$:

$$\frac{d\mu}{dt} = \gamma \mu \times B_o \tag{2.8}$$

In a frame rotating at frequency ω about the z–direction the effective magnetic field is B_{eff}:

$$B_{eff} = (B_o - \frac{\omega}{\gamma})k \tag{2.9}$$

By replacing B_o with the effective field B_{eff}, in the rotating frame, equation 2.8 becomes

$$\frac{d\mu}{dt} = \gamma \mu \times [(B_o - \frac{\omega}{\gamma})k] \tag{2.10}$$

If the frame rotates at the Larmor frequency $\omega=\omega_o$, μ is constant. When, in addition to B_o, a radio frequency field B_1 is applied perpendicular to B_o, equation 2.10 becomes as

$$\frac{d\mu}{dt} = \gamma \mu \times [(B_o - \frac{\omega}{\gamma})k + B_1 i] \tag{2.11}$$

If the rotating frame frequency is equal to the at Larmor frequency, equation 2.11 simplifies to:

$$\frac{d\mu}{dt} = \mu \times \gamma B_1 i \tag{2.12}$$

Therefore, in the rotating frame only the radio-frequency field exists and interacts with the magnetization along z axis causing it to rotate about the x-axis. As a result, this field may be used to perturb the magnetization and subsequently the NMR signal may be detected. Experimental details on pulsed FT NMR are given in section 3.1.

The nuclear spins with I=1/2 aligned with B_o are in thermodynamic equilibrium and this is given by the Boltzmann equation as

$$\frac{N_-}{N_+} = \exp\left(-\frac{\Delta E}{k_B T}\right) \tag{2.13}$$

Where N_- and N_+ respectively are the number of spins in the energy levels for m=-1/2 and m=1/2. The equilibrium is disturbed by applying a rf pulse (B_1). Then the nuclear spins come back to equilibrium via the interactions (see section 2.2) between the nuclear spins and the surroundings. One can define this process with the transition probability per unit time by considering $W_\downarrow$ and $W_\uparrow$ respectively as the probabilities of the transition from m=1/2 to m=-1/2 and vice versa. This process is characterized by a time called the spin lattice relaxation time ,T_1, defined such that

$$\frac{1}{T_1} = W_1 + W_1 \qquad (2.14)$$

Further details on the basic theory of NMR can be found elsewhere[1,2] from both classical and quantum mechanical point of views.

2.2. Nuclear Spin Interactions In Solids.

In this section the dominant nuclear spin interactions in solids will be treated, since they are the basic characteristics of a nucleus and its environment.

The total spin Hamiltonian can be given as

$$H = H_z + H_{rf} + H_D + H_{CS} + H_{KS} + H_Q \qquad (2.15)$$

The first two terms (H_z and H_{rf}) are called external interactions and they are the interactions of the spins with the applied static field and rf fields, respectively (see section 2.1). In this section, the basic principles of the internal interactions, namely; dipolar (H_D), chemical shift (H_{CS}), Knight shift (H_{KS}) and Quadrupolar (H_Q), are described. Further details can be found elsewhere[1,3,4].

2.2.1. Dipole Dipole Interaction.

The dipole dipole interaction is the coupling of a nuclear spin with the local field of its neighbouring spins. This interaction depends on the magnitude and orientation of the magnetic moments. The corresponding energy for the dipolar interaction between two magnetic moments μ_1 and μ_2 is[1]:

$$E=\frac{\overline{\mu_1}\,\overline{\mu_2}}{r^3}-3\frac{(\overline{\mu_1}\,\overline{r})(\overline{\mu_2}\,\overline{r})}{r^5} \qquad (2.16)$$

where $\overline{r}$ is joining vector between these two moments. The magnetic moments of the nuclear spins in terms of their spin angular momenta are:

$$\begin{aligned}\overline{\mu_1}&=\gamma_1\hbar\overline{I_1}\\ \overline{\mu_2}&=\gamma_2\hbar\overline{I_2}\end{aligned} \qquad (2.17)$$

Thus the dipole dipole interaction between two nuclei can be written (equations 2.16 and 2.17) as

$$H_{12}=\frac{\gamma_1\gamma_2\hbar^2}{r^3}[\overline{I_1}\,\overline{I_2}-3\frac{(\overline{I_1}\,\overline{r})(\overline{I_2}\,\overline{r})}{r^5}] \qquad (2.18)$$

After choosing the z axis along the applied magnetic field and using the polar coordinates of the vector $\overline{r}$, the Hamiltonian becomes as[1]:

$$H_{12}=\frac{\gamma_1\gamma_2\hbar^2}{r^3}(A+B+C+D+E+F) \qquad (2.19)$$

where

$$A = I_{1z}I_{2z}(1-3\cos^2\theta) \tag{2.20.a}$$

$$B = -\frac{1}{4}(1-3\cos^2\theta)(I_{1+}I_{2-}+I_{1-}I_{2+}) \tag{2.20.b}$$

$$C = -\frac{3}{2}\sin\theta\cos\theta e^{-i\phi}(I_{1z}I_{2+}+I_{1+}I_{2z}) \tag{2.20.c}$$

$$D = -\frac{3}{2}\sin\theta\cos\theta e^{-i\phi}(I_{1z}I_{2-}+I_{1-}I_{2z}) \tag{2.20.d}$$

$$E = -\frac{3}{4}\sin^2\theta e^{-2i\phi}(I_{1+}I_{2+}) \tag{2.20.e}$$

$$F = -\frac{3}{4}\sin^2\theta e^{2i\phi}(I_{1-}I_{2-}) \tag{2.20.f}$$

Since $\langle\exp(\pm i\phi)\rangle = \langle\exp(\pm 2i\phi)\rangle = 0$, the averages of the terms from C to F are zero and do not effect the static spectrum. Detailed discussion can be found elsewhere[1,2]. Then the simplified Hamiltonian (with the contributions coming from only A and B) becomes as[1]:

$$H_D = \frac{1}{4}\gamma^2\hbar^2\sum_{j,k}\frac{(1-3\cos^2\theta_{jk})}{r^3_{jk}}(3I_{jz}I_{kz}-\vec{I}_j\vec{I}_k) \tag{2.21}$$

For solids this interaction can result in broad NMR lines (powder patterns) which obscure high resolution information. Since the dipolar interaction is proportional to r^{-3}, it is very sensitive to the changes in internuclear distances. This interaction is orientational dependent with a geometric factor of $(1-3\cos^2\theta)$. Averaging this geometric factor to zero using MAS (Magic Angle Spinning) is discussed in section 2.4.

The dipole dipole interaction is often the dominant source of line broadening for nuclei with spin I=1/2.

2.2.2. The Chemical Shift Interaction.

The chemical shift effect corresponds to a magnetic shielding of the nucleus, which is produced by the electrons circulating around the nucleus. Therefore for a particular nucleus, NMR signals have different frequencies for different chemical environments. Because of this shielding, the magnetic field at the nucleus will be

$$\boldsymbol{B}=\boldsymbol{B}_o(1-\sigma) \tag{2.22}$$

where σ is the shielding factor called chemical shift. The chemical shift Hamiltonian can be expressed as[3]:

$$H_{CS}=\hbar\gamma \boldsymbol{I}\cdot\sigma\cdot\boldsymbol{B} \tag{2.23}$$

Therefore the resonance frequency of the nucleus is

$$\omega = \gamma B_o(1-\sigma) \tag{2.24}$$

For a particular nucleus, the shielding factor σ is measured relative to a reference sample. Discussion on the reference sample is given in section 3.3.1.

In molecules, σ has two contributions namely; a diamagnetic σ_d and a paramagnetic σ_p term:

$$\sigma = \sigma_d + \sigma_p \tag{2.25}$$

The diamagnetic term is due to the applied magnetic field producing an electronic charge circulation around the nucleus. This circulation creates a magnetic field opposing the applied magnetic field (Lenz's law). The diamagnetic term for spherical charge distribution can be represented by Lamb's equation[5]

$$\sigma_d = \frac{\mu_o e^2}{3m_e}\int_0^\infty r\rho_e dr \tag{2.26}$$

The paramagnetic term is a correction for the distortion of the electron motion and the non-spherical charge distribution of the electrons. The paramagnetic term can be written as[5]

(2.27)

where P_u is p electron imbalance, ΔE is an average excitation energy and $\langle r^{-3} \rangle$ is the expectation value of r^{-3}.

The chemical shift is anisotropic i.e. it differs along various axes within the molecule with respect to the applied magnetic field. Therefore it can be described as a second rank tensor:

$$\sigma = \begin{pmatrix} \sigma_{xx} & \sigma_{xy} & \sigma_{xz} \\ \sigma_{yx} & \sigma_{yy} & \sigma_{yz} \\ \sigma_{zx} & \sigma_{zy} & \sigma_{zz} \end{pmatrix} \qquad (2.28)$$

In the principal axis system the principal components of the tensor are: σ_{11}, σ_{22}, σ_{33} and the case $\sigma_{11} < \sigma_{22} < \sigma_{33}$ is valid. Magnetic shielding σ_{zz}, along B_o, is defined in terms of principal components:

$$\sigma_{zz} = \frac{1}{3} Tr\sigma + \frac{1}{3} \sum_{j=1}^{3} (3\cos^2\theta_j - 1)\sigma_{jj} \qquad (2.29)$$

where $Tr\sigma = \sigma_{11} + \sigma_{22} + \sigma_{33}$ and $(1/3)Tr\sigma$ are the trace and the isotropic average of chemical shielding tensor, respectively. In a solution state experiment, because of the rapid molecular motion only the isotropic part of the chemical shift ($(1/3)Tr\sigma$) is observed. For solids, chemical shift anisotropy gives anisotropic powder patterns shown in fig.2.3 for different cases. Broadening caused by chemical shift anisotropy

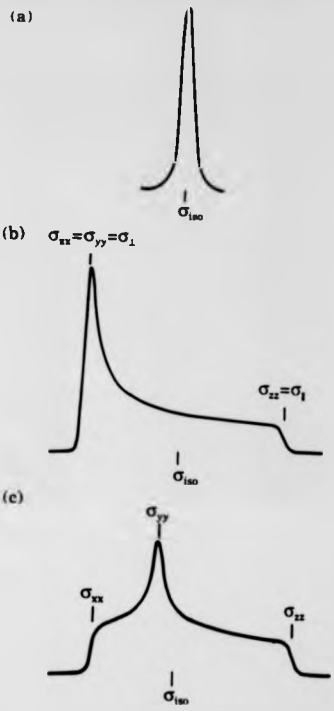

Fig.2.3. Anisotropic powder patterns for (a) cubic symmetry (b) axial symmetry and (c) the general cases.

is inhomogeneous.

In general this chemical shielding is independent of temperature.

2.2.3. The Knight Shift Interaction.

The Knight shift is a measure of the magnetic hyperfine field at the nucleus produced by the polarized conduction electrons in an applied magnetic field. The Knight shift effect was first observed by Knight[6] who found that the resonance frequency of ^{63}Cu in metallic copper was shifted to a value higher than in diamagnetic CuCl. In metallic substances, this is an additional shift to the chemical shift.

The total Hamiltonian for the Knight shift from the three interactions between nucleus and conduction electrons is[7]:

$$\begin{aligned} H_{KS} = & -2\frac{8\pi}{3}\mu_B\gamma_n\hbar\vec{I}\cdot\vec{S}(r)\delta(r) \\ & -2\mu_B\gamma_n\hbar\vec{I}\cdot\left\{\frac{\vec{S}}{r^3}-\frac{3\vec{r}(\vec{S}\cdot\vec{r})}{r^5}\right\}-\gamma_n\hbar\frac{e}{mc}\left[\vec{I}\cdot\frac{(\vec{r}\times\vec{p})}{r^3}\right] \end{aligned} \qquad (2.30)$$

where I and S are nuclear and electron spins, respectively and r is the radius vector of the electron with the nucleus.

In this equation, the first term is called the Fermi contact interaction which describes the interaction between the magnetic moments of the s electrons and the nucleus. (This term also has the contribution from the unpairing inner s-core electron spins as a result of an exchange interaction with s, d and f electrons). The Knight shift contribution of this term is given by[7]

$$K_C = \frac{8\pi}{3}\chi_s P_F \qquad (2.31)$$

Where χ_s and P_F are the Pauli spin susceptibility and the probability density for conduction electrons at the nucleus, respectively. The Knight shift is usually dominated by this contribution. The Pauli spin susceptibility can be defined as a function of the electronic density of states at the Fermi level

$$\chi_s = \mu_B^2 N(E_F) \qquad (2.32)$$

An average magnetic hyperfine coupling constant <a> is defined in terms of probability density by the equation.

$$\langle a \rangle = \frac{8\pi}{3} P_F \qquad (2.33)$$

The second term in equation 2.30, a source of anisotropic Knight shift interaction, is the spin dipolar interaction between the spins of nucleus and conduction electrons. This interaction is orientation dependent and results in line broadening in powders in a similar way to the chemical shift anisotropy (previous section). There is no contribution from the s-like conduction electrons for this term because of their spherical symmetry.

The third contribution to the Knight shift interaction comes from the orbital effect from the non-s electrons.

In simple metals a theoretical relationship between K and T_1 known as the Korringa relation found by Korringa is given as[8]:

$$K^2T_1T=\frac{\hbar}{4\pi k_B}\left(\frac{\gamma_e}{\gamma_n}\right)^2 \tag{2.34}$$

where K and T_1 respectively are the contributions to the Knight shift and spin lattice relaxation time coming from the coupling between the magnetic moments of the nuclei and the s-state electrons via the contact interaction.

2.2.4. The Quadrupolar Interaction.

Nuclei with a spin I>1/2 possess an electric quadrupole moment because of the non-spherically symmetric electric charge distribution. The electric quadrupole moment of the nucleus will interact with the electric field gradient which is produced by atomic electrons. The Hamiltonian for this interaction, called the quadrupole interaction, is given by[2]:

$$\begin{aligned}H_Q=&\frac{e^2qQ}{4I(2I-1)}\{\frac{1}{2}(3\cos^2\theta-1)(3I_z^2-I(I+1))\\&+\frac{3}{2}\sin\theta\cos\theta[I_z(I_++I_-)+(I_++I_-)I_z]+\frac{3}{4}\sin^2\theta(I_+^2+I_-^2)]\end{aligned} \tag{2.35}$$

where eq and eQ are electric field gradient and quadrupole moment, respectively. After using perturbation theory[1,2,4] the energy levels for the first order quadrupolar interaction for the situation when $H_z >> H_Q$ are given by

$$E_m^{(1)} = \frac{e^2qQ}{8I(2I-1)}(3\cos^2\theta - 1)[3m^2 - I(I+1)] \qquad (2.36)$$

The quadrupolar interaction has an orientational dependence similar to the chemical shift. In fig.2.4, (a) the energy levels and (b) the schematic NMR spectra for a nucleus I=3/2 are illustrated for the first order quadrupolar interaction. As seen from the fig. 2.4 and equation 2.36, the central transition (1/2, −1/2) is not effected by the first order quadrupolar interaction. Since the entire powder pattern of most quadrupolar nuclei is often wider than the bandwidth of many NMR spectrometers, only the central transition is observable. Therefore, satellite transitions such as (−1/2,−3/2) and (3/2,1/2) are obtained separately.

If e^2qQ is large enough in comparison to the Larmor frequency ω_o, the second order quadrupolar effect is observed and broadens the central transition. Detailed theory on the first and second order quadrupolar interactions can be found elsewhere[1-4].

2.2.5. RKKY Interaction.

The RKKY interaction is the interaction between the localized moments of an impurity atom and the conduction electrons, first studied by Ruderman and Kittel[9]. The development and extension of this theory to s-d and s-f electrons was presented first by Kasuya[10] and then by Yosida[11]. This interaction was called after their names; Ruderman-Kittel-Kasuya-Yosida; RKKY interaction.

The energy for this interaction is given by[12]

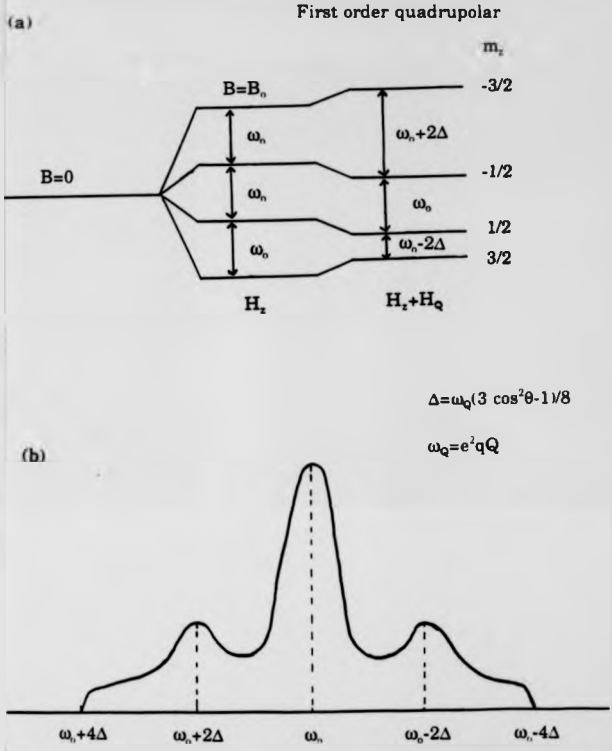

Fig.2.4. (a) Separation of energy levels and (b) the schematic spectrum for a nucleus I=3/2 in the case of first order quadrupolar interaction.

$$E_{ind}(R_{12}) = -C\frac{2k_fR_{12}\cos(2k_fR_{12}) - \sin(2k_fR_{12})}{(2k_fR_{12})^4}(\vec{S}_1\cdot\vec{S}_2) \qquad (2.37)$$

The conduction electrons are polarized by the localized magnetic moments of an impurity atom. The magnetization around the magnetic impurity dies off in an oscillating manner because of the exchange with the conduction electrons. This behaviour of conduction electron wave functions and the distribution of conduction electron spin density are shown in fig.2.5[13].

This indirect interaction results in line broadening which can not be removed by the MAS technique.

2.3. Spin Lattice Relaxation.

The spin lattice relaxation time is the measure of the time in which magnetization along the applied magnetic field B_0 returns to its equilibrium after perturbation. During this time the spin system loses its energy due to the interaction with its environment. It is also called longitudinal relaxation time. This relaxation process is exponential for spin 1/2 systems and can be written as

$$M_z = M_0(1 - e^{-\frac{t}{T_1}}) \qquad (2.38)$$

with no magnetization along z axis at t=0.

Fluctuating magnetic fields at a nucleus are the sources of the relaxation mechanism; these include dipole-dipole interaction, electric quadrupole interaction,

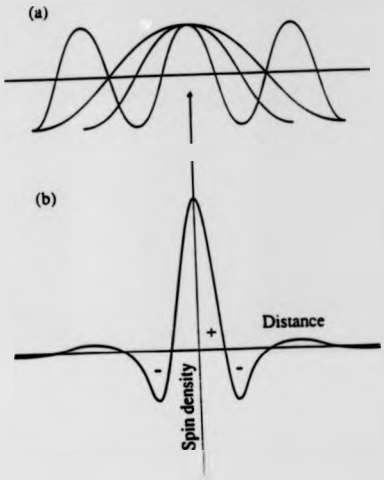

Fig.2.5. (a) The conduction electron wave functions and (b) the distribution of conduction electron spin density around the impurity atom in RKKY interactions[13].

chemical or Knight shift anisotropy and so on[5,14].

Since the dipole-dipole interaction is often the dominant source of the fluctuating magnetic field for spin I=1/2 nuclei, it will be discussed in this work. The relaxation rate due to the dipolar interaction in solids is given by[15]

$$T_1^{-1} = \frac{2\gamma^4\hbar^2}{5r^6} I(I+1)\left[\frac{\tau_c}{1+\omega_o^2\tau_c^2} + \frac{4\tau_c}{1+4\omega_o^2\tau_c^2}\right] \qquad (2.39)$$

Where ω_0 and τ_c are the resonance frequency and correlation time, respectively. The correlation time describes random molecular motions creating fluctuating local magnetic fields.

2.4. MAS and Averaging of the Anisotropic Interactions.

In polycrystalline solids, because of the anisotropic interactions namely, chemical and Knight shift anisotropies, dipolar and first order quadrupolar interactions which have been discussed in section 2.2, very broad lines, which are not very informative, are observed. However in order to eliminate these anisotropic interactions there are several techniques employed[16]. One of these line narrowing techniques is what is called "Magic Angle Spinning (MAS)" first discovered by Andrew[17] and Lowe[18], independently.

As discussed in section 2.2, anisotropic interactions namely, chemical shift or Knight shift anisotropy, dipolar interaction and first order quadrupolar interaction involve the geometric factor term $(3\cos^2\theta-1)$, where θ is the angle between a specific fixed molecule direction and the applied static magnetic field. When the

sample is spun at an angle of β=54.7° with respect to the applied magnetic field as shown in fig.2.6 , the angle of the geometric factor term θ will vary between β-χ and β+χ. Thus, it is necessary to take the average of (3 $\cos^2\theta$−1) and it is given by[5]

$$\langle 3\cos^2\theta - 1\rangle = \frac{1}{2}(3\cos^2\beta - 1)(3\cos^2\chi - 1) \qquad (2.40)$$

As (3 $\cos^2\beta$−1) becomes zero for β=54.7°, spinning at this angle, Magic angle, results in narrowed lines by averaging away the anisotropic interactions.

For the dipolar interaction the broadening is homogeneous. Therefore in order to narrow the homogeneously broadened lines spinning speed must be greater than the broadening (i.e> the line width). In the case of inhomogeneous broadening (Chemical shift or Knight shift anisotropy, heteronuclear dipole and first order quadrupolar interactions) when the spinning speed is less than the anisotropic interaction itself, a series of spinning side bands around the isotropic line separated by the spinning frequency are observed. As an example ^{51}V NMR spectra in 2.5% V doped $YBa_2Cu_3O_{7-\delta}$ with different spinning rates are shown in fig 2.7. This behaviour was first reported by Andrew et al[19]. More importantly they found that intensity pattern of the spinning side bands reflects the chemical shift anisotropy observed in a nonspinning experiment. In order to determine the principal values of a chemical shift tensor from MAS powder spectra by using MAS sideband intensities, a graphical method has been developed[20]. An extension of this graphical method has been reported by D. Frenzke et al[21].

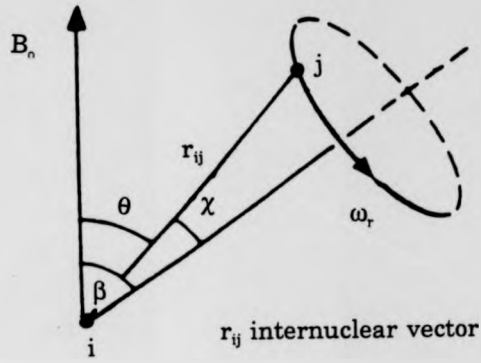

Fig.2.6. Definition of angle geometry for Magic Angle Spinning technique.

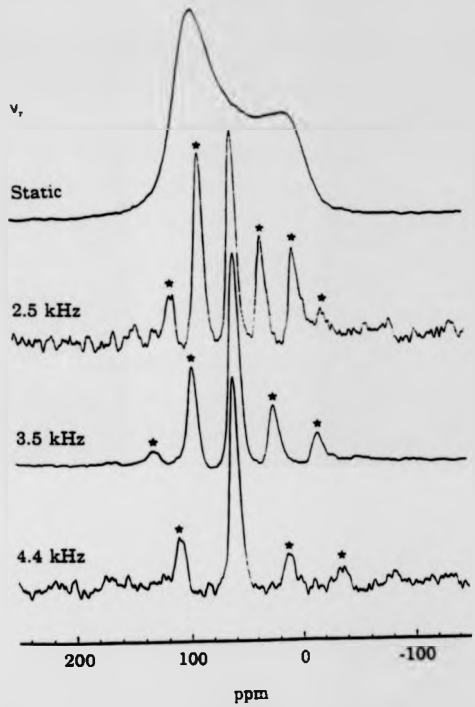

Fig.2.7. ^{51}V NMR spectra in 2.5 % V doped $YBa_2Cu_3O_{7-\delta}$ with different spinning rates. The asterisks denote the spinning side bands.

The anisotropy of second order quadrupolar interaction causes a broadening in the central transition of quadrupolar nuclei with half integer spins. This broadening can not be averaged to zero by MAS. For this case, the Variable Angle Spinning (VAS) technique was employed[22] as suggested before[23]. In the VAS technique it is unfortunate, however, that, since the sample is not spun at the magic angle any more, there exists a broadening due to the chemical shift anisotropy and dipolar interaction. Recently there have been two techniques, namely; Dynamic Angle Spinning (DAS)[24] and Double Rotation (DOR)[25] employed to overcome this problem.

2.5. NMR Theory of High T_c Superconductivity.

2.5.1. General Introduction.

In a metallic system the total spin susceptibility can be written as

$$\chi_s(q,\omega)=\chi'_s(q,\omega)+\chi''_s(q,\omega) \qquad (2.41)$$

where $\chi_s'(q,\omega)$ and $\chi_s''(q,\omega)$ are respectively the real and imaginary parts of spin susceptibility of the conduction electrons at a specific site. They are probed by the Knight shift and relaxation time measurements respectively (see section 2.5.3). Therefore NMR has been widely used (see chapter 1) to characterize the magnetic and electronic properties of the high T_c copper oxides which have large unit cells and different atomic sites.

There have been several attempts which have developed models to describe the behaviour of NMR in high T_c superconductors[26-36]. Most of them are based on the one component model[26,27,30-36]. In section 2.5.2 a brief description of this

model together with the spin Hamiltonian is given. Section 2.5.3 describes the spin Knight shift and relaxation rate in this model.

2.5.2. One component Model and the Spin Hamiltonian.

In the one component model it was assumed that each CuO_2 plane has a free electronic spin S=1/2 as suggested from Cu NMR study of $YBa_2Cu_3O_7$[37]. It was also assumed that these are centred on the Cu(2) sites and are antiferromagnetically correlated[38]. A model for the coupling of the electronic spins in CuO_2 planes to the nuclear moments was suggested[27] and has been extended[30,33-36].

The total electron nuclear hyperfine coupling hamiltonian in $YBa_2Cu_3O_{7-\delta}$ following Mila-Rice[27] and MMP[33] can be written down by the equation[39];

$$H = {}^{63}\gamma_n\hbar\left({}^{63}\vec{I}\cdot\vec{A}\cdot\vec{S}\right) + {}^{63}\gamma_n\hbar\sum_{j=1}^{4}\left({}^{63}\vec{I}\cdot\vec{B}\cdot\vec{S}_j\right) + {}^{17}\gamma_n\hbar\sum_{j=1}^{2}\left({}^{17}\vec{I}\cdot\vec{C}\cdot\vec{S}_j\right) + {}^{89}\gamma_n\hbar\sum_{k=1}^{8}\left({}^{89}\vec{I}\cdot\vec{D}\cdot\vec{S}_k\right) \qquad (2.42)$$

Where i, j and k label the four unit cells nearest to the Cu site, two electronic spins of Cu atoms nearest to O site and eight electronic spins (four in one plane and four in another) nearest to Y site, respectively. A is the direct (on site) hyperfine coupling constant and B, C and D are transferred hyperfine coupling constants. Fig.2.8 shows the hyperfine couplings in CuO_2 planes for $YBa_2Cu_3O_{7-\delta}$.

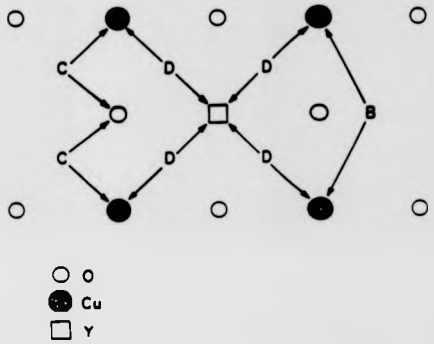

Fig.2.8. The illustration of the hyperfine couplings in the CuO_2 planes[33].

2.5.3. The Knight Shift and Relaxation Rate.

In the one component model[33] the free electronic spins on the Cu(2) sites are assumed to be the source for spin Knight shift and relaxation for ^{63}Cu and ^{17}O on the plane and ^{89}Y in the Y based superconductors (e.g. $YBa_2Cu_3O_{7-\delta}$) via the interaction between the nuclei and the one component spin system.

In terms of the hyperfine coupling constants (A,B,C and D) and the spin susceptibility of conduction electrons at a specific site the spin Knight shifts for ^{63}Cu, ^{17}O and ^{89}Y (in $YBa_2Cu_3O_7$) are given as[33]:

$$^{63}K_{\parallel} = \frac{A_{\parallel} + 4B}{\gamma_e {}^{63}\gamma_n \hbar^2} \chi_o \qquad (2.43.a)$$

$$^{63}K_{\perp} = \frac{A_{\perp} + 4B}{\gamma_e {}^{63}\gamma_n \hbar^2} \chi_o \qquad (2.43.b)$$

$$^{17}K_{iso} = \frac{2C}{\gamma_e {}^{17}\gamma_n \hbar^2} \chi_o \qquad (2.43.c)$$

$$^{89}K_{iso} = \frac{8D}{\gamma_e {}^{89}\gamma_n \hbar^2} \chi_o \qquad (2.43.d)$$

In equation 2.43.d (for ^{89}Y nucleus) 8 represents the 8 nearest Cu neighbours to Y site. The transferred hyperfine coupling constant, D, between ^{89}Y nucleus and CuO_2 plane has been calculated as $- -3.0$ kOe/μ_B[34].

By using the general expression given by Millis and Monien[36], the spin lattice relaxation rate arising from the fluctuation of the free electronic spins for ^{89}Y in $YBa_2Cu_3O_7$ can be written as

$$^{89}T_1^{-1} = \frac{1}{4}\lim_{\omega \to 0} \frac{k_B T}{\hbar^2 \omega} \sum_{q,\alpha} [^{89}F_\alpha(q)]^2 \frac{\chi''(q,\omega)}{\mu_B^2} \qquad (2.44)$$

Where $^{89}F_\alpha(q)$ is a form factor defined as:

$$^{89}F_\alpha(q) = 8D_\alpha(\cos\frac{q_x}{2})(\cos\frac{q_y}{2})(\cos\frac{q_z}{2}) \qquad (2.45)$$

This relaxation rate expression is also valid for ^{17}O and ^{63}Cu with different form factors including direct and transferred hyperfine coupling constants.

References.

1. C.P.Slichter,Principles of Magnetic Resonance,Springer-Verlag (3rd edition), 1990.
2. A. Abragam, Principles of Nuclear Magnetism, Oxford,
3. M. Mehring, High Resolution NMR in Solids, Springer Verlag, 1983.
4. B.C. Gerstein and C.R. Dybowski, Transient Techniques in NMR of Solids, Academic Press, 1985.
5. R.K. Harris, Nuclear Magnetic Resonance Spectroscopy, Longman Scientific and Technical, 1986.
6. W.D Knight, Phys. Rev. **76** (1949) 1259.
7. G.C. Carter, L.H. Bennet and D.J. Kahan, Metallic Shifts in NMR (Prog. In Mat. Scien. vol.20) 1977.
8. J. Korringa, Physica, **16** (1950) 601.
9. M.A. Ruderman and C. Kittel, Phys. Rev. **96** (1954) 99.
10. T. Kasuya, Prog. Theor. Phys. Jpn. **16** (1956) 45.
11. K. Yosida, Phys. Rev. **106** (1957) 893.
12. Y. Ishikawa and N. Miura (eds), Physics and Engineering applications of Magnetism, Springer-Verlag 1991, p.306.
13. J. Crangle, Solid State Magnetism, Edward Arnold, 1991 p.144.
14. T.C. Farrar and E.D. Becker, Pulse and Fourier Transform NMR: Introduction to Theory and Methods, Academic Press, 1971.
15. U. Haeberlen and J. S. Waugh, Phys. Rev. **185** (1969) 420.
16. J. Mason (Ed), Multinuclear NMR, Plenum Press, New York, 1987.
    R. Richards and K.J. Packer (Eds.), NMR spectroscopy in Solids, The Royal Society of London, 1981.
17. E.R. Andrew, A. Bradbury and R.G. Eades, Nature **183** (1959) 1802.
18. I.J. Lowe, Phys. Rev. Lett. **2** (1959) 285.
19. E.R. Andrew, W.S. Hinshaw and R.S. Tiffen, J. Mag. Res. **15** (1974) 191.
20. J. Herzfeld and A.E. Berger, J.Chem. Phys, **73** (1980) 6021.
21. D. Frenzke, B. Maeβ and H. Pfeifer, J. Mag. Res. **88** (1990) 172.
22. S. Ganapaty, S. Schramm and E. Oldfield, J. Chem. Phys. **77** (1982) 4360.
23. M.M. Maricq and J.S. Waugh, J. Chem. Phys. **70** (1979) 3300.
24. K.T. Mueller, B.Q. Sun, G.C. Chingas, J.W. Zwanziger, T. Terao and A. Pines, J. Mag. Res. **86** (1990) 470.
25. A. Samoson, E. Lippmaa and A. Pines, Mol. Phys. **65** (1988) 1013.
26. F. Mila and T.M. Rice, Phys. Rev. B **40** (1989) 11382
27. F. Mila and T.M. Rice, Physica C **157** (1989) 561.
28. T. Koyama and M. Tachiki, Phys. Rev. B **39** (1989) 2279.
29. D.L. Cox and B.R. Trees, Phys. Rev. B **41** (1990) 11260.
30. T. Imai, J Phys. Soc. Jpn. **59** (1990) 2508.
31. T. Moriya, Y. Takahashi and K. Ueda, J Phys. Soc. Jpn. **59** (1990) 2905.
32. J.P. Lu, Q. Si, J.H. Kim and K. Levin, Physica C **179** (1991) 191.
33. A.J. Milles, H. Monien and D.Pines, Phys. Rev. B **42** (1990) 167.
34. H. Monien, D. Pines and M. Takigawa, Phys. Rev. B **43** (1991) 258.
35. H. Monien, P. Monthoux and D. Pines, Phys. Rev. B **43** (1991) 275.
36. A.J. Millis and H. Monien, Phys. Rev. B **45** (1992) 3059.
37. M. Horvatic, P. Segransan, C. Berthier, Y. Berthier, P. Butaud, Y.J. Henry,

M. Couach and J.P. Chaminade, Phys. Rev. B 39 (1989) 7332.
38. R.E. Walstedt, W.W. Warren, Jr, R.F. Bell, G.F. Brennert, G.P. Espinosa, R.J. Cava, L.F. Schneemeyer and J.V. Waszcak, Phys. Rev. B 38 (1988) 9299.
39. T. Ohno, T. Kanashiro and K. Mizuno, J. Phys. Soc. Jpn. 60 (1991) 2040).

Chapter 3. Experimental.

3.1.Pulsed FT NMR.

This section describes some of the elementary features of the pulsed NMR spectrometer.

In a pulsed NMR experiment, an oscillating radio frequency magnetic field B_1, is applied perpendicular to the existing static field B_0 along the z axis. In the laboratory frame, the oscillating field B_1 is in the x-y plane and given as;

$$\overrightarrow{B_1} = B_1(i\cos\omega t + j\sin\omega t) \qquad (3.1)$$

then the field B_1, oscillating at the Larmor frequency ($\omega=\omega_0$) of the nuclei being observed, will be along the x′ axis in the rotating frame. As seen in section 2.1, the effective field is $B_{eff}=B_1$ when the nucleus is on resonance. In this case precession of the magnetization will be around B_1. The magnetization, M_0, is rotated by an angle θ, which is called the pulse angle and it depends on the gyromagnetic ratio of the perturbed nuclei γ, and the strength of the alternating magnetic field B_1. The pulse width, t_p, which is the time between turning on the B_1 and turning it off again, is related to θ by

$$\theta = \gamma B_1 t_p \qquad (3.2)$$

The pulse width should be a short time compared to T_1 and T_2, so that no relaxation

occurs during the pulse. By applying a pulse one is able to place the magnetization in any direction in the y′−z plane. For example, as seen in fig.3.1, a $\pi/2(90^0)$ and a $\pi(180^0)$ pulses will rotate the magnetization into the y′ and −z axis, respectively. Following a 90^0 pulse, the magnetization lying along the y′ axis will be detected as the intensity of the signal,which is maximum just after the pulse, by the receiver coil. The same coil could be used as a receiver coil and also to generate B_1 or there could be two separate coils for these two processes. The induced signal intensity will decay as a function of T_2, called spin spin relaxation time in the x−y plane after the B_1 field is turned off. This is called the **Free Induction Decay (FID)** which is the simplest form of an NMR signal. At the same time, the magnetization along the z axis will come back to equilibrium with a time (T_1) called the spin lattice relaxation time.

Lowe and Norberg[1] were the first to show that the Fourier transform (FT) of the FID, after a 90^0 pulse, was identical to the steady state spectrum. An experimental design for pulsed nuclear resonance has been given by Clark[2]. The first pulsed FT high resolution NMR spectrometer was built by Ernst and Anderson[3]. The development of the fast Fourier transform algorithm by Cooley and Tukey[4] was a significant contribution. Fig.3.2 shows the typical FID signal (a) and its Fourier transformation (b).

The block diagram of a typical pulsed FT NMR spectrometer is shown in fig.3.3. The main parts of a pulsed FT NMR spectrometer are followings:

(a) A large magnet; providing a homogeneous high magnetic field B_0. It is desirable to have a superconducting magnet for high resolution experiments.

(b) The probe, is situated inside the magnet and has the parts required for

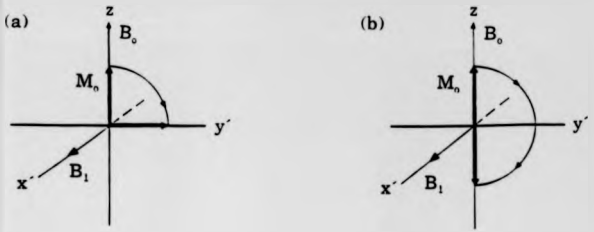

Fig.3.1. The effect of (a) a $\pi/2$ and (b) a π pulse.

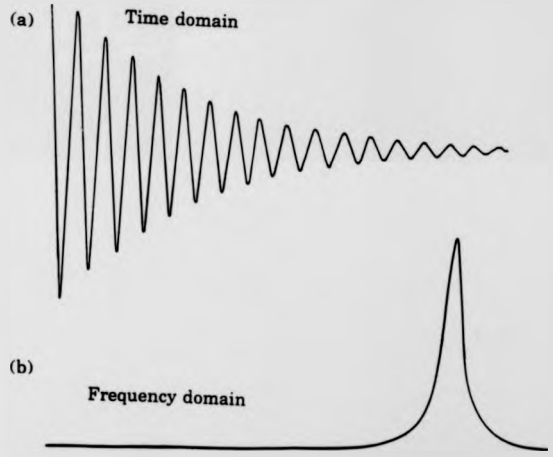

Fig.3.2. (a) Typical FID signal and (b) its Fourier transformation.

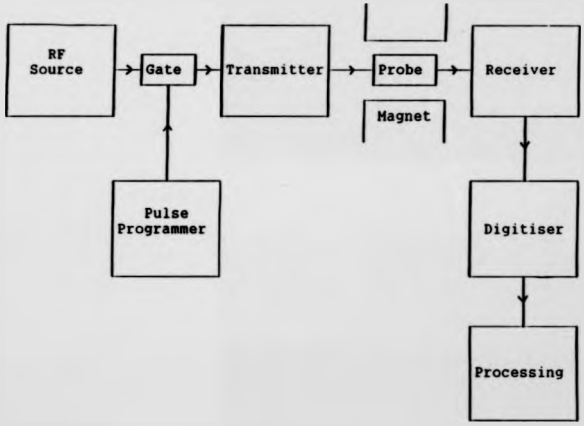

Fig.3.3. The block diagram of the Pulsed FT NMR spectrometer.

variable temperature experiments. It contains the coils and radio frequency electronics which allow the excitation and the detection of an NMR signal.

(c) A transmitter; as a source of a rf oscillating magnetic field B_1. The radio frequency signal is amplified by the transmitter before it is applied to the transmitter coil inside the probe. The required power depends on the characteristics of the probe and the sample under investigation.

(d) The pulse programmer, is used for timing and providing the stable pulses. It switches the gate on and off by sending control pulses to the transmitter.

(e) A receiver; to amplify and detect the signal.

3.2. The Bruker MSL-360 Spectrometer.

In this section a brief description of the Bruker MSL (Multipurpose Solid and Liquid)-360 spectrometer is given. Further details are available from the Bruker manuals[e.g.5].

The MSL-360 spectrometer has an Oxford superconducting high field (8.45T) magnet with a wide bore of 89mm. Details on the superconducting magnet assembly are given elsewhere[5]. By using the shim coils very small local field gradients are generated in order to improve the homogeneity of the magnetic field. The shimming varies with the orientation of the probes inside the magnet and for every new probe placed into the magnet, a new shim is required.

Generation of the frequencies (1-200 MHz) is performed by a PTS 200 frequency synthesizer. For the frequencies above 200MHz generation is established by the converter.

All the operations such as data acquisition, data manipulation, storage,

plotting e.g. are performed by the Aspect-3000 computer[6]. The DISMSL program is used to perform the spectrometer operation; with this program, one can easily control the parameters and carry out the processing using short commands from the keyboard.

Fig.3.4 shows the block diagram of the Bruker MSL-360 spectrometer[7].

3.2.1. The NMR Probes and Spinners.

The Bruker MSL-360 spectrometer has a range of static and spinning probes operating at frequencies between 10 and 360 MHz. The static and spinning high resolution experiments are performed by using the Bruker double bearing (DB) Magic Angle spinning (MAS), static, Doty and "woty" (home made doty) probes. Also decoupling and Cross Polarisation (CP) experiments can be achieved with the DB MAS probe. The DB MAS probe is equipped with a single coil resonance system. Detailed description on the operation of a single coil probe is given elsewhere[8-9]. Description of the complicated electronics of these Bruker probes are given elsewhere[10]. Spinners made from zirconia (with internal diameter 5.5mm, external diameter 7mm and length 17.7mm) are used in the Bruker DB MAS probes. Since spinning with these spinners is very sensitive to sample imbalance, finely powdered sample and careful packing of the sample are required. With these spinners a spinning rate of up to 5kHz can be achieved although with the high density high T_c superconductors maximum spinning speed was typically 3.5 kHz.

In the Doty and Woty probes, hollow cylindrical silicon nitride,(or zirconia or sapphire) spinners (with external diameter 5.0mm) with a smaller sample volume were used. Spinning with these spinners is easier and higher spinning rates are

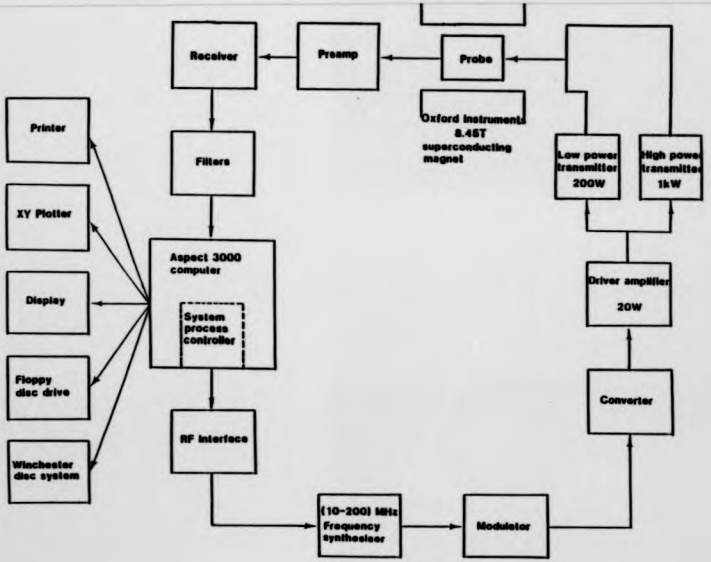

Fig.3.4. The block diagram of the Bruker MSL-360 spectrometer system[7].

achieved typically 10–15 kHz. The diagrams of the spinners used in the Bruker DB MAS, doty and woty probes are shown in fig.3.5. The coils of all the spinning probes are orientated at the magic angle (54° 35') to B_o.

3.3. Setting and Operation of the Spectrometer.

3.3.1. Setting up on a Nucleus.

For each nucleus studied setting up the spectrometer basically includes hardware changes, tunings and determination of the acquisition parameters and shimming the magnet.

Hardware changes consist of the selection of the relevant high power transmitter plug–in, if high power is used, and changing the preamplifier box in order to match and tune the carrier frequency and also placing the appropriate probe into the magnet. In this work nuclei given in table 3.1, were studied using the Bruker DB MAS, Woty and Doty probes. After tuning the probe and preamplifier box, appropriate acquisition parameters are set. Shimming of a particular probe is performed by reading the appropriate shim file. Since all of the lines investigated in this work are relatively broad > 10 ppm, a measurement of the spectrum reference (SR) which determines the zero shift was performed using the reference sample for the particular nucleus given in table 3.1.

3.3.2. Magic Angle Spinning.

Averaging of the broadenings from the anisotropic interactions in solids (section 2.4) can be achieved by spinning the sample at the angle of 54.7°, called the Magic Angle, relative to the external magnetic field. This experiment known as

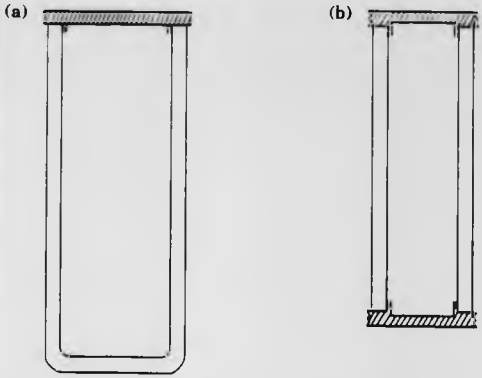

Fig.3.5. The spinners used in (a) DB MAS (b) Doty and Woty probes.

Table 3.1. Larmor frequencies of the nuclei and their reference samples used in this study together with their abundances and spin numbers.

Nucleus	Larmor Frequency at 8.45T (MHz)	Reference Sample	Natural Abundance (%)	Spin Number
^{89}Y	17.646	YCl_3(Solution)	100	1/2
^{51}V	94.675	YVO_4(Powder)	99.76	7/2
^{27}Al	93.848	$AlCl_3$(Solution)	100	5/2

Magic Angle Spinning (MAS) was first proposed independently by Andrew[11] and Lowe[12].

In this study MAS was carried out for the nuclei given in table 3.1. MAS especially for ^{89}Y nucleus in substituted $YBa_2Cu_3O_{7-\delta}$ and $YBa_2Cu_4O_8$ samples was essential to narrow the resonance line so that the small shift changes which occur with substitution at room temperature and with variable temperatures could be detected. As an example ^{89}Y static and MAS NMR spectra of $YBa_2Cu_4O_8$ are presented in fig.3.6. For this case, the broadening averaged out by MAS is mostly due to the chemical shift anisotropy (sections 2.2.2 and 2.4). The Full Width at Half Maximum (FWHM) $\nu_{1/2}$ are 900 and 80Hz for the static and MAS spectra, respectively.

If the spinning rate is less than the anisotropic inhomogeneous broadenings due to the chemical shift anisotropy and first order quadrupolar interaction (see section 2.4), spinning side bands are observed. The effect of MAS on ^{51}V NMR in 20 % V doped $YBa_2Cu_3O_{7-\delta}$ is illustrated in fig.3.7 with different spinning rates. As seen the isotropic shift position remains the same with the changes in the spinning rate whereas the positions for the spinning side bands shift linearly with spinning rate. This is because the spinning sidebands are separated by the spinning frequency. Detailed theoretical discussion on MAS is given in section 2.4.

The setting of the Magic angle must be accurate in order to get high resolution signal. A common method for the setting of the magic angle is to adjust the angle by running a suitable reference sample with a quadrupolar nucleus having a cubic environment[13]. Details on the accurate magic angle setting for different range of frequencies are given elsewhere[7,14] where ^{79}Br (in KBr) and ^{85}Rb (in

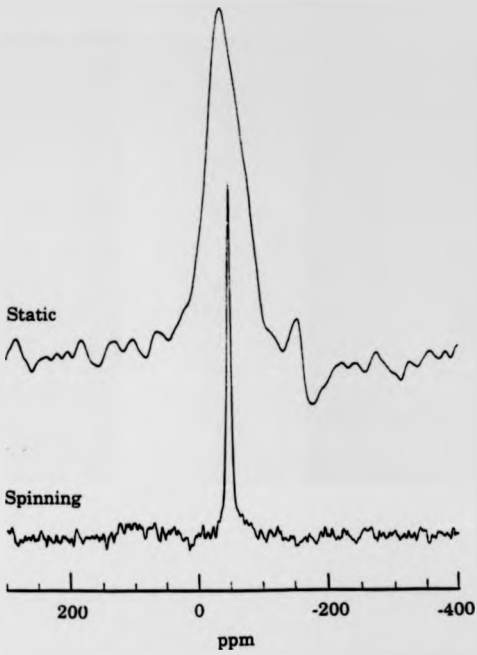

Fig.3.6. ^{89}Y Static and MAS NMR spectra in $YBa_2Cu_4O_8$.

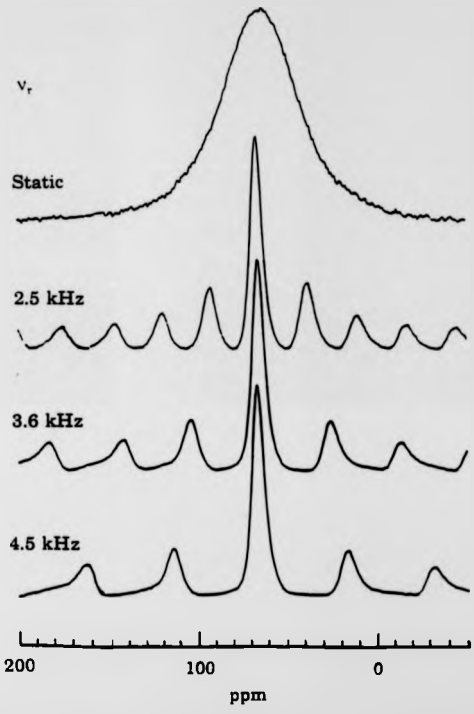

Fig.3.7. ^{51}V Static and MAS. with different spinning rates. NMR spectra in $YBa_2(Cu_{1-x}V_x)_3O_{7-\delta}$ (x=0.2).

RbCl) quadrupolar nuclei were used to set the magic angle.

3.3.3. Spin–Echo Method.

The spin spin relaxation time, T_2, (also called transverse relaxation time) is concerned with the exchange of energy between spins in the x–y plane. For a Lorentzian the line width is related to T_2 by[9];

$$\nu_{1/2} = \frac{1}{\pi T_2} \tag{3.3}$$

When the external magnetic field varies between $B_0-\Delta B_0/2$ and $B_0+\Delta B_0/2$ over the sample, inhomogeneity of the magnetic field ΔB_0 leads to a contribution to the line width following a single 90° pulse given by

$$\nu_{1/2(\text{inhom})} = \gamma \frac{\Delta B_0}{\pi} \tag{3.4}$$

Therefore the effective spin-spin relaxation time T_2^* including the contribution coming from the inhomogeneous field is defined as

$$\frac{1}{T_2^*} = \frac{1}{T_2} + \gamma \Delta B_0 \tag{3.5}$$

In order to remove inhomogeneous line broadening and as a result to enable to

measure the real spin-spin relaxation time T_2, a method called spin-echo was first employed by Hahn[15] and then extended by Carr and Purcell[16]. The simplest form of this spin echo sequence is:

$$\frac{\pi}{2} - \tau - \pi - \tau - echo \qquad (3.6)$$

This is illustrated in fig.3.8. The first, $\pi/2$ pulse is applied as a preparation pulse. Then the π pulse is applied. As a result spins are refocused and produce an echo at 2τ. The effect of the spin echo on the magnetization is illustrated in fig.3.9. In the rotating frame, initially (a) magnetization M_0 is along z' axis. After the 90^0 pulse (b) it is turned to the y' axis. As the inhomogeneity of the magnetic field over the sample results in different resonance frequencies for identical spins in the different parts of the NMR sample, magnetization vectors (c) begin to fan out. At $t=\tau$ a 180^0 pulse is applied (d). Because the relative positions of the magnetization vectors, during the second τ time they will come together along $-y'$ axis and magnetization vectors continue to move in the same direction. As a result of the spin echo sequence all effects of the inhomogeneous magnetic field have been removed. The maximum signal (echo) is then obtained.

3.3.4. Data Collection.

After setting up on a nucleus and spinning the sample (sections 3.3.1 and 3.3.2) the experiment can be started by an automatic command ZG (Zero the memory and go) on the computer keyboard. Data acquisition can be stopped any

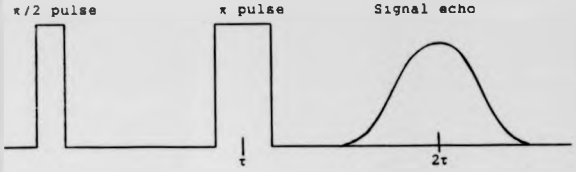

Fig.3.8. The illustration of the simplest form of spin echo sequence.

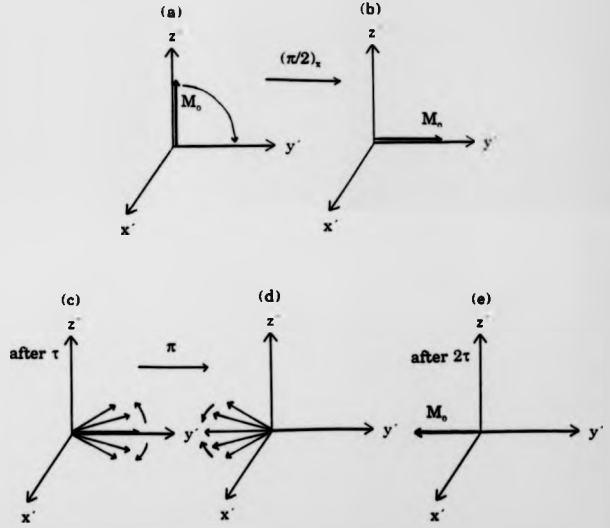

Fig.3.9. The vectorial representation of the extended spin echo sequence.

time by pressing Ctrl/H or Bs. Also automatic stop can be performed by setting NS (Number of scans).

For ^{89}Y nucleus CYCLOPS (CYCLically Ordered Phase Sequence) phase cycling and mostly spin echo (section 3.3.3) pulse sequences were used. In the case of ^{51}V and ^{27}Al only CYCLOPS phase cycling was employed. CYCLOPS phase cycling was introduced by Hoult and Richards[17].

After stopping the acquisition, the collected data is saved on the computer hard disk and processing of the data can be performed by retrieving it from the disk.

3.3.5 Data Manipulation.

After collection, the data is processed in order to get a conventional absorption spectrum which allows the interpretation of the spectrum. Basic data processing consists of exponential multiplying, Fourier transformation, phasing and baseline correction.

One can begin processing by left shift (LS) to remove the dead time of the FID. An exponential multiplying which multiplies the FID by $\exp(-\alpha t)$ is applied in order to improve the Signal/ Noise ratio, where α is given as a line broadening parameter in Hz. But exponential multiplying broadens the line width (FWHM) by LB. Then Fourier transformation of the FID gives the frequency dependent spectrum to which the phasing and baseline correction are applied.

3.4. Variable Temperature Experiments.

MAS and static variable temperature experiments for ^{89}Y nucleus in substituted $YBa_2(Cu_{1-x}M_x)_3O_{7-\delta}$ and $YBa_2(Cu_{1-y}M_y)_4O_8$ samples were carried out

using the Bruker DB MAS probe over the temperature range 100–400K.

For high temperature experiments dry compressed air or N_2 gas is required. The temperature control unit[5] is connected to the probe thermocouple and heater. The bearing gas is used to heat the sample by passing through the probe heater. In the case of low temperature experiments, dry nitrogen gas must be used. The sample, spinning or static, is cooled by passing the bearing gas through the heat exchanger loop which is immersed into the 25l liquid nitrogen dewar. The desired temperature and spinning rate can be adjusted with the temperature control unit and pneumatic unit systems, respectively.

3.5. T_1 Measurements.

When a spin system is perturbed from equilibrium, the system relaxes back by an energy transfer to the lattice. A theoretical description of T_1 has been given in section 2.3.

There are many pulse techniques for measuring spin lattice relaxation time. These techniques are described in detail elsewhere[18]. In this study the Saturating Comb method has been used to determine the ^{89}Y spin lattice relaxation time in substituted $YBa_2(Cu_{1-x}M_x)_3O_{7-\delta}$ and $YBa_2(Cu_{1-y}M_y)_4O_8$ using the spin echo pulse sequence since T_1 is rather long typically around 10s. It is best for samples having a long T_1, because there is a short waiting time between the pulses in this method. First the spin system is saturated by applying a series of identical ($\pi/2$) pulses with a short delay τ' between pulses. Where $n\tau' < T_1$ and $\tau' > T_2$. At a variable time t after this pulse train, a $\pi/2$ pulse or a spin echo train is applied and the z–magnetization is thus monitored. The saturation comb sequence followed by a spin

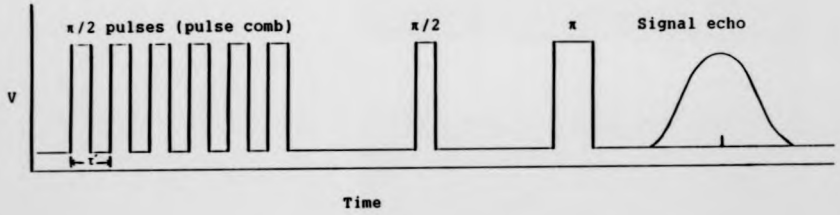

Fig.3.10. The illustration of saturation combs sequence for T_1 measurements.

echo is shown in fig.3.10. The time dependence of the z–magnetization is then expressed by equation (section 2.3)

$$M_z = M_o(1 - e^{-\frac{t}{T_1}}) \qquad (3.7)$$

^{89}Y T_1 measurements were performed with a series of experiments with different NS (Number of Scans) and t values. M_z values were obtained from the Fourier transformed FID signal by taking the signal intensity. The M_z value for the case of $t=4T_1$ was taken as M_o. The equation 3.7 can be written as

$$\ln(M_o - M_z) = \ln M_o - \frac{t}{T_1} \qquad (3.8)$$

whence the slope of the plot of $\ln(M_o - M_z)$ versus t gives $-1/T_1$.

3.6. Sample Preparation and Characterisation.

The superconducting properties of the copper oxide compounds are very senaitive to the preparation method, annealing time and temperature. Therefore, the preparation procedure should be followed carefully. After the preparation it is necessary to check the sample quality from the structural and superconducting point of views. X-ray powder pattern and A.C. susceptibility are the basic methods to determine the crystal structure phase purity and transition temperature of the superconducting sample, respectively.

3.6.1. Sample Preparation.

The samples of $YBa_2(Cu_{1-x}M_x)_3O_{7-\delta}$ (M=V,Fe,Co,Ni,Zn,Al and Ga) and $YBa_2(Cu_{1-y}M_y)_4O_8$ (M=Fe and Zn) were prepared via the solid state reaction method.

3.6.1.1. Preparation of $YBa_2(Cu_{1-x}M_x)_3O_{7-\delta}$.

Stoichiometric amounts of Y_2O_3,Ba_2CO_3,CuO and substituent oxides (V_2O_5,Fe_2O_3,CoO,NiO,ZnO,Al_2O_3 and Ga_2O_3) were mixed and ground. The resulting sample was calcined twice in air at 900- 950°C for 18-24 hours and the pulverised sample was pressed into pellets. These pellets were annealed under flowing oxygen at 925°C for 15 hours. Then the temperature was lowered to 600°C at which the sample was annealed for 5 hours. After that the sample was allowed to cool slowly to room temperature. The resulting pellets were pulverised in order to carry out XRD, A.C. susceptibility and NMR measurements. The prepared samples were stored in a desiccator.

3.6.1.2. Preparation of $YBa_2(Cu_{1-y}M_y)_4O_8$.

Superconducting $YBa_2(Cu_{1-y}M_y)_4O_8$ (M=Fe and Zn; y=0, 0.009, 0.018 and 0.03) samples have been prepared at one atmosphere oxygen pressure using a two step process first developed by Cava et al[19].

First $YBa_2(Cu_{1-x}M_x)_3O_{7-\delta}$ (where x=0, 0.012, 0.024 and 0.04; and δ=0.5) samples were prepared from the stoichiometric amounts of Y_2O_3,Ba_2CO_3,CuO and substituent oxides (Fe_2O_3 and ZnO) without annealing under flowing oxygen. Then the stoichiometric amounts of $YBa_2(Cu_{1-x}M_x)_3O_{7-\delta}$ and CuO were mixed to

provide $YBa_2(Cu_{1-y}M_y)_4O_8$ (y=3x/4). After that, as a flux, an equal volume of Na_2CO_3 was added to the resulting mixture and ground. Finally the mixture was annealed under flowing oxygen at 800°C for 4 days and allowed to cool slowly to room temperature.

3.6.2. X-Ray Diffraction.

The XRD powder pattern method using a Phillips Powder Diffractometer has been used to determine the crystal structures of superconducting $YBa_2(Cu_{1-x}M_x)_3O_{7-\delta}$ and $YBa_2(Cu_{1-y}M_y)_4O_8$ compounds. CuK_α radiation was used with a λ=1.54178Å.

A typical XRD powder pattern of orthorhombic $YBa_2Cu_3O_{7-\delta}$ is given in fig.3.11. The (200),(020) and (006) peaks correspond to the lattice parameters a,b and c,respectively. In the case of the orthorhombic structure, the calculated lattice parameters from these peaks are a=3.827,b=3.882 and c=11.682Å. The splitting of the (013) and (103) and also (020) and (200) peaks simply indicate that the structure is orthorhombic. It is well known and agreed that for V,Ni and Zn substitution the structure remains orthorhombic whereas for Fe,Co,Al and Ga substitution the structure changes from orthorhombic to tetragonal with a small amount of substitution (2-2.5%)[20,21]. The detailed results and discussion of the O-T transition for those substitutions are given in section 4.2.

In fig.3.12, the XRD powder pattern is presented for $YBa_2Cu_4O_8$. The (200),(020) and (0014) peaks in the case of $YBa_2Cu_4O_8$ correspond to the (200),(020) and (006) peaks in the powder pattern of $YBa_2Cu_3O_{7-\delta}$ and the corresponding lattice parameters are a=3.8364,b=3.8635 and c=27.2083Å which are

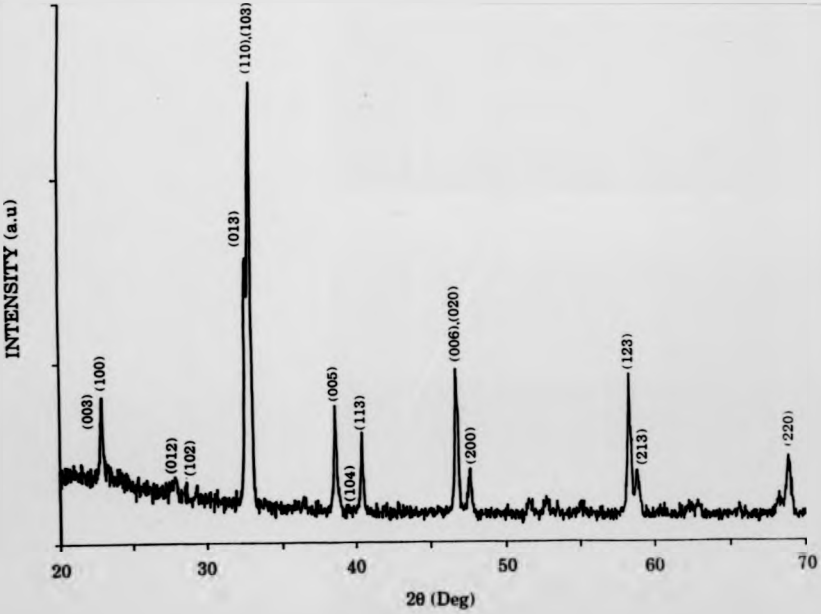

Fig.3.11. XRD powder pattern of orthorhombic $YBa_2Cu_3O_7$ at room temperature.

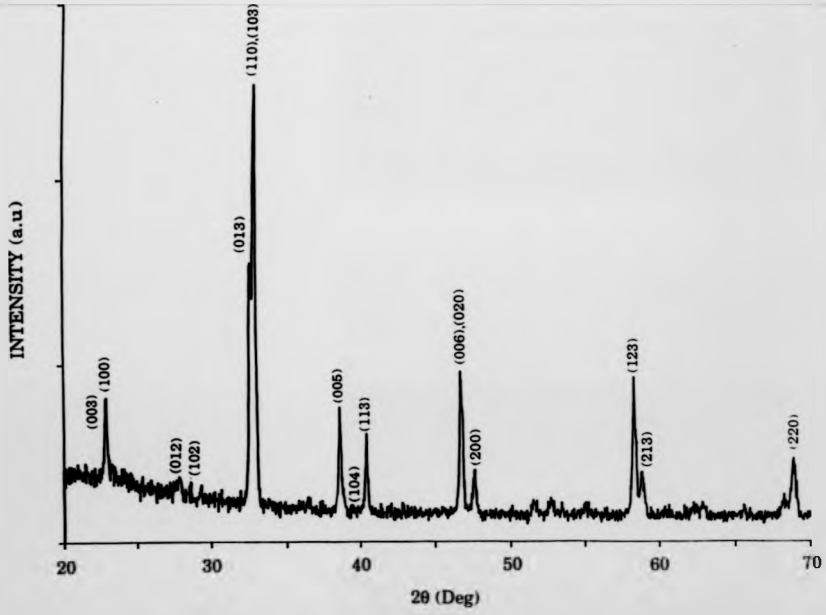

Fig.3.11. XRD powder pattern of orthorhombic $YBa_2Cu_3O_7$ at room temperature.

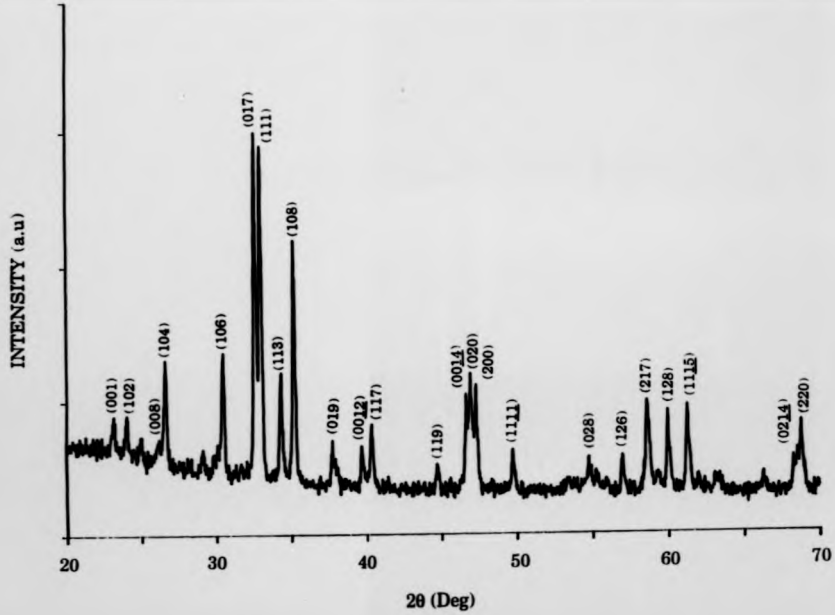

Fig.3.12. XRD powder pattern of $YBa_2Cu_4O_8$ at room temperature.

in good agreement with references[22,23]. In $YBa_2(Cu_{1-y}Zn_y)_4O_8$ the structure remains orthorhombic and lattice parameters do not change with doping (up to y=0.03). For $YBa_2(Cu_{1-y}Fe_y)_4O_8$, the structure is still orthorhombic with y=0.03 but the lattice parameters become similar. For Fe the structure probably undergoes an orthorhombic to tetragonal transition for 4-5% dopant concentration (see section 5.2).

3.6.3. A.C. Susceptibility.

Two unique characteristics of the superconducting state, namely, zero resistance and perfect diamagnetism are two classical ways to determine the transition temperature of a superconductor. Since the susceptibility technique is a bulk and therefore the preferred method, A.C. Susceptibility has been used in order to carry out the critical temperature, T_c, measurements. The A.C. Susceptibility method is based on the behaviour of perfect diamagnetism of the superconducting state.

The A.C. Susceptibility system has one primary coil and two secondary coils. The secondary coils situated inside the primary coil are connected in series and in a direction opposite to each other. All the coils are located in a cryostat in which the cooling takes place. Fig.3.13 displays the basic schematic diagram of the A.C. Susceptibility system. The sample sits in one of the secondary coils. An alternating current is applied to the primary coil, an e.m.f will be created in the secondary coils. Total e.m.f,ε, is

$$\varepsilon = \varepsilon_1 - \varepsilon_2 \qquad (3.9)$$

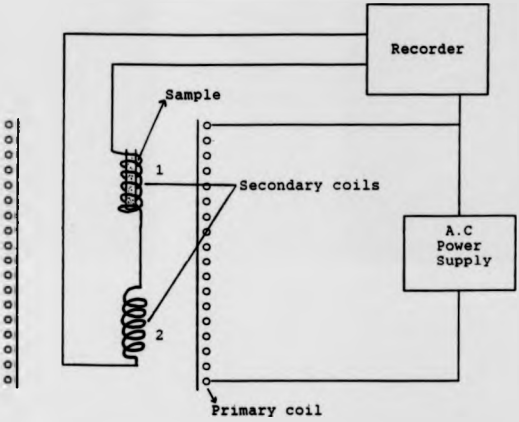

Fig.3.13. Basic schematic diagram of the A.C. susceptibility system.

Total ε is observed by varying the temperature. Because of the perfect diamagnetic behaviour of the superconducting sample inside the first secondary coil, $\varepsilon_1-\varepsilon_2$ will start decreasing just below T_c. This is shown in fig.3.14 for $YBa_2Cu_3O_{7-\delta}$. In this measurement the sharpness of the superconducting transition displays the sample quality.

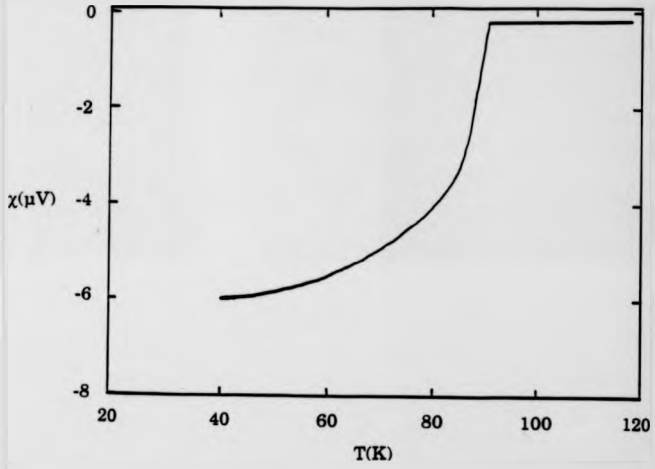

Fig.3.14. A.C. susceptibility vs. temperature curve for $YBa_2Cu_3O_7$.

References.

1. I.J. Lowe,and R.E. Norberg, Phys.Rev. **107** (1957) 46.
2. W.G. Clark, Rev.Sci.Inst.,**35** (1964) 316.
3. R.R.Ernst and W.A.Anderson, Rev. Sci.Inst. **37** (1966) 93.
4. J.W.Cooley and J.W.Turkey, Math.Computation **19** (1985) 297.
5. MSL System description, Bruker Manual, Ref.No:432001.
6. Aspect 3000 MSL Software Manual, Bruker Manual, 1986.
7. M.E.Smith, Ph.D. Thesis, Department of Physics, University of Warwick, UK, 1987.
8. I.J. Lowe and C.E. Tarr, J. Scien. Instrum (J. Phys. E) Series (2) **1** (1968) 320.
9. T.C. Farrar and E.D. Becker, Pulse and Fourier Transform NMR, 1971 Academic press, New York.
10. NMR Probehead Series MAS-DB, Bruker Manual,1985.
11. E.R.Andrew, A. Bradbury and R.G. Eades, Nature, **183** (1959) 1802.
12. I.J.Lowe, Phys.Rev.Lett. **2** (1959) 285.
13. J.S.Frye and G.E.Maciel, J.Mag.Res. **48** (1982) 125.
14. M.G.Mortuza, Ph.D. Thesis, Department of Physics, University of Warwick, UK, 1989.
15. E.L. Hahn, Phys. Rev. **80** (1950) 580.
16. H.Y. Carr and E.M. Purcell, Phys. Rev. **94** (1954) 630.
17. I. Hoult and R.E. Richards, Proc. Roy. Soc. (Lond.) A **344** (1975) 311.
18. E. Fukushima and S.B.W. Roeder, Experimental Pulse NMR, Addisson Wesley, 1981.
19. R.J. Cava, J.J. Krajewski, W.F. Peck Jr, B. Batlogg, L.W. Rupp Jr, R.M. Fleming, A.C.W.P. James and P. Marsh, Nature **338** (1989) 328.
20. G. Xiao, M.Z. Cieplak, D. Musser, A. Gavrin, F.H. Streitz, C.L. Chein, J.J. Rhyne and J.A. Gotaas, Nature **332** (1988) 238.
21. J.M. Tarascon, P. Barboux, P.F. Miceli, L.H. Greene, G.W. Hull, M. Eibschultz and S.A. Sunshine, Phys. Rev. B **37** (1988) 7458.
22. I.Felner and B.Brosh, Phys.Rev. B **43** (1991) 10364.
23. D.E.Morris, J.H. Nickel, J.Y.T. Wei, N.G. Asmar, J.S. Scott, U.M. Scheven, C.T. Hultgren, A.G. Markelz, J.E. Post, P.J. Heaney, D.R. Veblen and R.M. Hazen, Phys.Rev. B **39** (1991) 7347.

Chapter 4. $YBa_2(Cu_{1-x}M_x)_3O_{7-\delta}$ System.

4.1. Introduction to $YBa_2(Cu_{1-x}M_x)_3O_{7-\delta}$ System.

Some basic properties of $YBa_2Cu_3O_{7-\delta}$ and the effects of substitution for Cu in this system have already been discussed in chapter 1. There have been many studies on substitution for Cu in this system[1-5] investigating structural and superconducting properties. The mechanism responsible for the reduction in T_c with substitution for Cu is still not understood. For some substitutions (Fe,Co, Al and Ga) the existence of a true structural transition from orthorhombic to tetragonal has been questioned[6-8]. Site occupancy studies by using the techniques other than NMR have been introduced in chapter 1. The results of these can be summarized as: (1) Co, Al and Ga occupy the Cu(1) site whereas Ni goes onto the Cu(2) site. (2) For Zn it is mostly agreed that substitution occurs in the Cu(2) site. (3) Fe substitutes into both sites but mostly into the Cu(1) site. (4) The situation regarding vanadium substitution is not yet clear although it appears to be pentavalent[9] and could occupy the Cu(2) site as reported by Shringi et al[10].

In this chapter, first the structural and superconducting properties of substituted $YBa_2(Cu_{1-x}M_x)_3O_7$ are given in section 4.2 where XRD and A.C. susceptibility results are presented. ^{89}Y MAS NMR data (shift and relaxation rate) in substituted $YBa_2(Cu_{1-x}M_x)_3O_7$ are presented and discussed in sections 4.3 and 4.5, taking into consideration other NMR work and theoretical studies on this system. ^{89}Y NMR evidence for a true O-T transition for substitution of Fe, Co, Ga and Al is provided in section 4.4. In section 4.6, the correlations between T_c and ^{89}Y shift for chain site substitution and between T_c and relaxation for the plane site

substitution are given. Also ^{51}V and ^{27}Al NMR data are presented and discussed in sections 4.7 and 4.8 for V and Al doped $YBa_2(Cu_{1-x}M_x)_3O_7$, respectively. Section 4.9 is the general discussion of the work presented here for this system.

4.2. XRD Results and Transition Temperatures.

As mentioned in chapter 3 XRD measurements have been carried out to identify the crystal structure of substituted $YBa_2(Cu_{1-x}M_x)_3O_{7-\delta}$ (M=V, Fe, Co, Ni, Zn, Ga and Al) samples. It has been observed that for some of the substitutions (Fe, Co, Ga and Al) XRD powder patterns present a tetragonal structure for x>0.025. As an example XRD powder patterns in $YBa_2(Cu_{1-x}Co_x)_3O_{7-\delta}$ for 2θ=45–50 are displayed in fig.4.1. They show that the splitting of the (200) and (020) peaks disappears for x>0.025 as the structure becomes tetragonal. Also XRD powder patterns of $YBa_2(Cu_{1-x}M_x)_3O_{7-\delta}$ (where M=Cu, V, Ni, Zn, Fe, Co, Ga and Al; and x=0.1) are presented in fig.4.2 with 2θ=45–50. Again the nonexistence of the splitting of the (020) and (200) peaks shows that the structure is tetragonal for Fe, Co, Ga and Al substitution. For other substitutions (V, Ni and Zn) the structure remains orthorhombic. There have been many structural studies in substituted $YBa_2(Cu_{1-x}M_x)_3O_{7-\delta}$[1-4,11]. Our XRD results are in good agreement with these studies.

Transition temperature measurements have been performed by using A.C. susceptibility (see section 3.6.3) in substituted $YBa_2(Cu_{1-x}M_x)_3O_{7-\delta}$ (M=V, Fe, Co, Ni, Zn, Ga and Al). The transition temperatures as a function of dopant concentration are plotted in fig.4.3(a) for Fe, Co, Ga and Al and fig.4.3(b) for Zn, Ni and V substitution in $YBa_2(Cu_{1-x}M_x)_3O_{7-\delta}$. All substitutions reduce T_c but with very

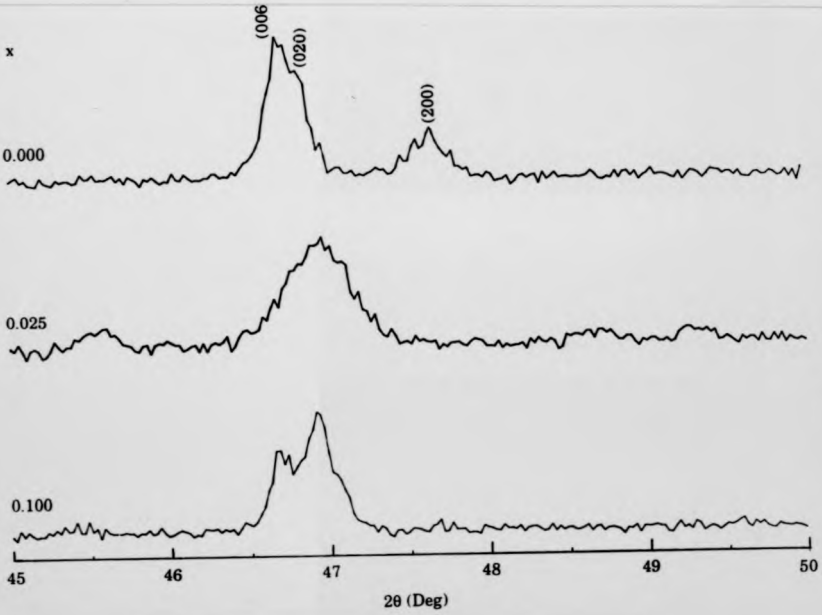

Fig.4.1. XRD powder patterns for $YBa_2(Cu_{1-x}Co_x)_3O_7$ with x=0-0.1 and 2θ=45-50.

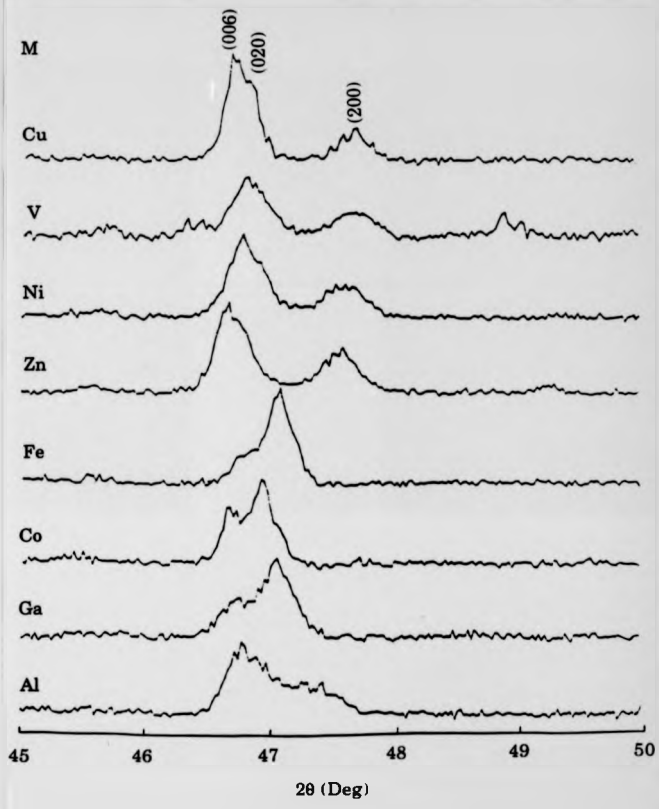

Fig.4.2. XRD powder patterns for $YBa_2(Cu_{1-x}M_x)_3O_7$ with 2θ=45–50. Where x=0.1 and M=Cu, V, Ni, Zn, Fe, Co, Ga and Al.

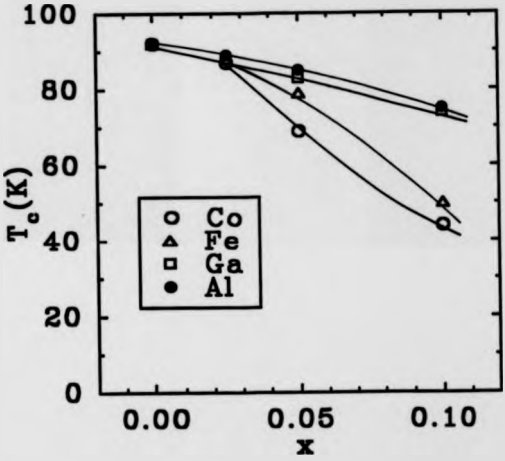

Fig.4.3(a). The transition temperatures as a function of dopant concentration x for Al, Ga, Fe and Co substitution in $YBa_2(Cu_{1-x}M_x)_3O_7$.The lines are drawn to guide the eye.

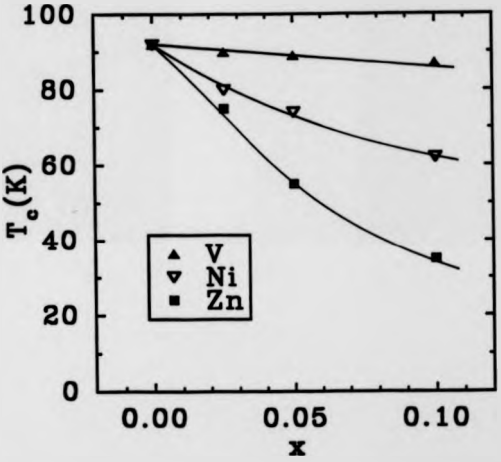

Fig.4.3(b). The transition temperatures as a function of dopant concentration x for V, Ni and Zn substitution in $YBa_2(Cu_{1-x}M_x)_3O_7$. The lines are drawn to guide the eye.

different rates as given in table.4.1. The largest reduction rates are ~7K/% for Zn substitution on the plane site and 5K/% for Co substitution on the chain site. Doping with V only slightly reduces the T_c. Transition temperature results presented here are in agreement with the data published elsewhere[1,2,4] to within experimental errors.

Table: 4.1. The reduction rates in T_c for a variety of substitutions in $YBa_2(Cu_{1-x}M_x)_3O_{7-\delta}$.

Substitution	Al	Ga	Fe	Co	V	Ni	Zn
$\Delta T_c/\Delta x$(K/%)±0.5	1.5	2.0	4.0	5.0	0.5	3.0	7.0

4.3. ^{89}Y shifts.

4.3.1. General.

The measured shift, $S=K+\sigma$, is the sum of a Knight shift contribution K, and σ the chemical shift. The Knight shift has two contributions: orbital K_{orb} and spin K_s. The spin contribution is temperature dependent and related to the static spin susceptibility χ_s as $K_s(T)=\alpha\chi_s(T)$ where α is the hyperfine coupling constant.

In an early ^{89}Y NMR study of $YBa_2Cu_3O_7$[12] (Where the total shift was observed as S=-103 ppm) it was suggested that the Chemical shift contribution is about 200 ppm and thus the Knight shift is −300 ppm. Although the existence of the negative Knight shift was first questioned theoretically[13], finally it was agreed that the ^{89}Y shift in $YBa_2Cu_3O_7$ was negative[14-16]. It is now generally accepted that the chemical shift of orthorhombic $YBa_2Cu_3O_7$ is close to +200ppm[17-20] (for a detailed discussion see reference 21). For $YBa_2Cu_3O_7$ the Knight shift is −303ppm (±10ppm) and the changes with substitution and with temperature are likely to be

due to the changes in Knight shift.

4.3.2. Room Temperature Results and Discussion.

The effect of Co substitution on the ^{89}Y spectrum at room temperature is shown in figure 4.4. In addition to the broadening produced by substitution, the shift becomes more positive as Co is added. The line broadening effect is probably due to the disorder in the structure produced by substitution. The same effect was also obtained in ^{89}Y spectra of the oxygen depleted $YBa_2Cu_3O_{7-\delta}$ samples[12]. As seen from fig.4.4, for Co doped $YBa_2Cu_3O_{7-\delta}$ samples an unknown phase appears at about 80 ppm. This phase was also seen in the other Cu site substituted $YBa_2Cu_3O_{7-\delta}$ and in Pr and Nd doped $YBa_2Cu_3O_{7-\delta}$[22]. In fig.4.5 ^{89}Y NMR shifts at room temperature vs. dopant concentration, x, are plotted for a variety of substitutions. All substitutions increase the ^{89}Y shift but with different rates; for Ni, Zn and V substitution the changes in shift are small whereas for Al, Co, Fe, and Ga substitution much more marked shift changes are observed. For these latter substitutions where the atoms are known to go on the chain sites and where the structure changes from orthorhombic to tetragonal a linear variation of shift with concentration is observed with the largest shift increase being for Co and the smallest for Al. Extrapolation of the shift to x=0 for all these substitutions gives -90 ± 2 ppm rather than the undoped $YBa_2Cu_3O_7$ shift of -103 ± 1 ppm[12]. This is probably because of the change in the chemical shift as the structure changes from orthorhombic to tetragonal. The discussion on O-T transition with these substitutions is given in section 4.4.

The ^{89}Y shift in $YBa_2Cu_3O_7$ has been interpreted theoretically by several

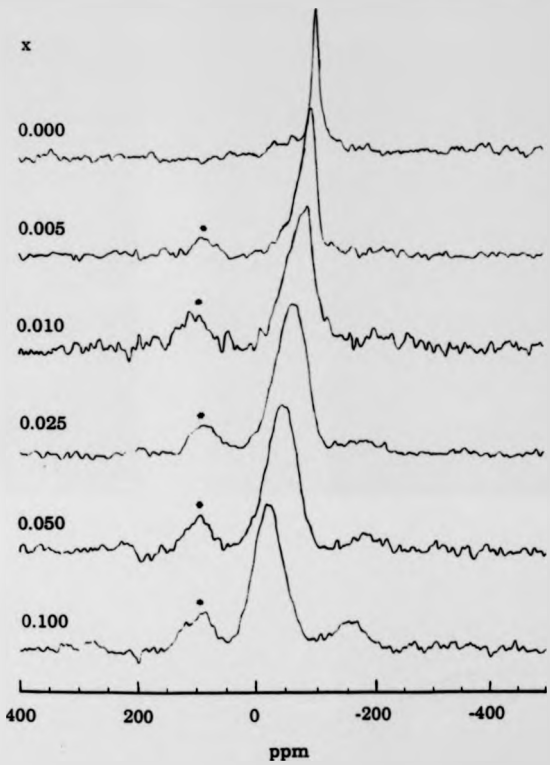

Fig.4.4. ^{89}Y MAS NMR spectra in $YBa_2(Cu_{1-x}Co_x)_3O_7$ with x=0-0.1. The asterisks denote an unknown phase.

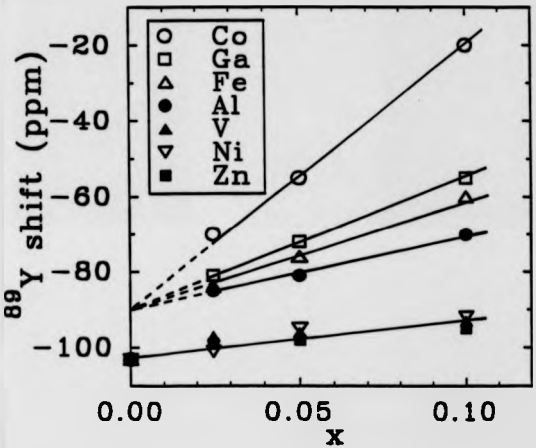

Fig.4.5. ^{89}Y shift at room temperature vs. concentration x for $YBa_2(Cu_{1-x}M_x)_3O_7$ with M=Co, Ga, Fe, Al, V, Ni and Zn.

authors (see section 2.5.3) in terms of the transferred hyperfine field, D, from the 8 nearest neighbour Cu(2) sites as[23]

$$K = \frac{8D}{\gamma_e \hbar \gamma_N} \chi_o \qquad (4.1)$$

where χ_o is the spin susceptibility. Within this model substitution onto the Cu(2) site might be expected to change K since there would no longer be 8 Cu(2) neighbours acting coherently. Although there is a small reduction in total shift experimentally observed with the plane site substitutions Ni and Zn, it is much smaller than would be predicted from this model as seen in table.4.2 unless χ_o also changes with increasing x.

Table: 4.2. The comparison of the experimental and the theoretical (in terms of transferred hyperfine field) values of total shift for the case of Ni and Zn substitution in $YBa_2Cu_3O_{7-\delta}$.

x	Calculated Shift* (ppm)	Observed Shift(ppm)	
		For Ni	For Zn
0.025	−89	−98±3	−96±3
0.050	−78	−92±3	−95±3
0.100	−55	−89±3	−92±3

* Note that the chemical shift was taken as 200 ppm.

4.3.3. Temperature Dependence.

4.3.3.1. Results.

The ^{89}Y shift against temperature for Co substitution in $YBa_2(Cu_{1-x}M_x)_3O_{7-\delta}$ is plotted for a range of x=0-10% dopant concentration in fig.4.6. Similar data for Al, Ga and V substitutions are given in figures 4.7, 4.8 and 4.9, respectively, for a range of substitution compositions (0-10%). The temperature dependence of the shift for various substitutions at the 2.5% level is shown in fig.4.10, and in fig.4.11 for 5% substitution together with the shift for pure 123 (this work and references 12 and 22). Once again the behaviour splits into two groups. For the substitutions on the chain site Al, Co, Fe, and Ga the shift increases with decreasing temperature whereas for Ni and Zn it becomes more negative having a fairly similar temperature dependence to the pure fully oxygenated $YBa_2Cu_3O_7$. The vanadium substituted sample has a shift at room temperature close to that of Ni and Zn doped $YBa_2Cu_3O_7$ (it is still orthorhombic) but it increases with decreasing temperature in a similar fashion to that of the Co, Fe, Al and Ga substituted samples.

The MAS width is shown as a function of temperature in fig 4.12(a) for 2.5% Al, Co, Ga, and Zn substitution together with that for pure $YBa_2Cu_3O_7$, and in fig 4.12(b) for Fe, Ni and V substituted material. At room temperature the width of the cobalt substituted sample, ~900Hz, is slightly greater than that for Al, 850Hz, or Fe and Ni,~800Hz, substitution with Zn substitution having least effect on the line width,~600Hz. The width increases with decreasing temperature in all these samples, increasing most rapidly for Fe and Ni and least rapidly for Zn. It is of interest that the width of pure $YBa_2Cu_3O_7$ is also temperature dependent increasing from ~150Hz at 380K to ~280Hz at 180K.

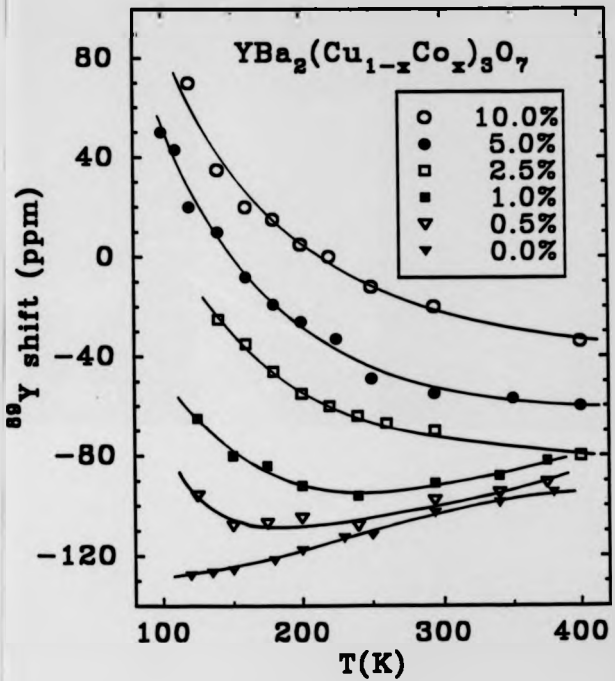

Fig.4.6. ^{89}Y shift as a function of temperature in $YBa_2(Cu_{1-x}Co_x)_3O_7$ with x=0-0.1. The lines are drawn to guide the eye.

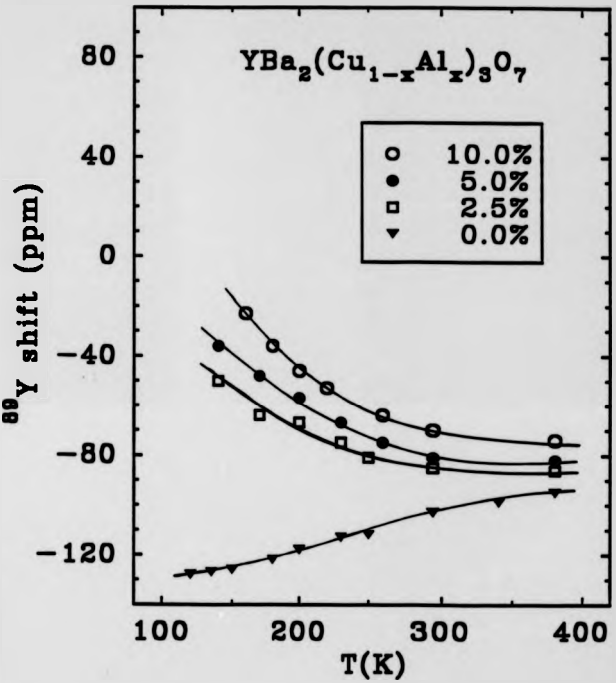

Fig.4.7. ^{89}Y shift as a function of temperature in $YBa_2(Cu_{1-x}Al_x)_3O_7$ with x=0-0.1. The lines are drawn to guide the eye.

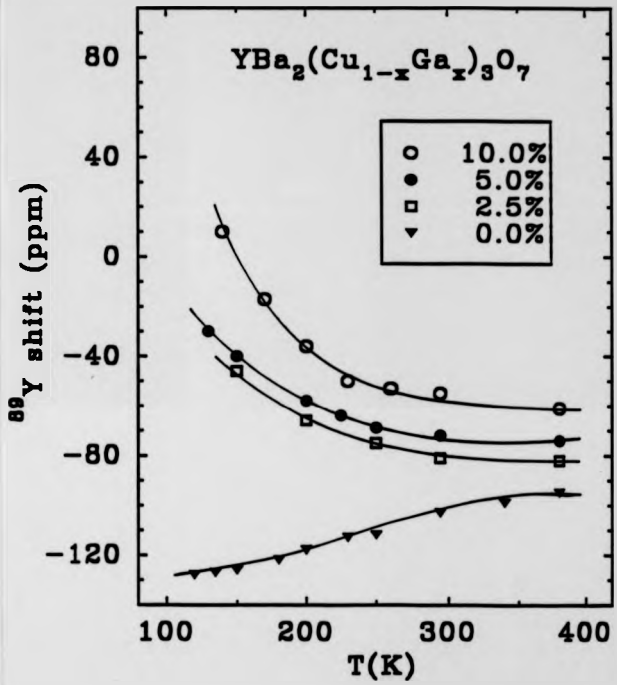

Fig.4.8. ^{89}Y shift as a function of temperature in $YBa_2(Cu_{1-x}Ga_x)_3O_7$ with x=0-0.1. The lines are drawn to guide the eye.

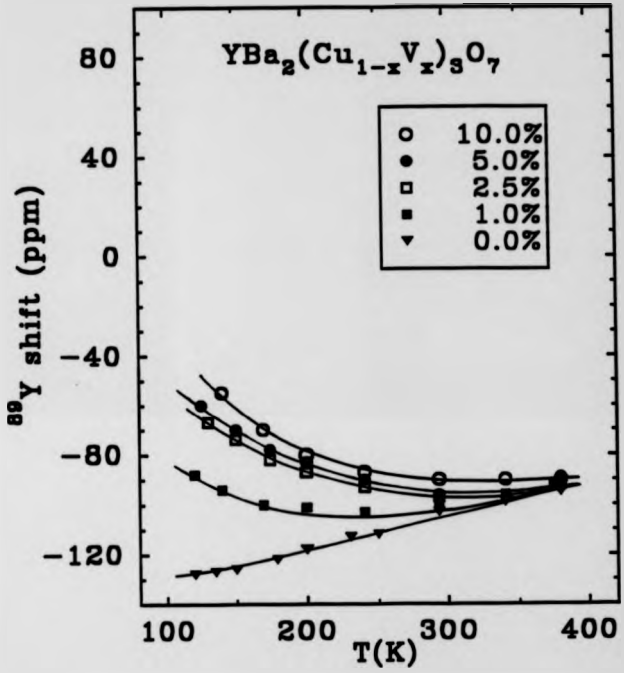

Fig.4.9. ^{89}Y shift as a function of temperature in $YBa_2(Cu_{1-x}V_x)_3O_7$ with x=0-0.1. The lines are drawn to guide the eye.

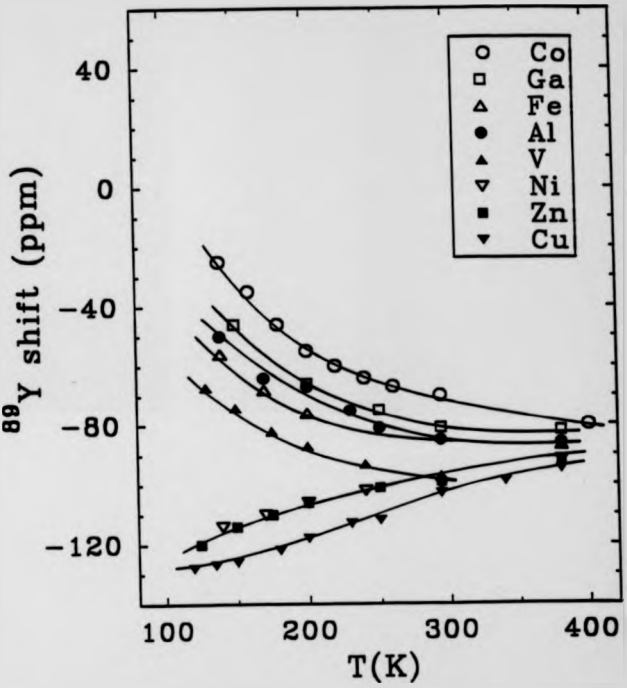

Fig.4.10. The temperature dependence of the ^{89}Y NMR shift for the 2.5% substituted samples. The lines are drawn to guide the eye.

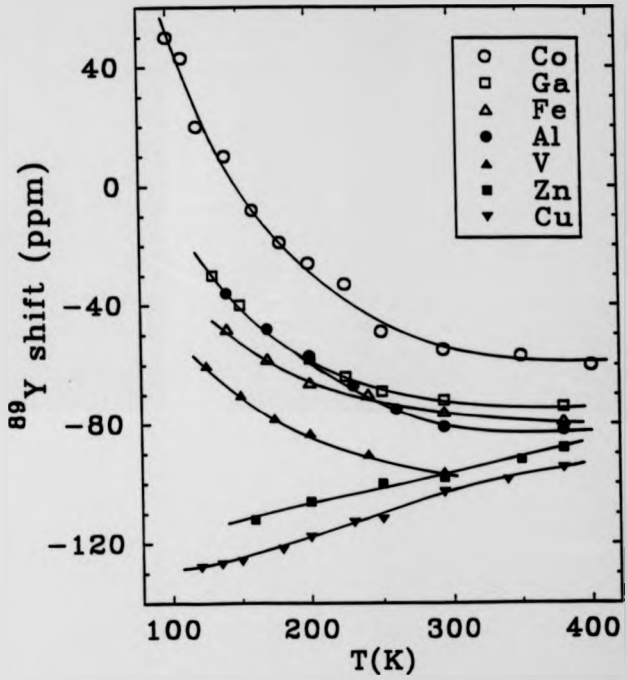

Fig.4.11. The temperature dependence of the ^{89}Y NMR shift for the 5% substituted samples. The lines are drawn to guide the eye.

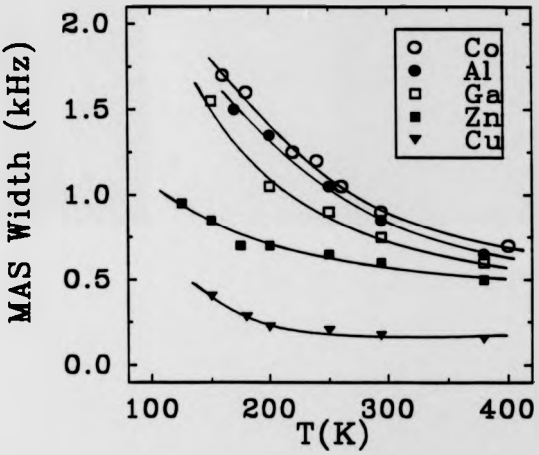

Fig.4.12(a). The ^{89}Y MAS NMR line width in $YBa_2Cu_3O_7$ and for 2.5% Al.Co.Ga and Zn substituted $YBa_2Cu_3O_7$. The lines are drawn to guide the eye.

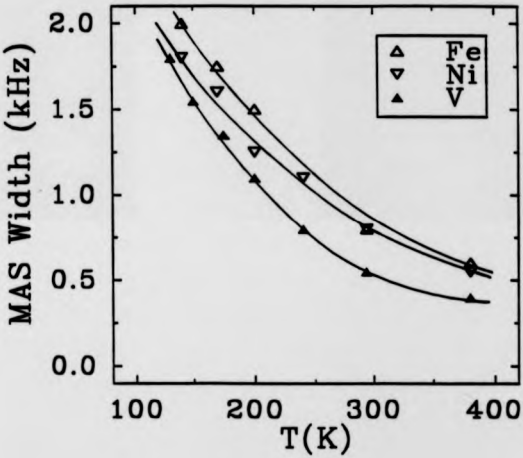

Fig.4.12(b). The ^{89}Y MAS NMR line width for 2.5% substituted Fe,Ni and V. The lines are drawn to guide the eye.

4.3.3.2. Discussion.

4.3.3.2.(a) Chain Site Substitution.

Figure 4.6 (for Co) clearly shows that the temperature dependence of the shifts increases as the dopant concentration increases from 0 to 2.5 %. The shift increases with decreasing temperature for the chain site substitutions (Co, Al, Ga and Fe) (figures 4.6, 4.7, 4.8, 4.10 and 4.11) with dopant concentrations more than 2.5% and shows a qualitatively similar behaviour to that observed for oxygen depleted 123[12,17]. This temperature dependence of shifts for the chain site substitutions might be due to the changes in $N(E_F)$ as was suggested[12] for oxygen depleted $YBa_2Cu_3O_{7-\delta}$ samples. Therefore this indicates that the mechanism responsible for temperature dependent behaviour for both chain site substituted and oxygen depleted $YBa_2Cu_3O_{7-\delta}$ systems might be the same.

A ^{89}Y NMR study of cobalt doped $YBa_2Cu_3O_7$ using a static sample which had been magnetically aligned has recently been reported[24]. The isotropic shift deduced from their parallel and perpendicular shift values for pure $YBa_2Cu_3O_7$ is fairly similar to that presented here (e.g fig.4.6) and elsewhere[12,22]. However for doped samples they found an isotropic shift which depended only weakly on concentration and which showed little or no temperature dependence contrary to the data in fig.4.6. In their static aligned samples cobalt doping caused a significant increase in the line width to ~5kHz for 4% Co. These large line widths might obscure the relatively small changes in shift.

In Magic Angle Spinning experiments homogeneous broadening which is less than the spinning speed (typically 3kHz) is narrowed, nevertheless the line width increases with decreasing temperature for all samples. Thus broadening is present

which cannot be narrowed by spinning. For the substitutions on the chain sites the line width follows an approximately Curie type temperature dependence over a factor of about 2.5 in 1/T and a plot of the width versus 1/T is shown in fig 4.13 for 2.5% Al, Co and Ga substitution together with that for pure $YBa_2Cu_3O_7$. It is interesting to note that the line width of the pure $YBa_2Cu_3O_7$ is also approximately Curie like with a temperature independent contribution to the line width of ~50Hz, much closer than the room temperature width to that expected for a non magnetic crystalline yttrium compound. The line width for the Co substituted sample at any given temperature is only slightly larger than that for Al or Ga substitution and for these chain site substitutions the width extrapolates roughly to the (extrapolated) line width of pure $YBa_2Cu_3O_7$ at infinite temperature. The effect of static magnetic moments such as Co in the sample would be to produce spinning sidebands rather than the large broadening observed here. In any case the widths of the Al and Ga substituted samples, where magnetic moments are not produced by the substitution, are very similar to the Co doped sample. For the undoped $YBa_2Cu_3O_{7-\delta}$ it is possible that small variations in oxygen stoichiometry could produce a temperature dependent line width via the different temperature dependencies of the shift as the oxygen content is changed with for instance a stoichiometry variation of 0.01-0.02 being sufficient if the ^{89}Y NMR shift variation with oxygen content is linear from δ=0.0 to 0.15. However the broadening is so large for the chain site doped samples that variable oxygen stoichiometry or concentration fluctuations in the doping cannot be the cause of the broadening. A possible cause of the temperature dependent broadening is via the RKKY interaction combined with the disorder present in these samples which would not be narrowed by spinning.

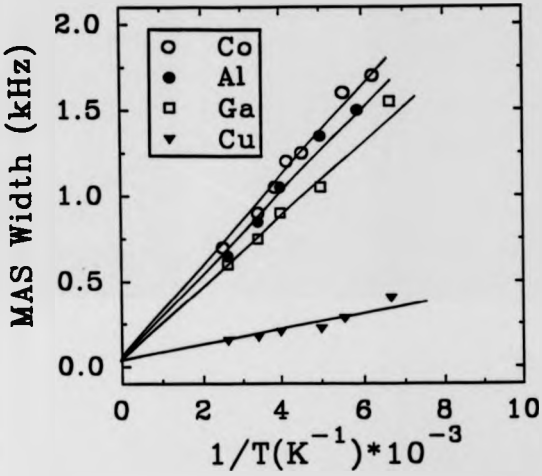

Fig.4.13. The ^{89}Y MAS NMR line width vs. 1/T for $YBa_2Cu_3O_7$ and for 2.5% Al, Co and Ga substituted $YBa_2(Cu_{1-x}M_x)_3O_7$.

4.3.3.2.(b) Plane Site Substitution (Zn and Ni).

As shown in figures 4.10 and 4.11 the temperature dependence of the shift for Zn and Ni substitution is similar to that of $YBa_2Cu_3O_7$. They all (Zn and Ni doped $YBa_2Cu_3O_{7-\delta}$ and also pure fully oxygenated $YBa_2Cu_3O_{7-\delta}$) show nearly temperature independent behaviour. For Zn, recently a similar temperature dependence of the ^{89}Y shift was observed in static measurements[25]. In that study[25] the temperature dependence of shift for oxygen depleted, Zn substituted $YBa_2Cu_3O_{7-\delta}$ samples was presented and a similar temperature dependence behaviour to oxygen depleted pure $YBa_2Cu_3O_{7-\delta}$ was observed.

In fig.4.14 the width versus 1/T is plotted for pure $YBa_2Cu_3O_{7-\delta}$ and 2.5% and 5% Zn substituted $YBa_2Cu_3O_{7-\delta}$. It clearly shows that the line width variation for zinc substitution is also rather different from that of the chain site substitutions, since it has a much smaller slope and extrapolates to a width of ~270Hz at 1/T=0 for 2.5% Zn. The effect of the zinc is to produce a fairly large temperature independent contribution to the broadening as well as the temperature dependent term observed in all doped samples. Measurements for a 5% Zn substituted sample show that this contribution scales roughly with concentration. For the Ni doped samples the line width varies more rapidly with temperature than for Zn or for the substitutions on the chain sites. The reason for this is not clear.

4.3.3.2.(c) V Substitution.

As seen in fig 4.9 the temperature dependences of the ^{89}Y shift for V substituted samples are very similar to that of the chain site substitutions. As the substitution composition increases the temperature dependence increases. This

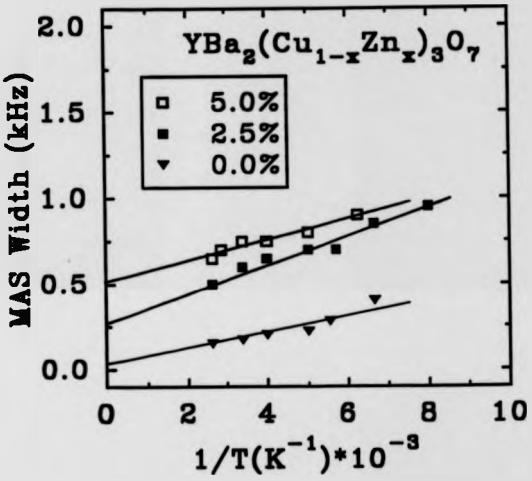

Fig.4.14. The ^{89}Y MAS NMR line width vs. 1/T for pure $YBa_2Cu_3O_7$ and for 2.5% and 5% Zn substituted $YBa_2(Cu_{1-x}Zn_x)_3O_7$.

implies that vanadium also substitutes on the chain sites even though the structure remains orthorhombic.

4.4. Evidence for O-T Transition for Fe, Co, Ga and Al Substitutions.

Structural studies by X-ray diffraction[1-4] and Neutron diffraction[2,4,11] experiments showed that the average structure of substituted $YBa_2Cu_3O_7$ with a small amount of Fe, Co, Ga and Al substitutions (2-3%) becomes tetragonal. However it is claimed that this appearance of tetragonal structure from XRD is due to the micro-twinning. Therefore further study was required to investigate the O-T transition. We believe that ^{89}Y MAS NMR is a good probe to study this O-T transition as the chemical shift is sensitive to the structure only to a distance of ~5A from the Y site.

As noted in section 4.3.2 (from fig.4.5) for Fe, Co, Ga and Al substitutions the shift varies linearly with concentration for $x \geq 2.5$ and extrapolates to -90 ± 2ppm at room temperature for $x=0$.

^{89}Y MAS NMR shifts at room temperature are plotted in fig.4.15 as a function of dopant concentration for Co, Ga, Al and V substitutions, including some data for $x<0.025$. As seen a linear variation of shift with concentration for concentration of substituent more than 2.5% is observed and for all the substitutions except V extrapolations of the shifts to $x=0$ give −90 ppm whereas for less than 2.5% concentration the curve (for Co and Al) extrapolate to the undoped $YBa_2Cu_3O_7$ shift value of −103 ppm. Similar behaviour was observed at 200K as shown in fig.4.16. For substitution more than 2.5% the shift varies linearly with Co, Al, Ga and V substitution and once again the difference between the extrapolated values for

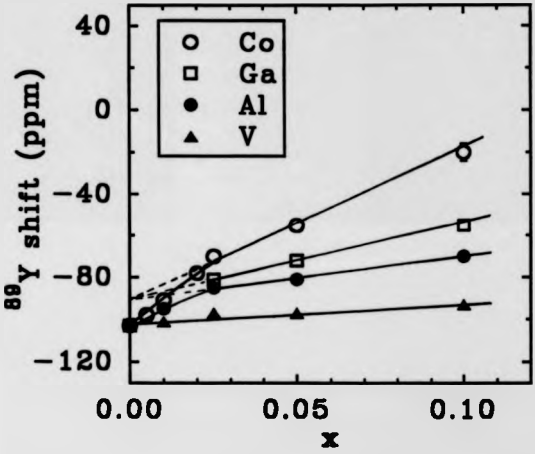

Fig.4.15. ^{89}Y shift at room temperature as a function of the dopant concentration x for $YBa_2(Cu_{1-x}M_x)_3O_7$ with M=Co, Ga, Al and V.

samples changing the structure (Co, Al, Ga) (-75 ppm) and for V which does not change the structure(-88 ppm) is 13 ppm. The difference between the values from the extrapolation of the lines (-75 ppm) for $x \geq 2.5\%$ and from the extrapolation of the curves (-118 ppm) for $x < 2.5\%$ is 43 ppm. This is because the temperature dependence of the shift for $x \geq 2.5\%$ is different from that for $x < 2.5\%$ as seen in fig.4.6 and 4.9 for Co and V substitution, respectively. This 13 ppm difference in figures 4.15 and 4.16 can be attributed as due to the change in chemical shift as the structure changes from orthorhombic to tetragonal. In fig.4.17 a plot of the ^{89}Y chemical shift change with Co substitution at room temperature, calculated from fig.4.15, is presented. The chemical shift varies for the low concentration rates ($x < 0.025$) in a similar way to the changes in the a and b lattice parameters[8] and becomes 213 ppm by 2.5%.

In fig.4.18 T_c versus ^{89}Y shift data at room temperature for Co and Al doped $YBa_2Cu_3O_{7-\delta}$ are plotted with x as the implicit parameter. For $x < 0.025$ the shift changes faster than the T_c whereas for $x > 0.025$ the shift and the T_c are very well correlated. This correlation is discussed in section 4.6. The faster shift change for $x < 0.025$ is most probably because of the contribution coming from the chemical shift change as the structure changes from orthorhombic to tetragonal. One can easily find out the change in chemical shift by using $\Delta S = \Delta K + \Delta\sigma$. Where $\Delta K = (dK/dx)x$ and dK/dx values were calculated from fig.4.5 as 7 ± 0.5 and 2 ± 0.4 ppm/% for Co and Al, respectively. Thus the change in chemical shift is 13 ± 2 ppm for 2.5% substitution of both Co and Al.

The ^{89}Y chemical shift is sensitive only to changes in the local environment, which differs in the tetragonal structure from that in the orthorhombic material with

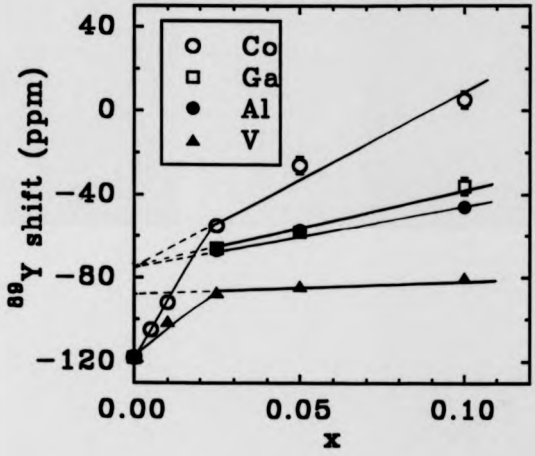

Fig.4.16. ^{89}Y shift at 200K as a function of the dopant concentration x for $YBa_2(Cu_{1-x}M_x)_3O_7$ with M=Co, Ga, Al and V.

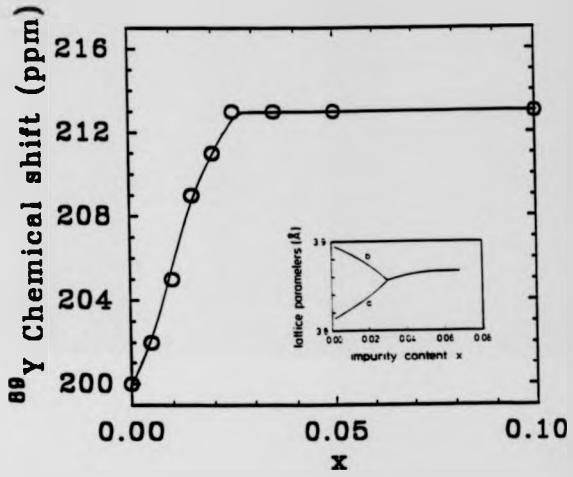

Fig.4.17. ^{89}Y chemical shift at room temperature as a function of the dopant concentration x for $YBa_2(Cu_{1-x}Co_x)_3O_7$.

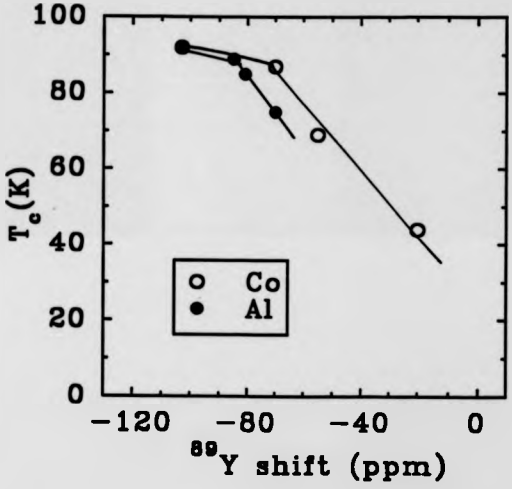

Fig.4.18. T_c versus ^{89}Y shift at room temperature for Co and Al substituted $YBa_2Cu_4O_7$ with x as the implicit parameter.

small changes in the bond distances (for example Y-Cu(2) bond distances are 3.2197 and 3.194Å for orthorhombic $YBa_2Cu_3O_7$ and Co doped tetragonal $YBa_2Cu_3O_7$, respectively). The explanation for a 13 ppm shift change for concentrations of substituent greater than –2.5% (from the extrapolations of the lines in fig.4.15 and 4.16; and from the calculation in fig 4.18) is the existence of a true O–T transition.

4.5. ^{89}Y Spin Lattice Relaxation.

4.5.1. Results.

The spin-lattice relaxation rates at room temperature for Ga, Al, Fe and Co substitution are shown in figure 4.19(a) and for Zn,Ni,V in figure 4.19(b). The relaxation rate *decreases* with dopant concentration for Ga, Al, Fe and Co substitution but *increases* for Zn,Ni and V substitution with the largest changes being for Co and Zn substitutions respectively. For 10% Zn substitution the relaxation rate has increased by a factor of 2, whilst for 10% Co it has halved. An early study of ^{89}Y resonance of Zn and Ga substitution at room temperature has presented[26] similar results on shift (section 4.3.2) and relaxation.

The plot of the relaxation rates is shown in fig.4.20 as (T_1T) versus temperature for 2.5% Co and Zn doped $YBa_2Cu_3O_{7-\delta}$ together with that for undoped $YBa_2Cu_3O_7$. T_1 values of undoped $YBa_2Cu_3O_7$ at 200 and 380K were taken from reference 12.

4.5.2. Discussion.

4.5.2.(a) Chain Site Substitution.

For simple metals the Knight shift and relaxation time T_1 are related through

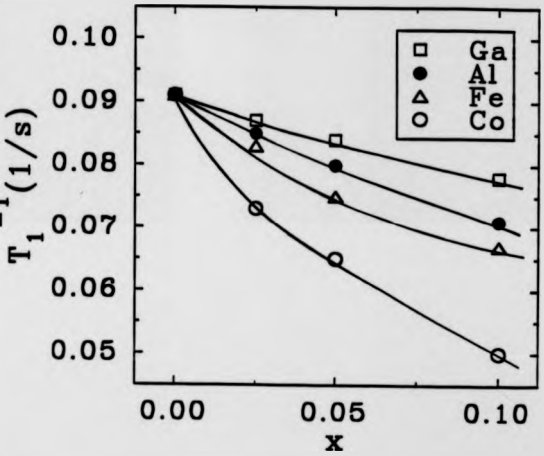

Fig.4.19(a). ^{89}Y spin lattice relaxation rates at room temperature versus concentration for Ga, Al, Fe and Co substituted $YBa_2Cu_3O_7$. The lines are drawn to guide the eye.

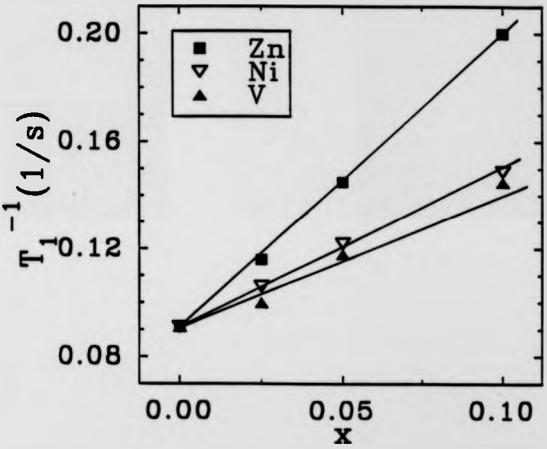

Fig.4.19(b). ^{89}Y spin lattice relaxation rates at room temperature versus concentration for Zn, Ni and V substituted $YBa_2Cu_3O_7$. The lines are drawn to guide the eye.

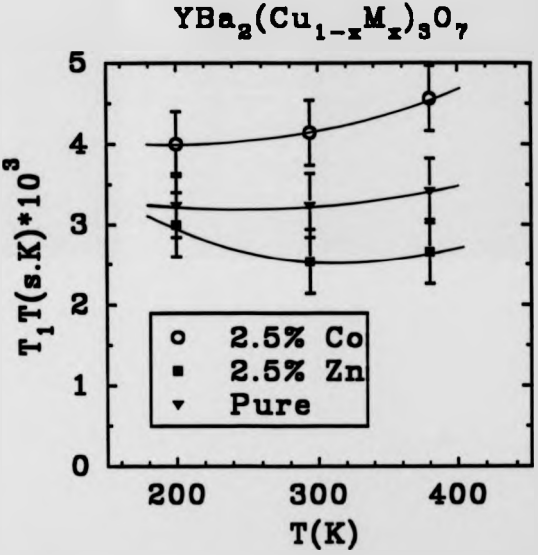

Fig.4.20. (T_1T) as function of temperature for 2.5% Co and Zn substituted $YBa_2Cu_3O_7$ and for pure $YBa_2Cu_3O_7$. The lines are drawn to guide the eye.

the Korringa relation K^2T_1T=constant and table 4.3 shows that this relation is obeyed as x increases in Co substituted $YBa_2(Cu_{1-x}Co_x)_3O_7$. (Uncertainties in K resulting from any uncertainty in σ are much smaller than the uncertainty in T_1). The smaller changes in relaxation and correspondingly shift for the other substitutions on the Cu(1) chain site are also consistent with a Korringa type of variation as shown in tables 4.4, 4.5 and 4.6 for Fe, Al and Ga substitution, respectively. This behaviour indicates that the dominant cause of the change in shift and relaxation for chain site substitution is a reduction in the $N(E_F)$

In fig.4.21 $^{89}K^2T_1T$ is plotted as a function of temperature for 2.5% Co doped $YBa_2Cu_3O_{7-\delta}$ and for undoped $YBa_2Cu_3O_7$. As seen for 2.5% Co doped $YBa_2Cu_3O_{7-\delta}$ the behaviour is not Korringa like whereas for undoped $YBa_2Cu_3O_{7-\delta}$ K^2T_1T=constant is obeyed.

4.5.2.(b) Plane Site Substitution.

The increase in relaxation rate is the most marked effect of these substitutions and since the shift changes very little there must be some additional source of relaxation present which does not cause a change in shift. In general one can write the relaxation rate arising from a fluctuating field, B_{loc}, as

$$T_1^{-1} = \gamma^2 B_{loc}^2 \tau \qquad (4.2)$$

For substitution in the CuO plane the B_{loc} could arise from the fluctuating components of the transferred hyperfine field of the Cu(2) ions no longer cancelling at the Y site, i.e. a simple estimate of B_{loc} would be D which is 3 kG[27] in $YBa_2Cu_3O_7$. If τ is taken as the spin fluctuation lifetime in the MMP model[23] then

Table: 4.3. K^2T_1T versus dopant concentration for $YBa_2(Cu_{1-x}Co_x)_3O_7$ at room temperature.

x	SHIFT(ppm) ±5ppm	K(ppm)* ±10ppm	T_1 (s)	$K^2T_1T*10^8$ ($ppm^2s.K$)
0.0	−103	−303	11±1.5	3.0±0.3
0.025	−70	−283	13±2	3.1±0.3
0.05	−55	−268	15±2	3.2±0.3
0.10	−20	−233	20±2	3.2±0.3

Table: 4.4. K^2T_1T versus dopant concentration for $YBa_2(Cu_{1-x}Fe_x)_3O_7$ at room temperature.

x	SHIFT(ppm) ±5ppm	K(ppm)* ±10ppm	T_1 (s)	$K^2T_1T*10^8$ ($ppm^2s.K$)
0.0	−103	−303	11±1.5	3.0±0.3
0.025	−84	−297	12±2	3.1±0.3
0.05	−76	−289	13±2	3.2±0.3
0.10	−55	−268	15±2	3.2±0.3

*Note that the chemical shift σ changes by 13ppm between x=0 and x=0.025.

Table: 4.5. K^2T_1T versus dopant concentration for $YBa_2(Cu_{1-x}Al_x)_3O_7$ at room temperature.

x	SHIFT(ppm) ±5ppm	K(ppm)* ±10ppm	T_1 (s)	$K^2T_1T*10^8$ (ppm^2s.K)
0.0	−103	−303	11±1.5	3.0±0.3
0.025	−85	−298	12±2	3.2±0.3
0.05	−81	−294	13±2	3.3±0.3
0.10	−70	−283	15±2	3.5±0.3

Table: 4.6. K^2T_1T versus dopant concentration for $YBa_2(Cu_{1-x}Ga_x)_3O_7$ at room temperature.

x	SHIFT(ppm) ±5ppm	K(ppm)* ±10ppm	T_1 (s)	$K^2T_1T*10^8$ (ppm^2s.K)
0.0	−103	−303	11±1.5	3.0±0.3
0.025	−81	−294	11.5±2	3.0±0.3
0.05	−72	−285	12±2	2.9±0.3
0.10	−55	−268	13±2	2.8±0.3

*Note that the chemical shift σ changes by 13ppm between x=0 and x=0.025.

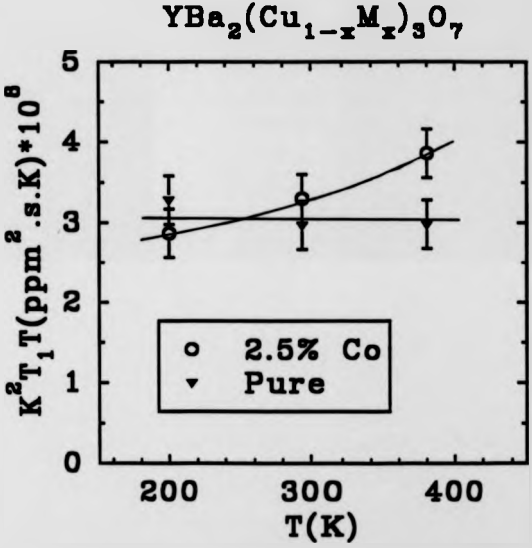

Fig.4.21. K^2T_1T as function of temperature for 2.5% Co substituted $YBa_2Cu_3O_7$ and for pure $YBa_2Cu_3O_7$.

for $YBa_2Cu_3O_7$ $\tau \sim h/T_{sf} \sim 4.8 \times 10^{-14} s$[28] and a (dT_1^{-1}/dc) of $2.5 s^{-1}$ is predicted in qualitative agreement with the observed values of $1.1 s^{-1}$ (Zn) and $-0.58 s^{-1}$ (Ni). However the small shift seems to militate against this explanation. An alternative explanation which might provide a consistent interpretation for both the shift and relaxation is that local moments are being formed in the CuO_2 plane and that these provide the B_{loc}. Magnetic susceptibility measurements of Zn and Ni doped $YBa_2Cu_3O_7$ give strong evidence for the formation of moments[1,29], as does the Cu(2) NMR of Warren et al[30], although the magnitude of the susceptibility implies that each Zn atom produces more than one spin half magnetic moment. An alternate way of describing the increased relaxation is to note that the form factor will be modified by substitutions in the CuO_2 plane which destroy the symmetry at the yttrium site and thus increase the relaxation. It is clear from the measurements nonetheless that the mechanism for the increase of T_1^{-1} is different for Ni and Zn substitution than for Al, Co, Fe and Ga.

4.6. Correlation Between T_c and ^{89}Y NMR Data (Shift and Relaxation).

4.6.1. Chain Site Substitution.

As seen from fig.4.18 for Co and Al, there is a linear correlation between the reduction in T_c and the change in shift with substitution. For $x<0.025$ the change in shift is faster than that in T_c. As discussed in section 4.4 this is due to the structural change from orthorhombic to tetragonal.

Figure 4.22 shows a plot of the rate of the change of shift dK/dx against the rate of chance of transition temperature dT_c/dx. For all the chain site substitutions (Co, Ga, Al and V), it can be seen that the points lie on a straight line through the

origin. Since the Knight shift is related to $N(E_F)$ (see the equations 2.31 and 2.32 in chapter 2), the correlation between the reduction in T_c and the change in shift (fig.4.22) indicates that the probable cause of the reduction in T_c for these substitutions is the reduction in $N(E_F)$. The point for Fe lies above the line, i.e.dT_c/dx is bigger than expected. However this probably comes from the fact that Fe substitutes on both the Cu(1) chain and Cu(2) plane sites[31-33]. As substitutions on the plane sites seem to have stronger effect on T_c whilst causing little change in shift (see e.g.Ni and Zn discussed in section 4.2), one would expect the point for Fe to lie above the line.

In fig 4.23 the shift of $YBa_2(Cu_{0.95}Co_{0.05})_3O_7$ (T_c =70K) is plotted against that of $YBa_2Cu_3O_{6.75}$ (T_c=70K) which was linearly interpolated from the shifts of $YBa_2Cu_3O_{6.80}$ and $YBa_2Cu_3O_{6.60}$[12] with temperature the implicit parameter. A linear relationship is observed with a slope of one indicating that the coefficients of the temperature dependent term are the same. Also shown in fig 4.23 is the shift of $YBa_2(Cu_{0.95}V_{0.05})_3O_7$ (T_c=89K) vs. that of $YBa_2(Cu_{0.975}Al_{0.025})_3O_7$ (T_c=89K). In this case despite the change in structure (the Al doped sample is tetragonal and the V doped sample orthorhombic), the temperature dependence of the shifts is identical to within error. It is noteworthy that the ^{89}Y shift in $YBa_2Cu_4O_8$ has the same temperature dependence as oxygen depleted $YBa_2Cu_3O_{7-\delta}$ (δ=0.2) with the same T_c[21] indicating the close connection between T_c and temperature dependence of the susceptibility in these systems. Also very recently a common magnetic behaviour of the ^{89}Y shift in the Cu-O layered $YBa_2Cu_3O_{7-\delta}$, $YBa_2Cu_4O_8$ and $(Pb_{0.75}Cu_{0.25})Sr_2(Ca_{1-x}Y_x)Cu_2O_7$ superconductors have been studied by Han et al[34] reporting similar values and temperature dependence of the shift in these different

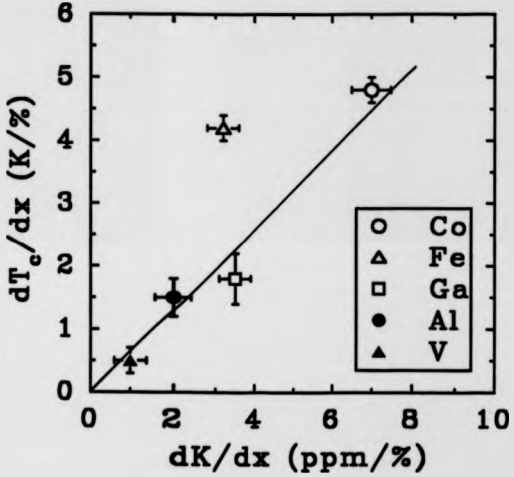

Fig.4.22. The reduction in T_c as a function of the change in ^{89}Y shift in $YBa_2(Cu_{1-x}M_x)_3O_7$ with M=Co,Fe,Ga, Al and V.

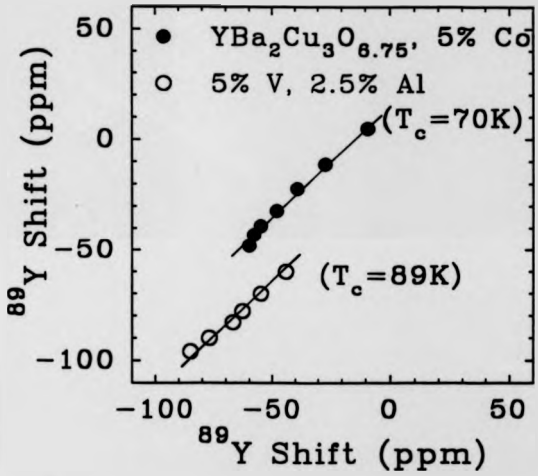

Fig.4.23. The ^{89}Y NMR shift in $YBa_2Cu_3O_{6.75}$ vs. $YBa_2(Cu_{1-x}Co_x)_3O_7$ (x=0.05) which both have T_c=70K with temperature as the implicit parameter. Also shown is the ^{89}Y NMR shift for $YBa_2(Cu_{1-x}V_x)_3O_7$ (x=0.05) vs. $YBa_2(Cu_{1-x}Al_x)_3O_7$ (x=0.025), both of which have a T_c=89K.

materials having similar T_c values.

4.6.2. Plane site substitution.

In fig.4.24 the rate of change of T_c with concentration dT_c/dx is plotted against the rate of change of relaxation rate dT_1^{-1}/dx for plane site substitution (Zn and Ni). It can be seen that there exists a straight line through the points for Zn, Ni and undoped $YBa_2Cu_3O_7$ (the origin). This correlation provides significant support for the idea that the cause for the reduction in T_c with plane site substitution is magnetic in origin.

4.7. ^{51}V NMR in $YBa_2(Cu_{1-x}V_x)_3O_{7-\delta}$.

The ^{51}V nucleus is 99.76% abundant with spin number I=7/2 (chapter 3). ^{51}V is a quadrupolar nucleus with a small electric quadrupolar moment. High resolution solid state NMR spectra of ^{51}V can be obtained by using the Magic Angle spinning technique[e.g.35,36].

^{51}V solid state NMR in $YBa_2(Cu_{1-x}V_x)_3O_7$ has been obtained with static and MAS experiments. The static and MAS ^{51}V NMR spectra in $YBa_2(Cu_{1-x}V_x)_3O_7$ (where x=0.025, 0.05 and 0.1) are shown in fig.4.25 (a) and (b), respectively. At low dopant concentration (2.5%), vanadium is in a site of axial symmetry, but at 5% dopant concentration, both static and spinning ^{51}V spectra show that vanadium occupies 2 sites. By 10% dopant concentration only one, approximately isotropic site is visible. The difference in shift of the two sites is –9 ppm (from 57 to 66 ppm).

^{51}V spectra in fig.4.25(a) and (b) clearly show the complexity of the substitution process. They demonstrate that whilst at low concentrations the

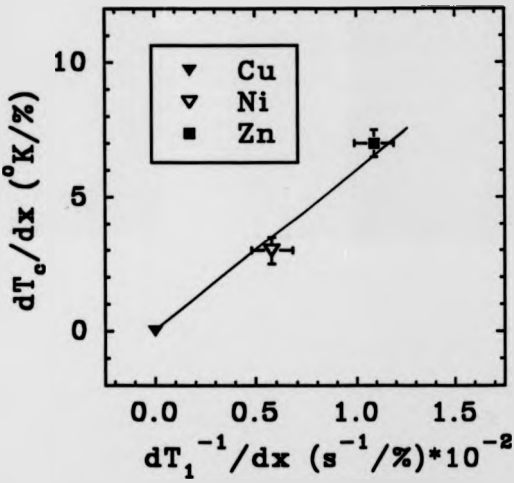

Fig.4.24. The reduction rate in Tc as a function of the change in relaxation rate in $YBa_2(Cu_{1-x}M_x)_3O_7$ with M=Cu, Ni and Zn.

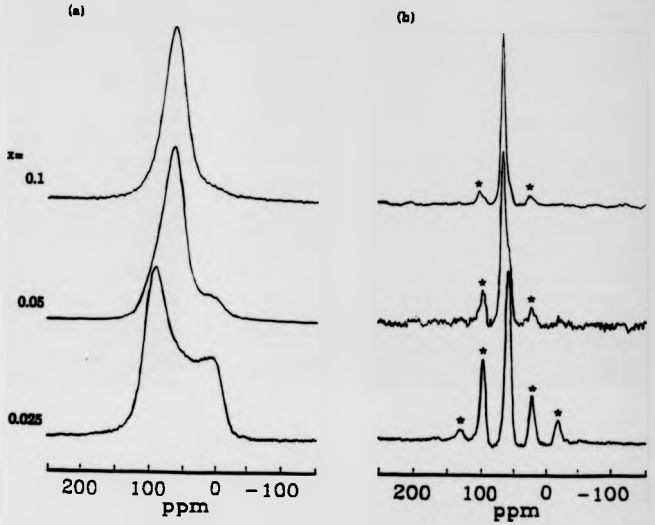

Fig.4.25. ^{51}V NMR spectra of $YBa_2(Cu_{1-x}V_x)_3O_7$ with x=0.025,0.05, and x=0.10.
(a) static, (b) spinning at 3.5kHz, asterisks denote the spinning sidebands.

vanadium occupies a site of axial symmetry, by 5% most of the vanadium atoms are in a more symmetric environment similar to that expected for a regular VO_4 tetrahedron (such as observed in YVO_4) i.e. the vanadium has pulled in an oxygen. This indicates that the vanadium is most likely to be substituted on the Cu(1) site where it is more easily able to pull in extra oxygen atoms. Mossbauer data have shown that iron substitutes on both Cu(1) and Cu(2) sites with relative proportions being a sensitive function of preparation conditions[33]. For Fe substitution on the Cu(1) sites three different local configurations are observed probably corresponding to fourfold, fivefold and sixfold ligand coordination in $YBa_2Cu_3O_7$ with a tetragonal structure being observed at higher concentrations[37]. The regular tetrahedral environment observed at higher vanadium concentrations indicates similar behaviour. The ^{51}V shift is small and close to insulator values for both sites indicating that there is little, if any, susceptibility at the vanadium sites.

4.8. ^{27}Al NMR in $YBa_2(Cu_{1-x}Al_x)_3O_{7-\delta}$.

The ^{27}Al nucleus (I=5/2 and 100% abundant) has a quadrupole moment of 0.149×10^{-28} m^2. ^{27}Al high resolution solid state NMR has been investigated e.g. in aluminium-oxygen compounds[38] alumina–silicates and zeolites[39], ceramics and glasses[e.g.40,41]. In this study ^{27}Al MAS NMR has been used in Al substituted $YBa_2(Cu_{1-x}Al_x)_3O_7$ superconductor.

The MAS ^{27}Al NMR spectra in $YBa_2(Cu_{1-x}Al_x)_3O_7$ (where x=0.025, 0.05 and 0.1) are shown in fig.4.26. Over the range of 2.5-10% Al, the ^{27}Al shift position is independent of concentration with a value of 76 ppm. As it can be seen from the spectra there is a small peak at 12ppm arising from a small amount of second phase

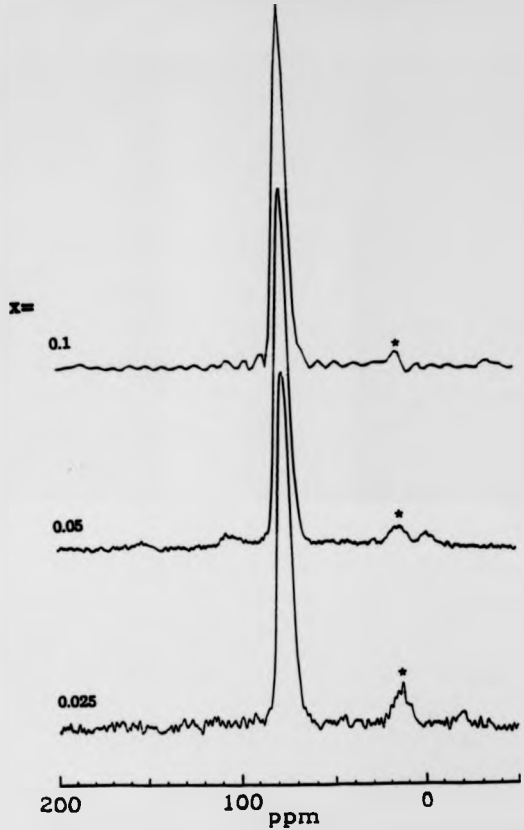

Fig.4.26. ^{27}Al MAS NMR spectra of $YBa_2(Cu_{1-x}Al_x)_3O_7$ with x=0.025, 0.05, and 0.10. asterisks donate the second phase Al_2O_3.

Al_2O_3.

The ^{27}Al spectra shows that aluminium, although occupying a chain site, has a relatively symmetric tetrahedral local environment suggesting that extra oxygen atoms may have been introduced into the chain layer sites[37]. The small ^{27}Al shift indicates that there is very little susceptibility at the aluminium sites.

4.9. General Discussion of $YBa_2(Cu_{1-x}M_x)_3O_{7-\delta}$ System.

XRD data for the substituted samples showed that for V, Ni and Zn the structure remains orthorhombic; and that Fe, Co, Al and Ga substitutions cause a structural change from orthorhombic to tetragonal. This behaviour was observed by several research groups[1-4,11] using XRD and Neutron diffraction techniques. There were some disagreements about the existence of a true O-T transition[6-8]. Our NMR measurements as discussed in section 4.4 by observing the change in the chemical shift have proved that there exists a true O-T transition with these substitutions.

In table 4.7 ^{89}Y NMR data of $YBa_2(Cu_{1-x}M_x)_3O_{7-\delta}$ have been summarized for a range of substitutions by dividing into three groups: (1) Ni and Zn ;(2) Fe, Co, Al and Ga ;(3) V. We now discuss this table for these three different cases.

The ^{89}Y NMR behaviour with Ni and Zn doping is completely different to the chain site doping. First there is only a small change in shift at room temperature, second in all cases the relaxation increases markedly with concentration of substituent, nearly doubling with the addition of ~10% Zn and third the temperature dependence of the shift for Zn and Ni substitution is similar to that of $YBa_2Cu_3O_7$. For these substitutions a dramatic increase in relaxation rate with very small shift changes (no Korringa behaviour) suggests that there exists some additional source

Table 4.7. Summary of ^{89}Y data for $YBa_2(Cu_{1-x}M_x)_3O_{7-\delta}$ system.

Substitution	Shift		Relaxation rate	Korringa Relation	T_c
	Room Temperature	Temperature Dependence	at room temperature	at room temperature	
Ni, Zn	Small changes	Similar to undoped Y123	increases	No	Correlated to T_1^{-1}
Fe,Co,Al,Ga	Linear increase	Similar to oxygen depleted Y123	decreases	Yes	Correlated to shift
V	Small changes	Similar to oxygen depleted Y123	increases	No	Correlated to shift

of relaxation rather than changes in the density of states. This is most probably fluctuating magnetic fields. Also the correlation between the T_c and relaxation rate for Ni and Zn substitution is evidence that these fluctuating magnetic fields are the mechanism responsible for the rapid decrease in T_c.

For the chain site substitutions Fe, Co, Ga and Al (we consider Fe as a chain site substitution since it mostly goes into the chain site) a linear variation in shift and a decrease in relaxation rate at room temperature with substitution are consistent with Korringa like behaviour, indicating that the density of states at the Fermi level ($N(E_F)$) is the dominant source for the change in shift and relaxation. For these substitutions the temperature dependence of the shift is similar to that for oxygen depleted $YBa_2Cu_3O_{7-\delta}$[12,17] suggesting that there exists a similar mechanism for these two systems. The mechanism for the temperature dependent susceptibility ($K(T)=\alpha\chi(T)$) in the normal state is not known although there have been several attempts at explaining the theoretical explanations of NMR data in $YBa_2Cu_3O_{7-\delta}$[e.g.23].

As shown in fig 4.18 and 4.22 the reduction in T_c and the shift change are very well correlated for the chain site substitution. This suggests that the reduction in $N(E_F)$ is the most probable cause for the decrease in T_c with these substitutions. In addition there is a close connection between T_c and temperature dependence of the shift for the chain site substituted and oxygen depleted $YBa_2Cu_3O_{7-\delta}$ as similar temperature dependences are observed for the samples with the same T_cs. Therefore this supports the idea that the T_c is related to the spin susceptibility and its temperature dependence in the CuO_2 planes[34].

For vanadium, small changes in shift at room temperature with substitution

are consistent with the slight reduction in T_c. For V the temperature dependence of ^{89}Y shift is very similar to that of chain site substituted $YBa_2(Cu_{1-x}M_x)_3O_7$ (M=Fe, Co, Ga and Al) samples. Therefore both ^{89}Y and ^{51}V (section 4.7) NMR data in $YBa_2(Cu_{1-x}V_x)_3O_7$ strongly suggest that the vanadium goes into the chain sites even though the structure remains orthorhombic. This is in disagreement with the ^{57}Fe Mossbauer study of $YBa_2(Cu,Fe,V)_3O_7$ of Shringi et al[10] who has suggested that V could occupy the Cu(2) site. It might be that addition of Fe modifies the behaviour of V since even for pure V doping 2 sites were evident. The increased relaxation and broadening of the ^{89}Y line in $YBa_2(Cu_{1-x}V_x)_3O_{7-\delta}$ suggest that some of the vanadium has a valence other than V^{5+} and is magnetic and thus unobservable in a ^{51}V NMR experiment.

From the Cu NQR studies of Zn doped $YBa_2Cu_3O_{7-\delta}$[42] it was found (consistent with our ^{89}Y data) that Zn mainly substitutes into the Cu(2) site. ^{63}Cu NMR data have been reported[30] for $YBa_2Cu_3O_7$ doped with small amounts of Zn, Al and Ga substitutions. Their data are also consistent with that Al and Ga substitute into the Cu(1) site and Zn into the Cu(2) site. In that study it was found that the Zn substitution in to the Cu(2) plane site leads to the formation of local moments on nearby sites. It was also suggested that the local moments lead to more rapid "metal-like" local field fluctuations at intermediate distances from the impurity (via the RKKY exchange interaction). These are the sources for the disruption of the antiferromagnetic fluctuations and thus for the suppression of superconductivity by Zn impurities. This explanation of ^{63}Cu NMR data is in good agreement with the conclusions made from ^{89}Y data.

References.

1. G.Xiao, M.Z.Cieplak, A.Gavrin, F.H.Streitz, A.Bakhshai and C.L.Chien, Reviews of Solid State Science, Vol.1, No.2 (1987) 323–328.
2. G.Xiao, M.Z.Cieplak, D.Musser, A.Gavrin, F.H.Streitz, C.L. Chien, J.J.Rhyne and J.A.Gotaas, Nature **332** (1988) 238.
3. Y.Maeno, T.Tomita, M.Kyogoku, S.Awaji, Y.Aoki, K.Hoshino, A.Minami and T.Fujita, Nature **238** (1987) 512.
4. J.M.Tarascon, P.Barboux, P.F.Miceli, L.H.Greene, G.W. Hull, M.Eibschutz and S.A.Sunshine, Phys.Rev.B **37** (1988) 7458.
5. Y.Xu, R.L.Sabatini, A.R.Moodenbaugh, Y.Zhu, S.G.Shyu, M. Suenaga, K.W.Dennis and R.W.McCallum, Physica C **169** (1990) 205.
6. E. Salamons and D.de Fontaine, Phys. Rev. B **42** (1990) 10152.
7. I.S. Lyubutin, Physica C **182** (1991) 315.
8. G. Baumgartel and K.H. Bennemann, Phys.Rev. B **40** (1989) 6711.
9. P.K.Mehta, O.Prakash, B.D.Padalia, P.D.Prabhavalkar, S.Natraj, D.T.Adroja and S.K.Malik, in Proc. Fifth Int. Conf.Ferrites (ICF-5) eds. C M Srivastava and M J Patni (New Delhi:IBH) **2** (1989) p.L597.
10. S.N.Shringi, R.V.Vadnere and Om.Prakash, Bull.Mater.Sci. **14** (1991) 709.
11. P.Bordet, J.L.Hodeau, P.Strobel, M.Marezio and A.Santoro, Solid State Comm. **66** (1988) 435.
12. G.Balakrishnan, R.Dupree, I.Farnan, D.M^{c}K Paul and M.E Smith, J.Phys.C **21** (1988) L847.
13. F.J. Adrian, Phys. Rev. Lett. **61** (1988) 2148.
14. R.Dupree, D.M^{c}K Paul, M.E Smith and G. Balakrishnan, Phys. Rev. Lett. **63** (1989) 688.
15 H. Alloul, Phys. Rev. Lett. **63** (1989) 689.
16. F.J. Adrian, Phys. Rev. Lett. **63** (1989) 690.
17. H.Alloul, T.Ohno and P.Mendels, Phys.Rev.Lett. **63** (1989) 1700.
18. R.E. Walstedt, W.W. Warren Jr., R.F. Bell, R.J. Cava, G.P. Espinosa, L.F. Schneemeyer and J. V. Waszczak, Phys. Rev. B **41** (1990) 9574.
19. T.Imai, J.Phys.Soc.Jpn. **59** (1990) 2508.
20. M. Takigawa, A.P. Reyes, P.C. Hammel, J.D. Thompson, R.H. Heffner, Z. Fisk and K.C. Ott, Phys. Rev. B **43** (1991) 247.
21. R.Dupree, Z.P.Han, D.McK.Paul, T.G.N.Babu and C.Greaves, Physica C **179** (1991) 311.
22. Z.P.Han, R.Dupree, D.McK.Paul, A.P.Howes and L.W.J.Caves, Physica C **181** (1991) 355.
23. A.J.Millis, H.Monien and D.Pines, Phys.Rev.B **42** (1990) 167.
24. W.J.Webster, D.P.Tunstall, P.F.Freeman and J.R.Cooper, Physica C **185-189** (1991) 1079.
25. H.Alluol, P.Mendels, H.Casalta, J.F.Marucco and J.Arabski, Phys.Rev.Lett. **67** (1991) 3140.
26. G.Balakrishnan, L.W.J.Caves, R.Dupree, D.McK.Paul and M.E.Smith, Physica C **161** (1989) 9.
27. H.Monien, D.Pines and M.Takigawa, Phys.Rev.B **43** (1991) 258.
28. H.Monien, P.M.Montheux and D.Pines Phys.Rev.B **43** (1990) 275.

29. R.Liang, T.Nakamura, H.Kawaji, M.Itoh and T.Nakamura, Physica C **170** (1990) 307.
30. W.W. Warren Jr., R.E. Walstedt, R.F. Bell, L.F. Schneemeyer, J.V. Waszczak, R. Dupree and A. Gencten, to be published.
31. S.Katano, T.Matsumoto, A.Matsushita, T.Hatano and S. Funahashi, Phys.Rev.B **41** (1990) 2009.
32. Y.Kohori, Y.Oda, H.Shibai, N.Okamoto, T.Kohara and K. Asayama, J.Phys.Soc.Jpn.**57** (1988) 2632.
33. M.E.Lines and M.Eibschutz, Physica C **166** (1990) 235.
34. Z.P. Han, R. Dupree, A. Gencten, R.S.Liu and P.P. Edwards, Phys. Rev. Lett. **69** (1992) 1256.
35. E. Oldfield, R.A. Kinsey, B. Montez, T. Ray and K.A. Smith, J. Chem. Soc. Chem. Commun. (1982) 254.
36. S. Ganapaty, S. Schramm and E. Oldfield, J. Chem. Phys. **77** (1982) 4360.
37. B.D.Dunlap and J.D.Jorgensen, C.Segre, A.E.Dwight, J.L.Matykiewicz, H.Lee, W.Peng and C.W.Kimball, Physica C **158** (1989) 397.
38. D. Müller, W. Gessner, H.J. Behrens and G. Scheler, Chem. Phys. Lett. **79** (1981) 59.
39. G. Engelhardt and D. Michel, High Resolution Solid State NMR of Silicates and Zeolites, John Wiley & Sons, 1987.
40. M.E. Smith, PhD Thesis, University of Warwick, 1987.
41. M.G. Mortuza, PhD Thesis, University of Warwick, 1989.
42. L. Albanese, C. Bucci, P. Carretta, R.De Renzi, G. Guidi, R. Tedeschi, F. Licci, C. Paris, G. Calestani, M.G. Francesconi, S.F.J. Cox and C.A. Scott, J. Magn. Magn. Mater., to be published.

Chapter 5. $YBa_2(Cu_{1-y}M_y)_4O_8$ System.

5.1. Introduction to $YBa_2(Cu_{1-y}M_y)_4O_8$ System.

As discussed in chapter 1 the structure of $YBa_2Cu_4O_8$ is closely related to $YBa_2Cu_3O_{7-\delta}$ with an addition of a CuO chain. Therefore it is of interest to make a comparative study of substitution effects in the $YBa_2Cu_4O_8$ system.

Substitution effects for Cu in $YBa_2(Cu_{1-y}M_y)_4O_8$ (M=e.g. Fe, Co, Ni and Zn) have been studied by several research groups[1-7]. A rapid decrease in T_c with Fe and Zn substitution was observed[2,3]. Structural properties of Zn and Fe substituted $YBa_2Cu_4O_8$ have been investigated by using X-Ray diffraction[1-3,5,7] and high resolution transmission electron microscopy[7] where it was found that the crystal structure undergoes an orthorhombic to tetragonal transition for 5% Fe substitution. Also Mossbauer spectroscopy studies of Fe substituted $YBa_2Cu_4O_8$ have been presented by Felner et al and Boolchand et al[1,5] who reported contradictory results on the site occupancy of Fe. For Zn substitution it was assumed[1] that it goes into the Cu(2) site. Miyatake et al[3] reported that the Zn substitution does not effect the oxygen content. On the other hand the oxygen concentration of Fe doped $YBa_2Cu_4O_8$ was assigned as $8+\delta$[1] since Fe has a valence larger than that for Cu and therefore attracts extra oxygen.

In this chapter , the effects of the Fe and Zn substitution for Cu in $YBa_2(Cu_{1-y}M_y)_4O_8$ are studied. First in section 5.2, XRD and transition temperature results are presented and discussed. ^{89}Y data (shift and relaxation rate) of $YBa_2(Cu_{1-y}M_y)_4O_8$ are presented and discussed in sections 5.3 and 5.4. Section 5.5 is the general discussion of $YBa_2(Cu_{1-y}M_y)_4O_8$ system.

5.2. XRD Results and Transition Temperatures.

XRD and A.C. susceptibility measurements of fully oxygenated powder samples of $YBa_2(Cu_{1-y}M_y)_4O_8$ (M=Fe and Zn) have been performed in order to determine the crystal structure and transition temperatures, respectively.

As discussed in sec 3.6.2, $YBa_2Cu_4O_8$ possesses an orthorhombic structure. In fig.5.1(a) and (b) XRD powder patterns of Zn and Fe doped $YBa_2(Cu_{1-y}M_y)_4O_8$ (where y=0–0.03) are illustrated,respectively, in the range of 2θ=45–50 showing the (0014), (020) and (200) peaks. The lattice parameters of $YBa_2(Cu_{1-y}M_y)_4O_8$ are plotted in fig.5.2(a) and (b) for Zn and Fe substitution, respectively.

For Zn doped $YBa_2Cu_4O_8$ samples XRD powder patterns (fig.5.1(a)) show that the crystal structure remains orthorhombic and as seen in fig.5.2(a) there are only very small changes in the lattice parameters. For Fe substitution the (020) and (0014) peaks move closer together until they nearly overlap with y=0.018. By 3% three peaks are almost together and the structure is close to being tetragonal. These results are in good agreement with the study by Felner and Brosh[2] who reported that the structure becomes tetragonal for y=0.05.

In fig.5.3 the transition temperatures determined from A.C. susceptibility measurements are plotted against dopant concentration y in $YBa_2(Cu_{1-y}M_y)_4O_8$ (where M=Zn and Fe and y=0–0.03). Both Fe and Zn substitutions cause a dramatic decrease in T_c with a rate of about 20K/%. The decreases in T_c are much faster than that for Fe and Zn substituted $YBa_2Cu_3O_{7-\delta}$.

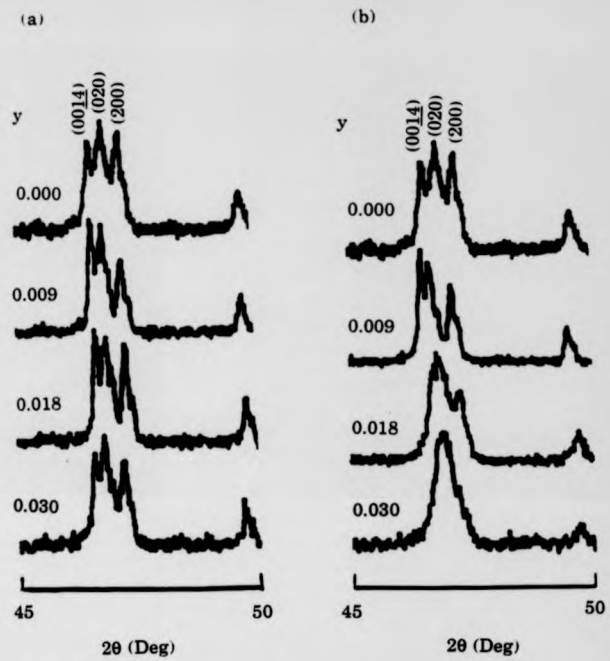

Fig.5.1. XRD powder patterns in $YBa_2(Cu_{1-y}M_y)_4O_8$ for M= (a) Zn and (b) Fe for y=0–0.03 and 2θ=45–50.

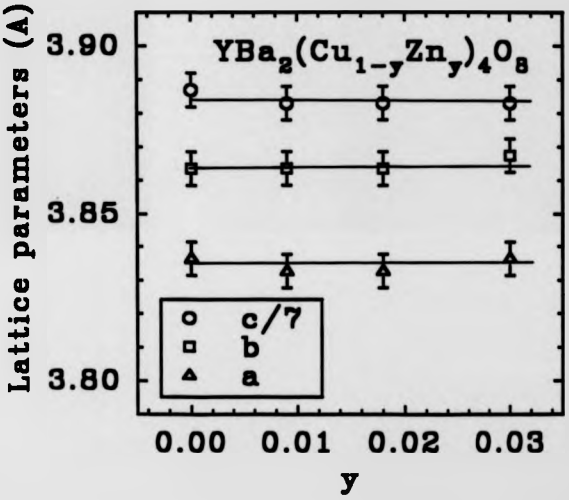

Fig.5.2(a). The lattice parameters of $YBa_2(Cu_{1-y}Zn_y)_4O_8$ as a function of dopant concentration y. The lines are drawn to guide the eye.

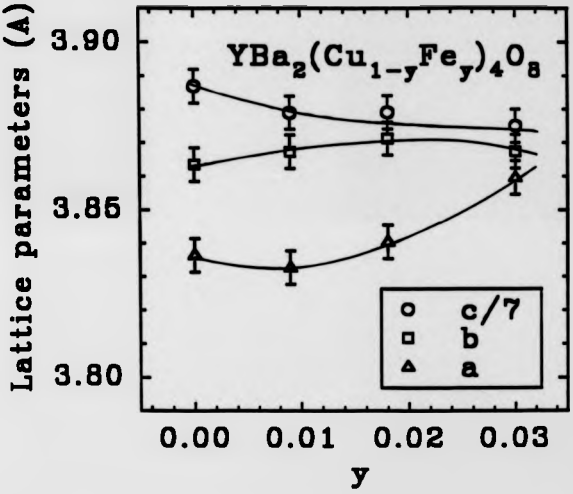

Fig.5.2(b). The lattice parameters of $YBa_2(Cu_{1-y}Fe_y)_4O_8$ as a function of dopant concentration y. The lines are drawn to guide the eye.

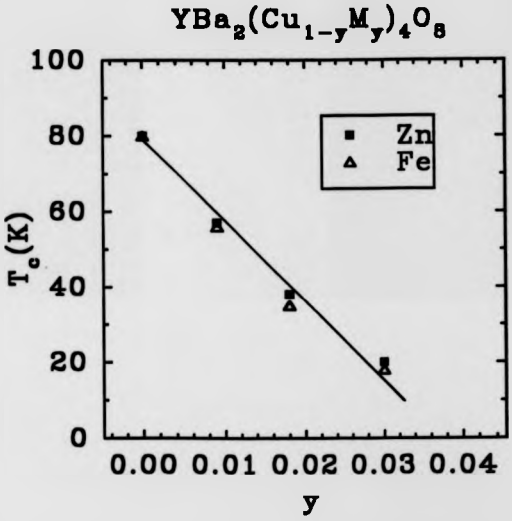

Fig.5.3. The transition temperatures as a function of dopant concentration y for Zn and Fe substitution in $YBa_2(Cu_{1-y}M_y)_4O_8$. The line is drawn to guide the eye.

5.3. ^{89}Y Shifts.

As discussed in chapter 4 the chemical shift for $YBa_2Cu_3O_7$ is ~200 ppm. Since in both $YBa_2Cu_3O_7$ and $YBa_2Cu_4O_8$ the yttrium atom has the same local chemical environment, one would expect the chemical shift to be very similar for $YBa_2Cu_4O_8$. As reported[8] the measured shift is -50 ppm, thus the Knight shift is ~-250 ppm. The changes in ^{89}Y shift with substitution and with temperature are likely to be due to the changes in Knight shift as the structure does not change.

5.3.1. Room Temperature Results and Discussion.

In fig.5.4 and 5.5 ^{89}Y MAS NMR spectra of $YBa_2(Cu_{1-y}M_y)_4O_8$ observed at room temperature are shown for a range of 0–3% dopant concentration for Zn and Fe substitution, respectively. There is hardly any change in shift with Zn substitution, but due to the disorder a line broadening was observed as the concentration increases for both (Zn and Fe) substitutions. In table 5.1 MAS line widths for $YBa_2(Cu_{1-y}M_y)_4O_8$ at room temperature are presented over the range of 0–3% substitution rate. For Fe, this broadening is greater than that for Zn. For Fe substitution also two additional peaks due to the additional phases appear at about 80 and 20 ppm. For Zn substitution the phase at 80 ppm was observed. The compositions of these phases are unknown. The phase at 80 ppm was also seen in some substituted $YBa_2(Cu_{1-x}M_x)_3O_{7-\delta}$ (Chapter 4) and; in Pr and Nd doped $YBa_2Cu_3O_{7-\delta}$[9]. From the ^{89}Y NMR spectrum of 3% Fe doped $YBa_2Cu_4O_8$ shown in fig.5.5, it appears ~50% of the yttrium is in the impurity phases. However these phases were not detected by XRD indicating that true amount of these impurity phases is less than 5%. In spectra acquired for shorter delays the relative intensity

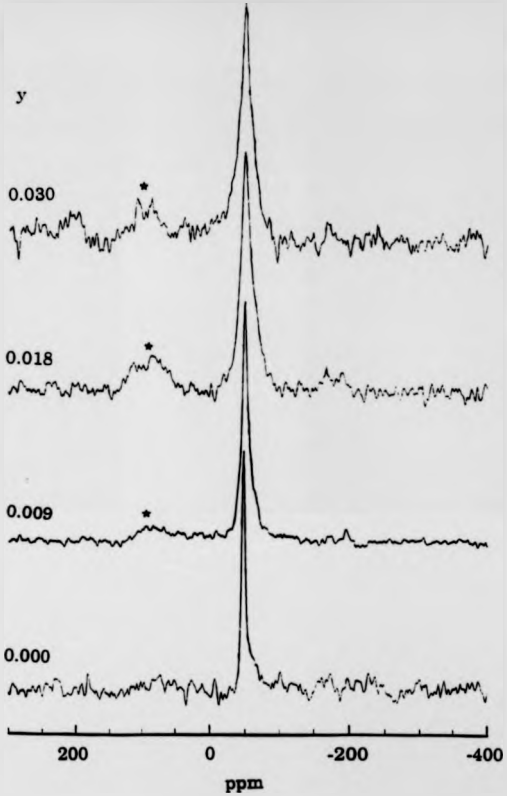

Fig.5.4. ^{89}Y MAS NMR spectra in $YBa_2(Cu_{1-y}Zn_y)_4O_8$ with x=0–0.03. The asterisks denote the unknown phase.

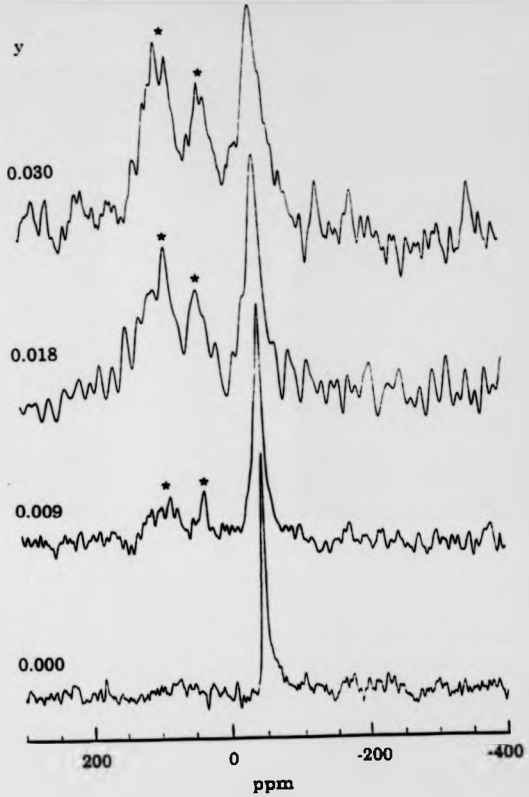

Fig.5.5. ^{89}Y MAS NMR spectra in $YBa_2(Cu_{1-y}Fe_y)_4O_8$ with x=0–0.03. The asterisks denote the additional phases.

of the lines at 80ppm and 20ppm increased indicating that their T_1 values are shorter than that in 3% Fe doped $YBa_2Cu_4O_8$. T_1 for 3% Fe doped $YBa_2Cu_4O_8$ could not be measured because of these impurity phases, but from fig.5.11 one would expect it to be about 28s. Therefore, for a delay of 30s used to obtain the spectrum, the line for 3% Fe doped $YBa_2Cu_4O_8$ is partially saturated. The peak at 80ppm may be due to some fraction of Y occupying the Ba site. ^{89}Y MAS NMR shifts are plotted in fig.5.6 as a function of dopant concentration y for both substitutions. For Fe substitution the ^{89}Y shift increases with substitution rate, becoming –42 ppm by 3%. For Zn, only very small shift changes observed. These changes in shift for Zn and Fe substituted $YBa_2Cu_4O_8$ are similar to those for Zn and Fe doped $YBa_2Cu_3O_{7-\delta}$.

Table: 5.1. MAS line widths for Zn and Fe substituted $YBa_2(Cu_{1-y}M_y)_4O_8$ at room temperature.

Substitution	MAS Width (Hz)	
y	For Zn	For Fe
0.000	80	80
0.009	150	250
0.018	250	400
0.03	300	700

5.3.2. Temperature Dependence.

In fig.5.7 ^{89}Y shift as a function of temperature is plotted for $YBa_2(Cu_{1-y}Zn_y)_4O_8$ with y=0,0.018 and 0.03. For pure $YBa_2Cu_4O_8$ the temperature dependence of the shift is similar to that reported by Dupree et al and Carretta et

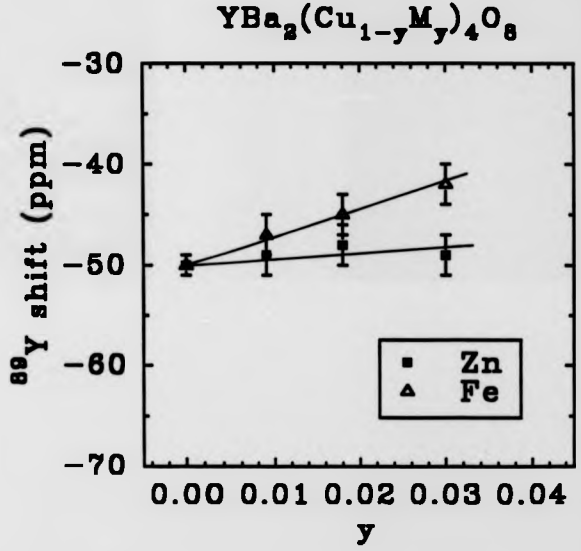

Fig.5.6. ^{89}Y shift at room temperature versus dopant concentration y for $YBa_2(Cu_{1-y}M_y)_4O_8$ with M=Fe and Zn.

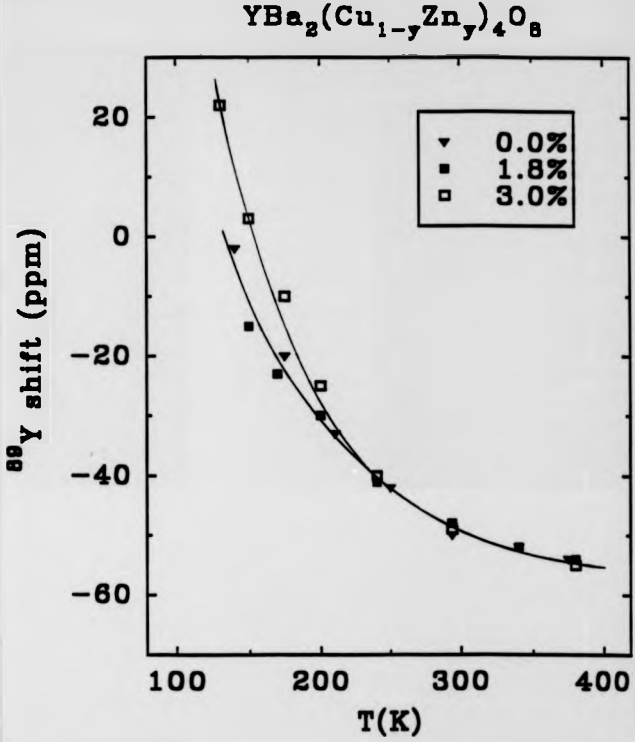

Fig.5.7. ^{89}Y shift as a function of temperature for 1.8% and 3% Zn substituted $YBa_2(Cu_{1-y}Zn_y)_4O_8$ and for pure $YBa_2Cu_4O_8$. The lines are drawn to guide the eye.

al[8,10]. For these three samples, pure $YBa_2Cu_4O_8$ and 1.8% and 3% Zn doped $YBa_2Cu_4O_8$, the temperature dependence of the shift shows a similar behaviour increasing as the temperature decreases. However for below 200K there is a slight divergence of the shift for 3% Zn as seen from the plot. The temperature dependence of shift for 1.8% Zn and Fe substitution is shown in fig.5.8 together with the shift for undoped $YBa_2Cu_4O_8$. For both substitutions the shift has a similar temperature dependence similar to that in undoped $YBa_2Cu_4O_8$ with only slight deviations.

The MAS width as a function of temperature is shown in fig.5.9 for 1.8% Zn and Fe substitution together with that for undoped $YBa_2Cu_4O_8$. The MAS width increases as the temperature decreases for all the samples. In fig.5.10 MAS width is plotted as a function of 1/T for pure $YBa_2Cu_4O_8$ and 1.8% Zn doped $YBa_2Cu_4O_8$. As seen from the figure, for both (pure $YBa_2Cu_4O_8$ and 1.8% Zn doped $YBa_2Cu_4O_8$) the line width follows a Curie Weiss type temperature dependence. For 1.8% Zn substitution a temperature independent contribution to the broadening is produced similar to that for Zn substituted $YBa_2Cu_3O_7$. These broadenings are 64 Hz/% and 88 Hz/% in Zn doped $YBa_2Cu_3O_7$ and $YBa_2Cu_4O_8$, respectively. For Fe the variation of the line width with temperature does not obey the Curie–Weiss behaviour.

5.4. ^{89}Y Spin Lattice Relaxation.

5.4.1. Results.

^{89}Y spin lattice relaxation rates at room temperature for both Fe and Zn substitutions are shown in fig.5.11 as a function of dopant concentration y. The relaxation rates decreases with Fe substitution but increases for Zn giving a similar

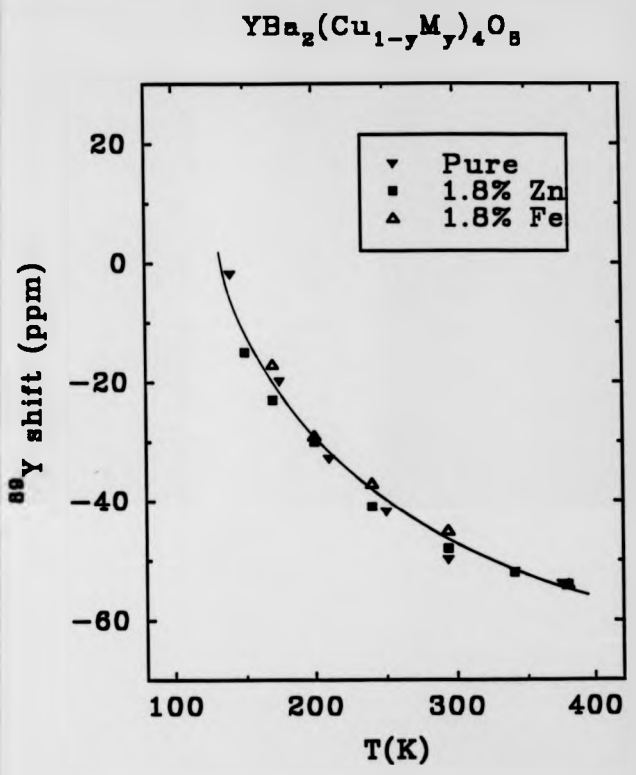

Fig.5.8. ^{89}Y shift as a function of temperature for 1.8% Zn and Fe substituted $YBa_2(Cu_{1-y}M_y)_4O_8$ and for pure $YBa_2Cu_4O_8$. The line is drawn to guide the eye.

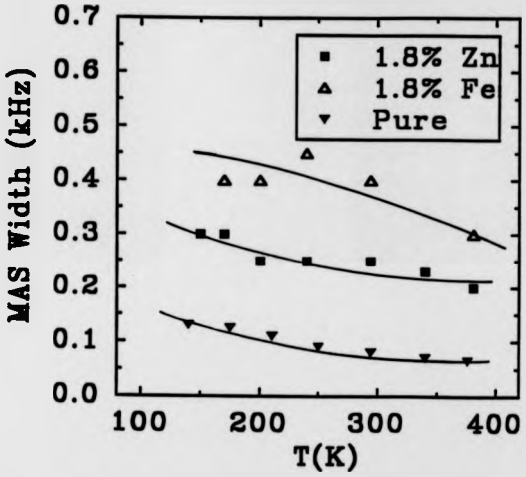

Fig.5.9. The ^{89}Y MAS NMR line width as a function of temperature for 1.8% Zn and Fe substituted $YBa_2(Cu_{1-y}M_y)_4O_8$ and for pure $YBa_2Cu_4O_8$. The lines are drawn to guide the eye.

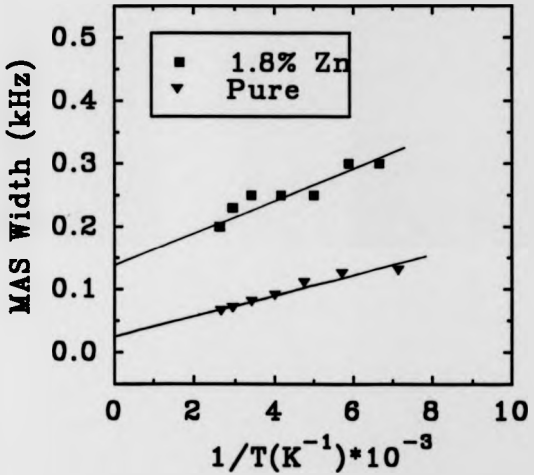

Fig.5.10. ^{89}Y MAS NMR line width versus 1/T for pure $YBa_2Cu_4O_8$ and 1.8% Zn doped $YBa_2Cu_4O_8$.

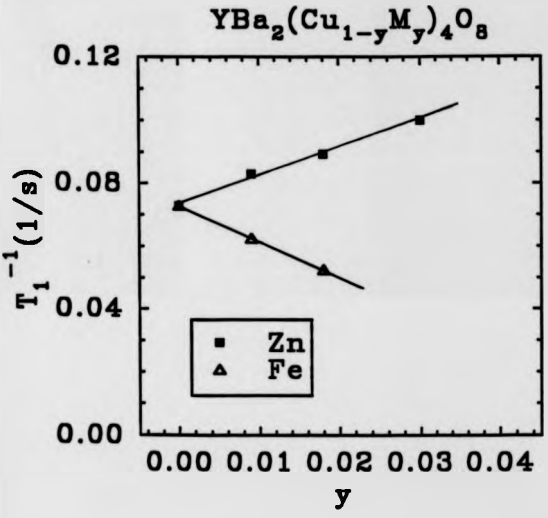

5.11. ^{89}Y T_1^{-1} at room temperature versus dopant concentration y for $YBa_2(Cu_{1-y}M_y)_4O_8$ with M=Fe and Zn. The lines are drawn to guide the eye.

behaviour to that for Fe and Zn substituted $YBa_2(Cu_{1-x}M_x)_3O_{7-\delta}$.

The relaxation data obtained for 1.8% Zn and Fe doped $YBa_2(Cu_{1-y}M_y)_4O_8$ together with undoped $YBa_2Cu_4O_8$ are shown in fig.5.12 as (T_1T) versus T. T_1 values for undoped $YBa_2Cu_4O_8$ at 150 and 380K were taken from reference 8.

5.4.2. Discussion.

For Zn, the increase in relaxation rate with only a small change in shift suggests that the source of this relaxation is not the changes in the density of states. This is similar to the behaviour for Zn and Ni substituted $YBa_2(Cu_{1-x}M_x)_3O_{7-\delta}$ in chapter 4.

Fig.5.13 shows relaxation rate, T_1^{-1} plotted as a function of transition temperature T_c for Zn substitution in $YBa_2Cu_4O_8$. It is clear that there is linear correlation between the reduction in T_c and the increase in relaxation rate. Assuming Zn substitutes on the plane sites, this suggest that the cause for the reduction in T_c with Zn substitution for Cu in $YBa_2Cu_4O_8$ is also magnetic as it was for Zn and Ni in $YBa_2(Cu_{1-x}M_x)_3O_{7-\delta}$.

Table: 5.2. K^2T_1T versus dopant concentration for $YBa_2(Cu_{1-y}Fe_y)_4O_8$ at room temperature.

y	Shift(ppm)	K (ppm)	T_1 (s)	K^2T_1T (ppm^2s.K)
0.000	−50	−250	14±1	2.6±0.3
0.009	−47	−247	16±1	2.9±0.3
0.018	−45	−245	19±2	3.4±0.3

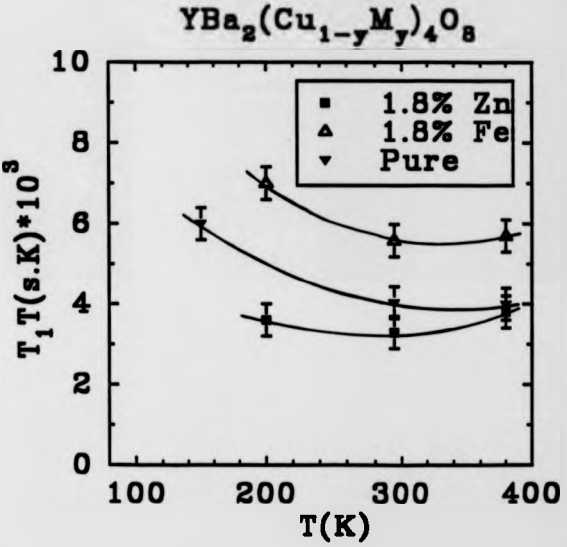

Fig.5.12. (T_1T) as a function of temperature for 1.8% Zn and Fe substituted $YBa_2(Cu_{1-y}M_y)_4O_8$ and for pure $YBa_2Cu_4O_8$[8].

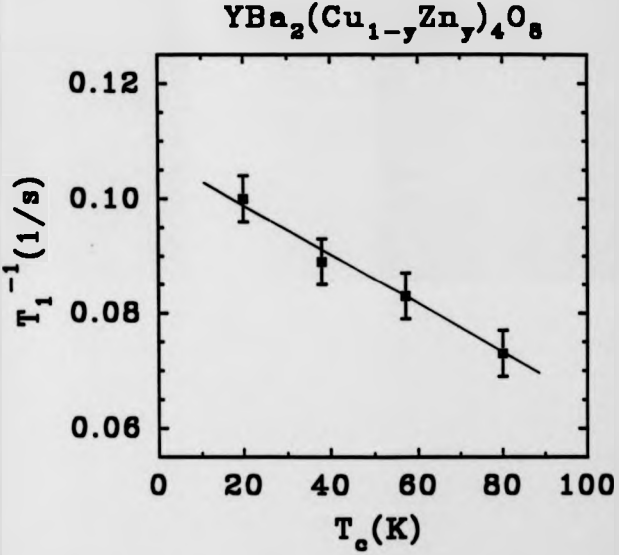

Fig.5.13. T_1^{-1} as a function of T_c for $YBa_2(Cu_{1-y}Zn_y)_4O_8$ with y as the implicit parameter.

In table 5.2 K^2T_1T is given for Fe substituted $YBa_2Cu_4O_8$. The behaviour is approximately Korringa like (K^2TT_1=constant).

In fig.5.14 K^2T_1T is plotted as a function of temperature for 1.8% Fe doped $YBa_2Cu_4O_8$ and for undoped $YBa_2Cu_4O_8$[8]. The plot shows that for 1.8% Fe doped $YBa_2Cu_4O_8$ and for undoped $YBa_2Cu_4O_8$ K^2T_1T=constant is obeyed. For ^{89}Y metal the Korringa constant is about $1.0*10^8$ $ppm^2s.K$. It is noteworthy that the actual magnitude of Korringa constant increases with Fe substitution and T_c is reduced.

5.5. General Discussion of $YBa_2(Cu_{1-y}M_y)_4O_8$ System.

XRD data have shown that the crystal structure remains orthorhombic for Zn substitution whereas Fe substitution causes changes in the lattice parameters towards becoming a tetragonal structure at about 5% substitution. This is consistent with earlier work[2,3,7]. For both Fe and Zn substitution a rapid decrease in T_c was observed. This is also in good agreement with earlier work[1,3].

We first discuss the NMR data for Zn substitution. Zn substitution cause very small changes in shift, but a dramatic increase in relaxation rate. This is not consistent with the Korringa relation and thus an indication for the existence of an additional source for the relaxation similar to that observed for Zn and Ni substituted $YBa_2Cu_3O_{7-\delta}$. The correlation between the relaxation rate and T_c as presented in section 5.4.2 is evidence that the fluctuating magnetic fields with Zn substitution creating extra relaxation are the probable source for the rapid decrease in T_c. The effects on the shift and relaxation rates with Zn substitution in $YBa_2Cu_4O_8$ are similar to those for Zn substitution in $YBa_2Cu_3O_{7-\delta}$ strongly suggesting that Zn substitutes onto the Cu(2) site. The suppression of T_c with Zn substitution has been

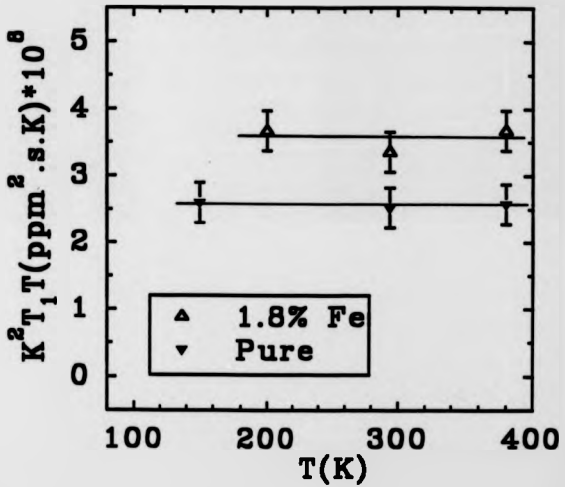

Fig.5.14. K^2T_1T as a function of temperature for 1.8% Fe substituted $YBa_2(Cu_{1-y}M_y)_4O_8$ and for pure $YBa_2Cu_4O_8$[8].

discussed by Miyatake et al[3] who have suggested that the destruction of the local antiferromagnetic correlations is the mechanism responsible for the rapid decrease in T_c. The fluctuating magnetic fields created by Zn doping as suggested by Warren et al[11] and discussed in section 4.9 for Zn doped $YBa_2Cu_3O_{7-\delta}$ might be the source for the destruction of the local antiferromagnetic correlations. Therefore the conclusion of Miyateka et al. agrees with what has been suggested from our ^{89}Y data. The temperature dependence of the ^{89}Y shift for Zn doped $YBa_2Cu_4O_8$ is similar to that for pure $YBa_2Cu_4O_8$ as was found for Zn doped $YBa_2Cu_3O_{7-\delta}$ i.e. consistent with substitution in the plane site and no change in $N(E_F)$.

^{89}Y shift and relaxation rate behaviour at room temperature for Fe substituted $YBa_2Cu_4O_8$ is similar to that for chain site substituted $YBa_2Cu_3O_{7-\delta}$ although there is a slight deviation from the Korringa relation. This could be taken to suggest that Fe mostly occupies the Cu(1) site. On the other hand (remembering that the temperature dependence of the shift for plane site substituted $YBa_2Cu_3O_{7-\delta}$ is similar to that for undoped $YBa_2Cu_3O_{7-\delta}$ (chapter 4)) for 1.8% Fe doped $YBa_2Cu_4O_8$ the temperature dependence of shift is similar to that for undoped $YBa_2Cu_4O_8$ consistent with Fe mainly occupying the plane site. From a ^{57}Fe Mossbauer study of 2.5% Fe substituted $YBa_2Cu_4O_8$, Felner et al[1] have observed that one quadrupole doublet is present at 90K. They have attributed this doublet to iron ions which replace copper in the Cu(1) site. However, it was claimed by Boolchand et al[5] that Fe appears to occupy the Cu(2) site. In their study Boolchand et al have analyzed Mossbauer spectra line shapes in terms of two majority (from the plane site) and two minority (from the chain site) quadrupole doublets. These contradictory results might be because of an unstable structure in Fe substituted

$YBa_2Cu_4O_8$ as reported elsewhere[7]. Also the ^{89}Y MAS widths of Fe substituted $YBa_2Cu_4O_8$ are broader than those of Zn substituted $YBa_2Cu_4O_8$ (table 5.1) suggesting that the structure in Fe substituted $YBa_2Cu_4O_8$ is much more disordered than that in Zn doped material. Although our ^{89}Y NMR results suggest that Fe might substitute on both Cu(1) and Cu(2), sites because of these complications discussed above we can not make a conclusion on the site occupancy of Fe. It also seems likely that some part of the reduction in T_c is due to the change in $N(E_F)$ with Fe substitution.

References.

1. I. Felner, I. Nowik, B. Brosh, D. Heckel and E. R. Bauminger, Phys. Rev. B **43** (1991) 8737.
2. I. Felner, B. Brosh, Phys. Rev. B **43** (1991) 10364
3. T. Miyatake, K. Yamaguchi, T. Takata, N. Koshizuka and S. Tanaka, Phys. Rev. B **44** (1991) 10139.
4. Y. Wu, S. Pradhan and P. Boolchand, Phys. Rev. Lett. **67** (1991) 3184.
5. P. Boolchand, S. Pradhan and Y. Wu, M. Abdegadir, W Huff, D. Farrell, R. Coussement and D. McDaniel, Phys. Rev. B **45** (1992) 921.
6. K. Yanagisawa, Y. Matsui, Y. Kodama, Y. Yamada and T. Matsumoto, Physica C **183** (1991) 197.
7. K. Yanagisawa, Y. Matsui, Y. Kodama, Y. Yamada and T. Matsumoto, Physica C **191** (1992) 32.
8. R. Dupree, Z.P. Han, D. McK. Paul, T.G.N. Babu and C. Graves, Physica C **179** (1991) 311.
9. Z.P. Han, R. Dupree, D. McK. Paul, A.P. Howes and L.W.J. Caves, Physica C **181** (1991) 355.
10. P. Carretta, M. Corti, A. Rigamonti, R.De Renzi, F. Licci, C. Paris, L. Bonoldi, M. Sparpaglione and L. Zini, Physica C **191** (1992) 97.
11. W.W. Warren Jr., R.E. Walstedt, R.F. Bell, L.F. Schneemeyer, J.V. Waszczak, R. Dupree and A. Gencten, to be published.

Chapter 6. Conclusions.

6.1. Comparison of These Two Systems.

It was found (in chapters 4 and 5) that the decreases in T_c with Fe and Zn substitution for Cu in $YBa_2Cu_4O_8$ are much faster than those observed for Fe and Zn substitution for Cu in $YBa_2Cu_3O_{7-\delta}$. For example the reduction rates in T_c for Zn substituted $YBa_2Cu_3O_{7-\delta}$ and $YBa_2Cu_4O_8$ are 7K/% and 20K/%, respectively (table: 6.1). The reduction rates in shift with Fe substitution for Cu in $YBa_2Cu_3O_{7-\delta}$ and $YBa_2Cu_4O_8$ are 3.0 and 2.7 ppm/%, respectively. But the reduction rates in T_c are very different (see table 6.2).

Table: 6.1 The changes in relaxation rate and T_c with Zn substitution for Cu in $YBa_2Cu_3O_{7-\delta}$ and $YBa_2Cu_4O_8$.

Substitution	dT_1^{-1}/dc $(s^{-1}/\%) \times 10^{-3}$	dT_c/dc (K/%)
Zn in $YBa_2Cu_3O_{7-\delta}$	11.00±1	7.0±1
Zn in $YBa_2Cu_4O_8$	9.50±1	20.0±2

Table: 6.2 The changes in shift and T_c with Fe substitution for Cu in $YBa_2Cu_3O_{7-\delta}$ and $YBa_2Cu_4O_8$.

Substitution	dK/dc (ppm/%)	dT_c/dc (K/%)
Fe in $YBa_2Cu_3O_{7-\delta}$	3.0±0.5	4.0±0.5
Fe in $YBa_2Cu_4O_8$	2.7±0.5	20.0±2

It is generally agreed and found in this work that Zn substitutes on the plane site in $YBa_2Cu_4O_8$. We have claimed (chapters 4 and 5) that the cause of the reduction in T_c for plane site substitution is magnetic in origin. As shown in table 6.1, dT_1^{-1}/dc values are nearly the same for both Zn substituted $YBa_2Cu_3O_{7-\delta}$ and $YBa_2Cu_4O_8$. Assuming the same cause for the depression in T_c for both Zn substituted $YBa_2Cu_3O_{7-\delta}$ and $YBa_2Cu_4O_8$, one would therefore expect the reduction rates in T_c also to be the same, but they are different. This (together with the comparison between the reduction rates in shift and the decreases in T_c for Fe substitution e.g. table 6.2) might be because for some reason T_c in $YBa_2Cu_4O_8$ is much more sensitive to magnetic effects than that in $YBa_2Cu_3O_{7-\delta}$.

6.2. General Conclusions.

6.2.1 $YBa_2(Cu_{1-x}M_x)_3O_{7-\delta}$ System.

The NMR behaviour of ^{89}Y upon substitution for copper in $YBa_2Cu_3O_7$ is very different for the substitutions which go on the chain site and change the structure to tetragonal (Al,Co,Fe,Ga) than for the other substitutions. ^{89}Y NMR data by means of the change in chemical shift for Al, Co, Ga and Fe substitutions have provided evidence for the existence of a true O–T transition. For the chain site substitutions the room temperature Knight shift increases linearly with substitution, the relaxation rate decreases, and the shifts become more positive with decreasing temperature. All the changes are consistent with a reduction in $N(E_F)$ and the shift variation at room temperature and the reduction in T_c seem to be well correlated suggesting that the reduction in T_c for these substitutions is also related to a reduction in $N(E_F)$. The temperature dependence of the shifts is similar for samples

with the similar T_cs emphasising the correlation between T_c and the susceptibility as evidenced in the ^{89}Y NMR shift. For the plane site substitutions (Ni,Zn) only small changes in shift are observed but the relaxation rate increases markedly. The increased relaxation suggests that some form of magnetic scattering, which is largest for Zn, is present and this combined with the small change in shift and the correlation between the reduction in T_c and the change in relaxation rate imply that some form of magnetic effect is most likely to be responsible for the decrease of T_c with the plane site substitutions (Zn and Ni) into $YBa_2Cu_3O_7$. The behaviour of both the ^{51}V NMR and the temperature dependence of the ^{89}Y shift in the vanadium doped sample suggest that at low concentrations vanadium reduces the hole concentration and substitutes on the chain sites.

The temperature dependence of ^{89}Y shift for Fe, Co, Al, Ga and V substituted $YBa_2Cu_3O_7$ is similar to that for oxygen depleted $YBa_2Cu_3O_7$[1,2] and supports the idea that Fe, Co, Al, Ga and V substitute on the chain site with a small portion of Fe going into the Cu(2) site.

6.2.2. $YBa_2(Cu_{1-y}M_y)_4O_8$ System.

The effect of substitution for Cu in $YBa_2Cu_4O_8$ upon ^{89}Y NMR at room temperature is different for Zn substitution than for Fe substitution. For Fe substitution, the room temperature shift increases by a roughly similar amount to that for Fe substituted $YBa_2Cu_3O_7$ and the relaxation rate decreases giving a nearly Korringa like behaviour. For Zn substitution, there are only small changes in shift but an increase in relaxation rate is observed as dopant concentration increases. This is not consistent with the Korringa relation. Therefore in similar fashion to the plane

site substituted $YBa_2Cu_3O_7$ case there must be some fluctuating magnetic fields producing extra relaxation with Zn substitution. The correlation between T_1^{-1} and T_c with Zn substitution indicates that these fluctuating magnetic fields are responsible for the reduction in T_c.

NMR data for Zn substituted $YBa_2Cu_4O_8$ combined with that for the Zn substituted $YBa_2Cu_3O_7$ system have provided the evidence that Zn occupies the Cu(2) site in $YBa_2Cu_4O_8$. For Fe, the shift and relaxation at room temperature is consistent with substitution in the Cu(1) site. However the temperature dependence of the shift similar to that for undoped $YBa_2Cu_4O_8$ and the rapid decrease in T_c imply that Fe substitutes on the Cu(2) site. Therefore, it is likely that Fe substitutes on both Cu(1) and Cu(2) sites.

6.3. Suggestions for Further Work.

In this thesis, ^{89}Y NMR study of substitution effects for Cu in $YBa_2Cu_3O_{7-\delta}$ and $YBa_2Cu_4O_8$ superconductors have been investigated. For substituted $YBa_2Cu_3O_{7-\delta}$ ^{89}Y shift behaviour and also some relaxation data for a variety of substitutions (Fe, V, Co, Ni, Zn, Al and Ga) have been provided in the normal state. In the case of $YBa_2Cu_4O_8$ ^{89}Y data in the normal state for Zn and Fe substitution have been obtained.

Further ^{89}Y NMR study of substitution for Cu in $YBa_2Cu_4O_8$ with some other substituent (e.g. V, Co, Ni, Al, Ga) is of particular interest regarding the entire combination of ^{89}Y data of substituted $YBa_2Cu_4O_8$ with that of substituted $YBa_2Cu_3O_{7-\delta}$. This further investigation might give some fruitful results to clarify the mechanism responsible for the rapid decrease in T_c with Cu site substitution in

$YBa_2Cu_4O_8$. Also ^{51}V and ^{27}Al NMR in V and Al substituted $YBa_2Cu_4O_8$ samples can be investigated. It seems that KT_1T=constant behaviour is obeyed more closely than Korringa behaviour for some substituted $YBa_2Cu_3O_{7-\delta}$ (chapter 4). The same behaviour was also obtained for $^{17}O^{(3)}$ and $^{89}Y^{(2)}$ in $YBa_2Cu_3O_{7-\delta}$. Therefore an understanding of this behaviour is of importance and further ^{89}Y relaxation time measurements of substituted $YBa_2Cu_3O_{7-\delta}$ and $YBa_2Cu_4O_8$ for a wider range of temperature might provide useful information regarding this behaviour.

Some work on ^{63}Cu NMR in substituted $YBa_2Cu_3O_{7-\delta}$[e.g.4-6] has been done and promising results have been obtained. Therefore, further ^{63}Cu NMR studies of these substituted $YBa_2Cu_3O_{7-\delta}$ and $YBa_2Cu_4O_8$ systems are required.

^{17}O has proved to be a useful probe in the study of high T_c superconductors[e.g.7-9]. However, to date, there has not been any ^{17}O NMR study of Cu site substituted $YBa_2Cu_3O_{7-\delta}$ and $YBa_2Cu_4O_8$. Thus, ^{17}O NMR might well be applied to the Cu site substituted $YBa_2Cu_3O_{7-\delta}$ and $YBa_2Cu_4O_8$ superconductors.

References.

1. G. Balakrishnan, R. Dupree, I. Farnan, D.McK. Paul and M.E. Smith, J.Phys.C **21** (1988) L847.
2. H. Alloul, T. Ohno and P. Mendels, Phy. Rev. Lett. **63** (1989) 1700.
3. Takigawa, A.P. Reyes, P.C. Hammel, J.D. Thompson, R.H. Heffner, Z. Fisk and K.C. Ott, Phys. Rev. B **43** (1991) 247.
4. Y. Kohori, Y. Oda, H. Shibai, N. Okamoto, T. Kohara and K. Asayama, J. Phys. Soc. Jpn. **57** (1988) 2632.
5. W.W. Warren Jr., R.E. Walstedt, R.F. Bell, L.F. Schneemeyer, J.V. Waszczak, R. Dupree and A. Gencten, to be published.
6. L. Albanese, C. Bucci, P. Carretta, R.De Renzi, G. Guidi, R. Tedeschi, F. Licci, C. Paris, G. Calestani, M.G. Francesconi, S.F.J. Cox and C.A. Scott, J. Magn. Magn. Mater., to be published.
7. E. Oldfield, C. Coretsopoulos, S. Yang, L. Reven, H.C. Lee, J. Shore, O.H. Han and E. Ramli, Phys. Rev. B **40** (1989) 6832.
8. R. Dupree, Z.P. Han, A.P. Howes, D.McK. Paul, M.E. Smith and S. Male, Physica C **175** (1991) 269.
9. A.P. Howes, PhD Thesis, University of Warwick, UK 1992.